A VERY HIGH FREQUENCY RADIO INTERFEROMETER FOR INVESTIGATING IONOSPHERIC DISTURBANCES USING GEOSTATIONARY SATELLITES

by

Robert Terry
Bernard J. Flaherty

Technical Report No. 45-1

DETERMINATION OF CHANGES IN EXOSPHERIC ELECTRON CONTENT BY A COMPARISON OF GROUP DELAY AND FARADAY ROTATION

by

Richard E. DuBroff

Technical Report No. 45-2

March 1972

Sponsored by

National Aeronautics and Space Administration
NGR 14-005-002
Ionosphere Radio Laboratory

ELECTRICAL ENGINEERING RESEARCH LABORATORY
ENGINEERING EXPERIMENT STATION
UNIVERSITY OF ILLINOIS
URBANA, ILLINOIS 61801

UILU-72-2539

A VERY HIGH FREQUENCY RADIO INTERFEROMETER FOR INVESTIGATING IONOSPHERIC DISTURBANCES USING GEOSTATIONARY SATELLITES

by

Robert Terry
Bernard J. Flaherty

Technical Report No. 45-1

DETERMINATION OF CHANGES IN EXOSPHERIC ELECTRON CONTENT BY A COMPARISON OF GROUP DELAY AND FARADAY ROTATION

by

Richard E. DuBroff

Technical Report No. 45-2

March 1972

Sponsored by

National Aeronautics and Space Administration
NGR 14-005-002
Ionosphere Radio Laboratory

ELECTRICAL ENGINEERING RESEARCH LABORATORY
ENGINEERING EXPERIMENT STATION
UNIVERSITY OF ILLINOIS
URBANA, ILLINOIS 61801

(Technical Report 45-2, DETERMINATION OF CHANGES IN EXOSPHERIC ELECTRON CONTENT BY A COMPARISON OF GROUP DELAY AND FARADAY ROTATION, begins on page 64. This report has its own pagination.)

A VERY HIGH FREQUENCY RADIO INTERFEROMETER FOR INVESTIGATING IONOSPHERIC DISTURBANCES USING GEOSTATIONARY SATELLITES

by

Robert Terry
Bernard J. Flaherty

March 1972

Sponsored by

National Aeronautics and Space Administration
NGR 14-005-002

Technical Report No. 45-1

Ionosphere Radio Laboratory

ELECTRICAL ENGINEERING RESEARCH LABORATORY
ENGINEERING EXPERIMENT STATION
UNIVERSITY OF ILLINOIS
URBANA, ILLINOIS 61801

ABSTRACT

This report deals with the theory and development of a VHF correlation radio interferometer for investigating ionospheric disturbances. The system was developed to receive signals from the geostationary Application Technology Satellite series satellites. Amplitude and phase variations of the signal passing through the ionosphere can be detected by this instrument.

The system consists of two superhetrodyne receivers separated by a distance known as the baseline of the system. Since the system is a phase sensitive instrument, the local oscillators of the two receivers must be phase coherent. This is accomplished by using phase-locked loops for generating the local oscillators. The system uses a frequency synthesizer as a stable reference source. All frequencies generated in the system are phase coherent with this source.

The two signals from the separate receivers are cross-correlated. This is accomplished by multiplying the two signals together and then time averaging the result.

The system developed uses the principle of frequency off-set to increase the sensitivity of the instrument. This is accomplished by off-setting one of the local oscillators by a small amount. The output of the multiplier now contains a signal component whose frequency is equal to the amount of the off-set. This signal contains the amplitude and phase information of the multiplied signal. Duel

channel correlation is accomplished by using quadrature phase detection of the multiplied signal. The integrated output of the phase detectors represents the sine and cosine components of the correlated signals. The effects of amplitude and phase variations can be separated using coordinate conversion techniques.

ACKNOWLEDGMENT

The authors wish to express their thanks to Dr. K. C. Yeh, for his advice and good counsel. Thanks are also extended to Mr. A. Szelpal who did the layout and building of the equipment. This work was sponsored by the National Aeronautics and Space Administration under Grant NGR 14-005-002.

TABLE OF CONTENTS

LIST OF FIGURES

1. INTRODUCTION

The first section of this work presents a review of the basic operating principles of the correlation type radio interferometer as applied to the monitoring of geostationary synchronous satellites. The basic interferometer consists of two spaced receiver sites. Signals from an external source enter the system at the receiver sites and are compared by cross-correlation or multiplication. This system is very sensitive to a change in position or apparent position of the source. This is because the spatial response of the system combines the individual directivity of each antenna site with that of a multibeam fan. The individual beams of the fan are comparable to that of a parabolic dish with a diameter equal to the receiver site spacing. [Clark and Frost, 1967].

Because of their phase sensitive characteristics, interferometers have become a valuable instrument for use in the investigation of the ionosphere. Its use with synchronous satellites is one such example. The synchronous satellite is a relatively stationary, coherent deterministic source. Variations in the ray path length from the source to the receiver sites occuring as the signal passes through the ionosphere can be detected using the principles of interferometry.

The second part of this work will deal with the design considerations and construction of a short base line inter-

ferometer. It was built to investigate the nature and occurrence of amplitude and phase scintillations of the signal received from a synchronous satellite caused by the ionosphere.

2. THEORY OF A SIMPLIFIED INTERFEROMETER

A simple idealized interferometer consisting of two spaced receiver sites is shown in the block diagram of Figure 1. The system shown shares a common local oscillator. (In systems where the receiver spacing is far apart and separate local oscillators are used, it is necessary that the local oscillators be phase locked together or to a common source.) The local oscillator signals must be phase coherent, otherwise the output of the multiplier-correlator will contain the unwanted phase variations between the local oscillators.

Assume a distant point source, such as a synchronous satellite, is radiating a monochromatic signal at some frequency f_0. The point source is oriented at some elevation angle θ with respect to the baseline of the system as shown in figure 1. The superhetrodyne output of both receivers will be at some intermediate frequency f_m. Since the local oscillator is common to both receivers, the output of receiver 'A' can be written as

$$S_{ma} = A \sin(\omega_m t + \phi + \phi_{ra}) + N_a(t) \qquad (1)$$

and from receiver 'B'

$$S_{mb} = B \sin(\omega_m t + \phi + \phi_{rb} - \phi_s) + N_b(t) \qquad (2)$$

Definition of terms:

ω_m the radian IF frequency of the output of the receivers

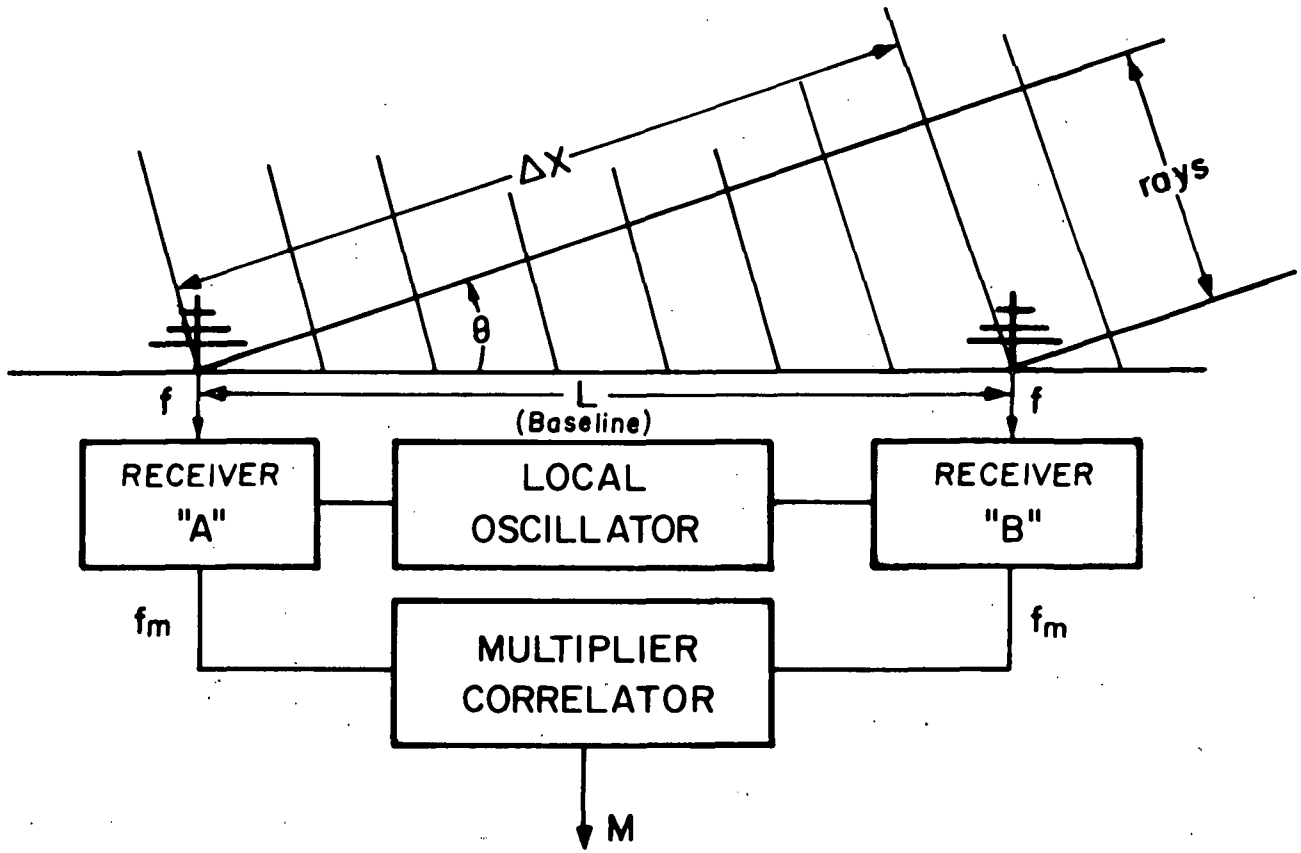

Fig. 1. Block diagram of a simple interferometer.

ϕ the phase of the transmitted signal from the source.

t time

ϕ_{ra}, ϕ_{rb} the phase shift in receiver A and B respectively

ϕ_s the phase shift due to the electrical path length ΔX (figure 1)

$N_a(t)$, $N_b(t)$ random noise terms

The noise terms are due to sources external to the system and also self noise generated in the receivers. This noise exhibits a broad spectrum but is limited by the IF bandwidth (Δf_m) of the receiver. If the bandpass of the receiver is considered to have an ideal rectangular bandpass, then the noise can be treated as bandlimited white noise centered about the IF frequency as shown in figure 2a.

In a well designed system the phase ϕ_{ra} and ϕ_{rb} are made insensitive to temperature and thus can be assumed constant. The transmitter reference phase ϕ is the same for both receivers. It is therefore convenient to lump together the phase angles to give

$$\phi_a = \phi + \phi_{ra} \quad \text{and} \quad \phi_b = \phi + \phi_{rb} - \phi_s$$

The outputs of the receivers can then be rewritten as

$$S_{ma} = A \sin(\omega_m t + \phi_a) + N_a(t) \qquad (3)$$

$$S_{mb} = B \sin(\omega_m t + \phi_b) + N_b(t) \qquad (4)$$

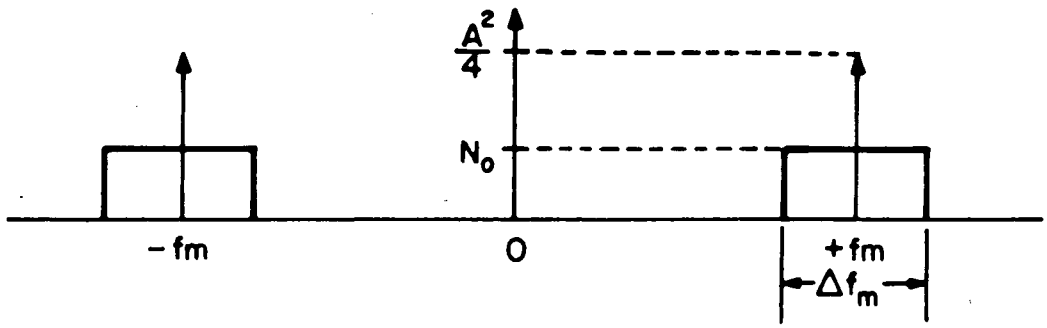

Fig. 2a. Frequency spectrum of the input signals to the multiplier.

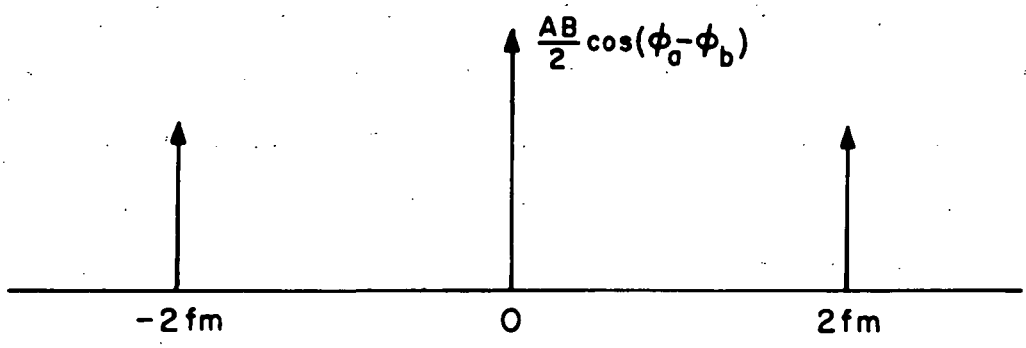

Fig. 2b. Frequency spectrum of the output of the multiplier.

A spectral analysis of these signals is now presented. They are composed of two parts, the deterministic signal from the source and the noise terms which are statistical in nature. Since the inputs of the receivers are identical except for a phase difference, only the 'A' receiver will be analyzed.

Since $N_a(t)$ is considered bandlimited white noise, its power spectrum is

$$\phi_{na}(f) = \begin{cases} N_0 & f_m - \frac{\Delta f_m}{2} < |f| < f_m + \Delta f_m/2 \\ 0 & \text{otherwise} \end{cases} \qquad (5)$$

The autocorrelation function $R_{na}(\tau)$ of this bandlimited white noise can be found through Fourier inversion. [Thomas, 1969.] The integral is given by

$$R_{na}(\tau) = \int_{-f_m+\frac{\Delta f_m}{2}}^{-f_m-\frac{\Delta f_m}{2}} N_0 e^{j2\pi f\tau}\, df + \int_{f_m+\frac{\Delta f_m}{2}}^{f_m-\frac{\Delta f_m}{2}} N_0 e^{j2\pi f\tau}\, df$$

The result of the integration is

$$R_{na}(\tau) = 2\Delta f_m N \frac{\sin \pi \Delta f_m \tau}{\pi \Delta f_m \tau} \cos 2\pi f_m \tau \qquad (6)$$

Since the noise is uncorrelated with the signal, the autocorrelation $R_{aa}(\tau)$ of the source signal is the time average because the signal is deterministic, [Thomas, 1969]

$$R_{aa}(\tau) = \text{AVE}\ \{A \sin(\omega_m t + \phi_a) A \sin(\omega_m (t + \tau) + \phi_a)\} \qquad (7)$$

where AVE represents the time average of the product.

This reduces to

$$R_{aa}(\tau) = \frac{A^2}{2} \cos(\omega_m \tau) \tag{8}$$

Taking the Fourier transform, the power spectral density is

$$\phi_{aa}(f) = \frac{A^2}{4} [\delta(f + f_m) + \delta(f - f_m)]$$

The total spectrum of the IF output which includes both noise and signal components is shown in figure 2a. The signal to noise ratio can be found using the following relation [Lathi, 1968].

$$R = \frac{R_{aa}(0)}{R_{na}(0)} = \frac{A^2}{4\Delta f_m N_0} \tag{9}$$

It is readily apparent the signal to noise ratio of the system can be increased by decreasing the bandwidth of the receiver, but in doing so the high frequency response of the system will suffer.

2.1 Detection By Cross-Correlation Or Multiplication

As shown in figure 1, the two IF signals from receiver A and receiver B are multiplied and then time averaged by the correlator. The correlator output is given by

$$R_{ab} = \text{AVE}\{S_{ma} \cdot S_{mb}\}$$

Performing the multiplication we get

$$M = S_{ma} \cdot S_{mb}$$

$$M = A \sin(\omega_m t + \phi_a) B \sin(\omega_b t + \phi_b) + \text{noise terms} \tag{10}$$

The noise terms are assumed to be uncorrelated, so they will not contribute to the time average of M. Using trigonometric identities this can be expanded to

$$M = \frac{AB}{2}\left\{\cos(\phi_a - \phi_b) - \cos[2\omega_m t + (\phi_a + \phi_b)]\right\} + \text{noise terms} \qquad (11)$$

Taking the Fourier transform, the spectrum of the multiplier output is

$$\phi(f) = \frac{AB}{2}[\delta(f)\cos(\phi_a - \phi_b) + \delta(f + 2f_m) + \delta(f - 2f_m)] + \text{noise terms} \qquad (12)$$

The spectrum is shown in figure 2b. It consists of line components at $\pm 2f_m$ and a DC term proportional to $\frac{AB}{2}\cos(\phi_a - \phi_b)$. The spectral lines are enclosed by a band of noise lying within the receiver bandwidth Δf_m. Since the noise terms are assumed to be uncorrelated, their time average value will be zero. The average value of the sinusoidal signal at $2f_m$ is also zero. Therefore AVE{M}, which represents the correlated output reduces to

$$R_{ab} = \frac{AB}{2}\cos(\phi_a - \phi_b) \qquad (13)$$

All the noise has been assumed to be uncorrelated, but in reality even incoherent noise sources from extra-terrestial sources would also be correlated and would be additive to expression (13). So the multiplier output has a DC term with a value lying within the range $\pm\frac{AB}{2}$ depending upon the value of the cosine term. The only term of interest is this

DC term which is a function of the phase angle $(\phi_a - \phi_b)$. The high frequency terms can be removed from the multiplier output by a low pass filter. This leaves the DC term in the presence of low frequency background noise. The level of this noise can be reduced by narrowing the overall receiver bandwidth.

Let $\phi_s = (\phi_a - \phi_b) + (\phi_{ra} - \phi_{rb})$

$(\phi_{ra} - \phi_{rb})$ is constant and can be neglected without a loss of generality. Therefore let

$$\phi_s = (\phi_a - \phi_b)$$

ϕ_s is the phase difference between the two signals arriving at the two receivers; given that the phase shifts introduced into the signals by the passive elements in the receivers and by the phase differences of the local oscillators remain fixed.

2.2 Spatial Response of the System

The angle ϕ_s can now be related to the geometry of the system. Assume the antennas are located on an east-west baseline of length L shown in figure 3. The source is in the west at an elevation angle of θ degrees. If the point source is far away, the rays appearing at the antenna sites can be assumed to be parallel. The electrical path length ΔX therefore represents the phase difference ϕ_s. From the geometry $\Delta X = L \cos\theta$ and $\phi_s = 2\pi\Delta X/\lambda_0$ where $\lambda_0 = c/f_0$.

Therefore

$$\phi_s = \frac{2\pi f_0 L \cos(\theta)}{c} \qquad (14)$$

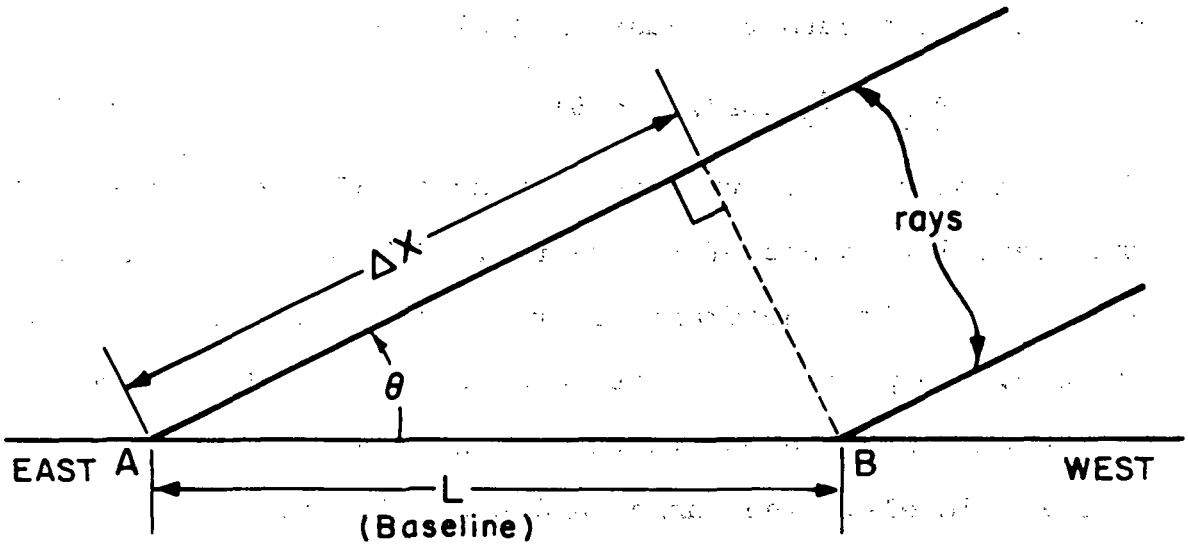

Fig. 3. The geometry of the interferometer system.

ϕ_s is a function of the baseline L, the input frequency, and elevation angle of the source. If the baseline is expressed in terms of multiple wavelengths, $L = N\lambda_0$ where N is the number of wavelengths. Equation (13) reduces to

$$\phi_s = 2\pi N\cos\theta$$

By substituting the above relation into the expression for the correlated output, equation (13), we get

$$R_{AB} = \frac{AB}{2}\cos(2\pi N\cos\theta) \qquad (15)$$

The plot of this function as a function of θ will represent the spatial response of the system. Figure 4 is a sample plot in the first quadrant for the case of $L = 2\lambda_0$. As can be seen, the pattern exhibits a succession of lobes. The lobe width is a minimum in the vicinity of 90° and increases at lower levels. The number and size of these lobes are dependent on the site separation L. The number of lobes in each quadrant will be 2N, where N is the baseline in wavelengths. As the baseline increases, the system becomes very sensitive to small changes in the elevation angle θ. Thus the system adapts well to the accurate tracking and location of R.F. sources. An R.F. source passing through this spatial antenna pattern produces D.C. fluctuations at the output of the correlator between $+\frac{AB}{2}$ and $-\frac{AB}{2}$. This fluctuating output is known as fringing.

It should be noted that the direction of motion of the source through the antenna pattern affects the fringe rate of the output. This is clearly seen when viewing a three

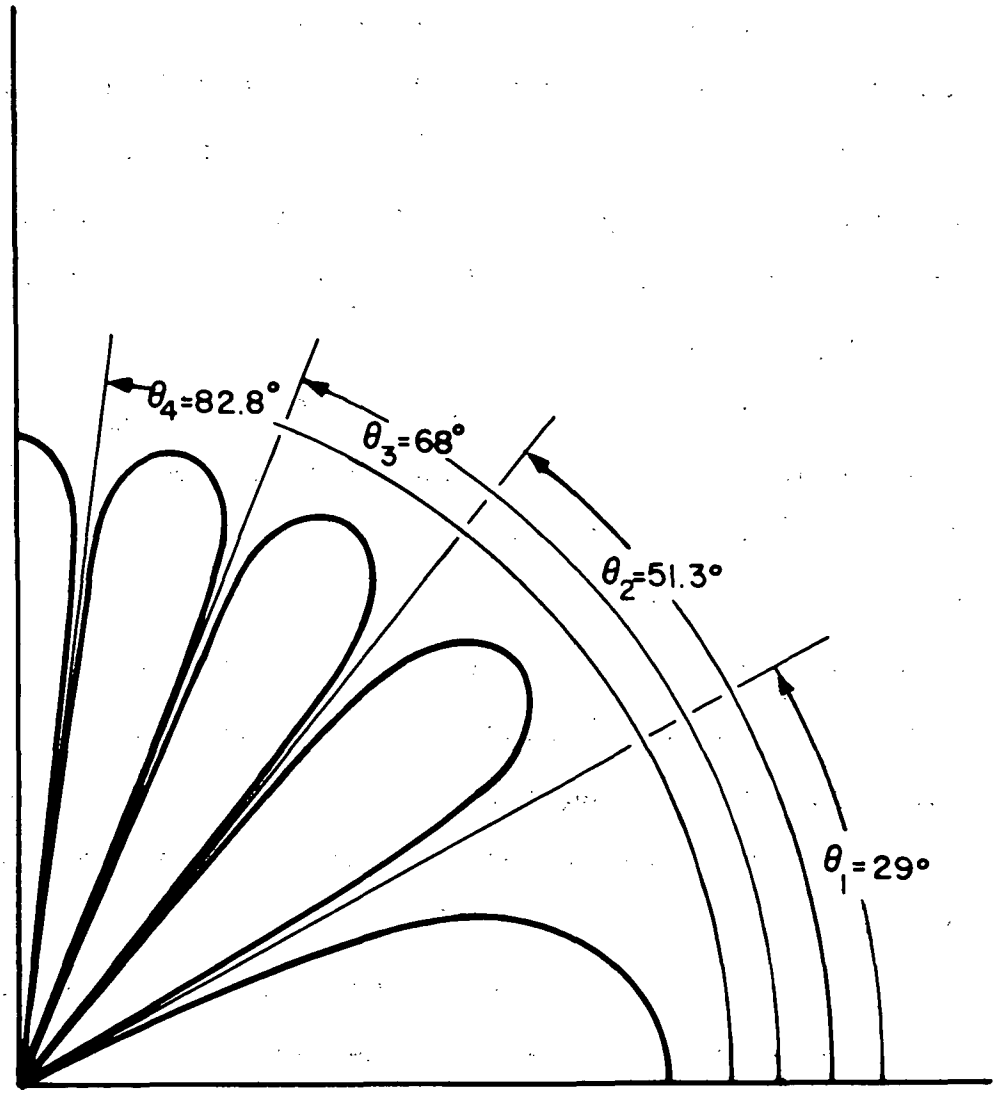

Fig. 4. The spatial response of the antenna pattern in the first quadrant for the case $N = 2\lambda_0$. θ_1, θ_2, θ_3, θ_4 represent the null points in the pattern.

dimensional portion of the antenna pattern generated with omni-directional antennas shown in figure 5. This fan beam structure is viewed end-on in figure 6. A source moving in direction 'a' would produce a maximum fringe rate whereas a source moving in the direction 'c' would produce a very slow fringe rate. Therefore the interferometer we have been describing is insensitive to the motion of a source in a direction which is perpendicular to the baseline.

2.3 Frequency Offset

The direct multiplication of S_{ma} and S_{mb} described in the previous section has been shown to contain both the desired correlated DC output and the undesired noise. It is noted from figure 2b that the desired DC output is embedded in a band of noise about the zero frequency point. Unless the signal to noise ratio is high, a substantial amount of filtering will be required and the systems ability to respond to rapid amplitude or phase changes of the input signal will be impared.

In order to increase the selectivity necessary for a good signal to noise ratio while still retaining the overall bandwidth required to pass information, a system using frequency offset and phase detectors can be used [Clark and Frost, 1967]. The block diagram of such a system is shown in figure 7. The local oscillator of one receiver is offset from the other receiver by a small amount Δf. The outputs of the two receivers now become

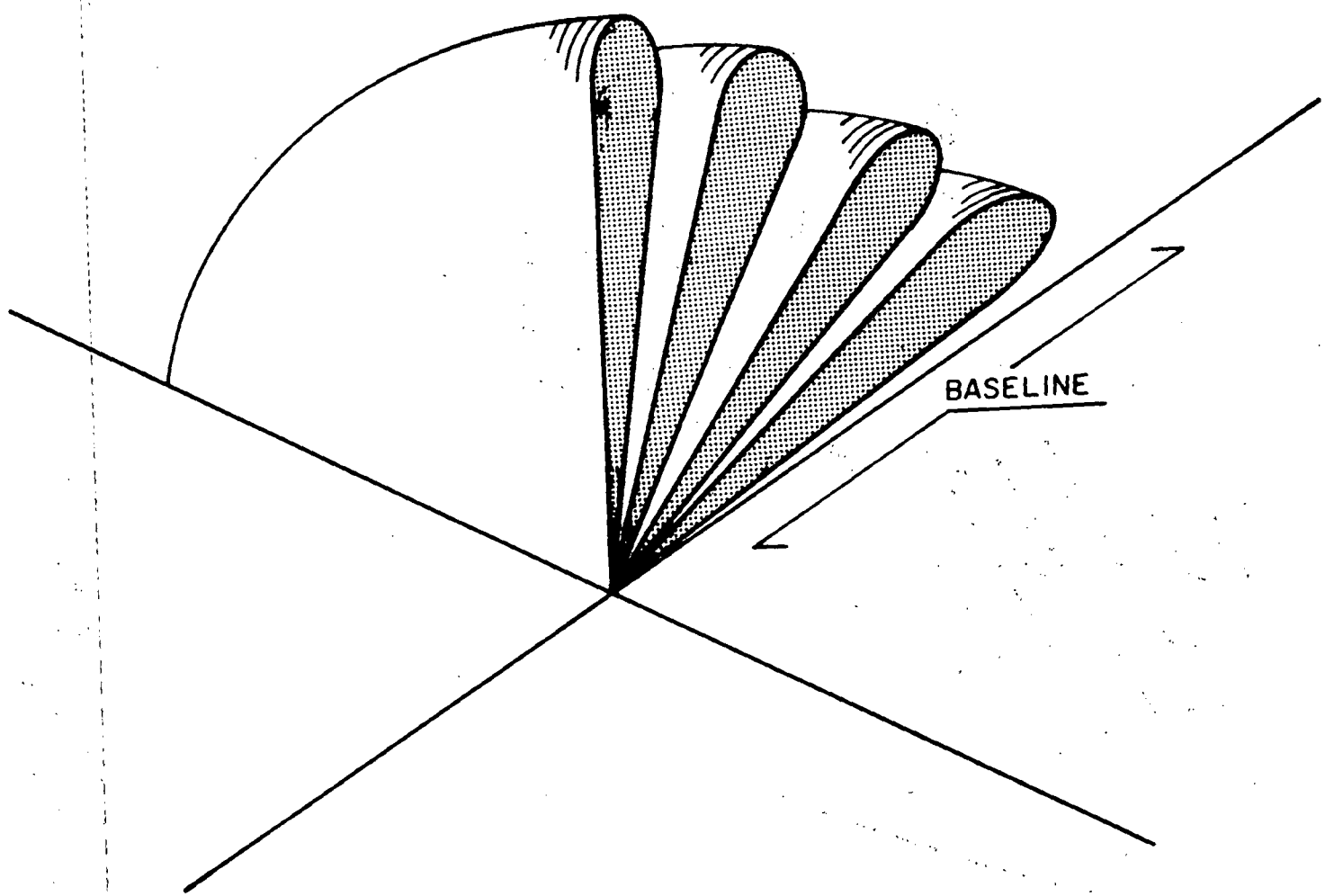

Fig. 5. Perspective view of a portion of the antenna pattern. [Clark, R. R. and Frost, A. D., Fig. 10, 1967].

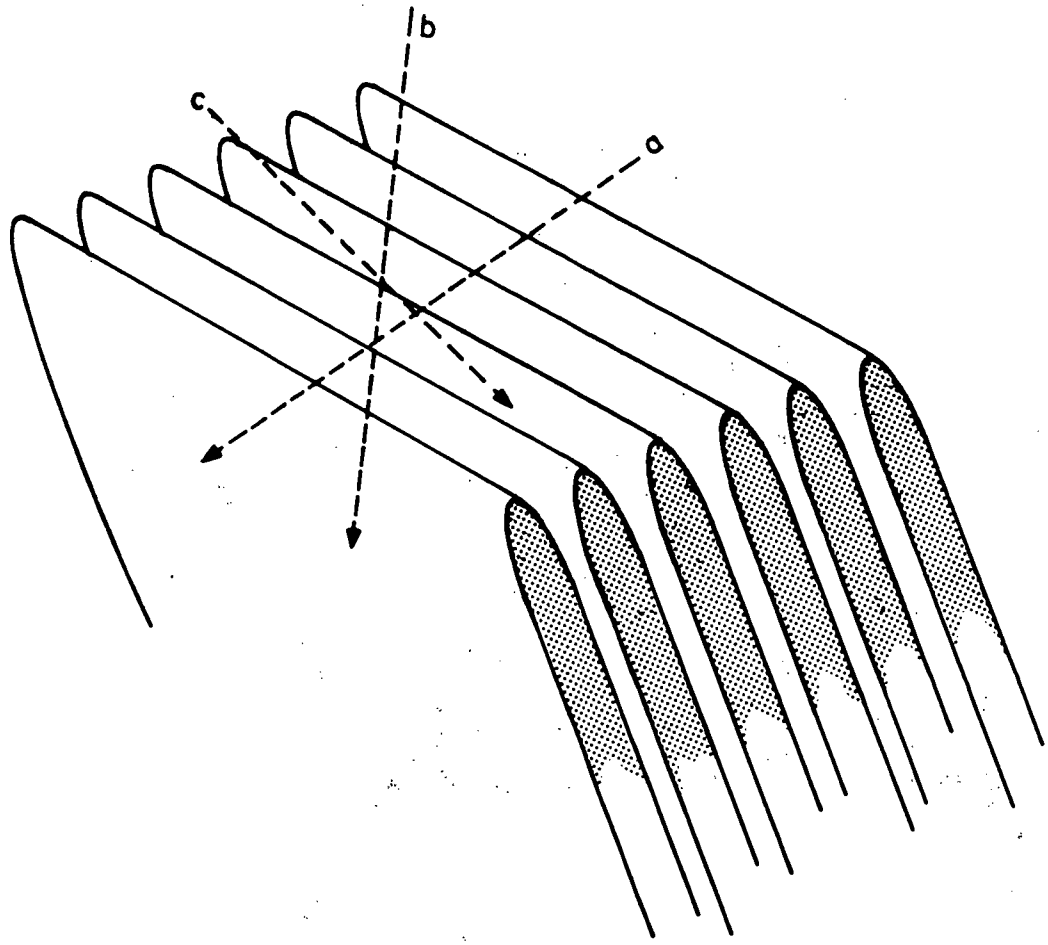

Fig. 6. End view representation of an interferometer antenna pattern. [Clark, R. R. and Frost, A. D., Fig. 11, 1967].

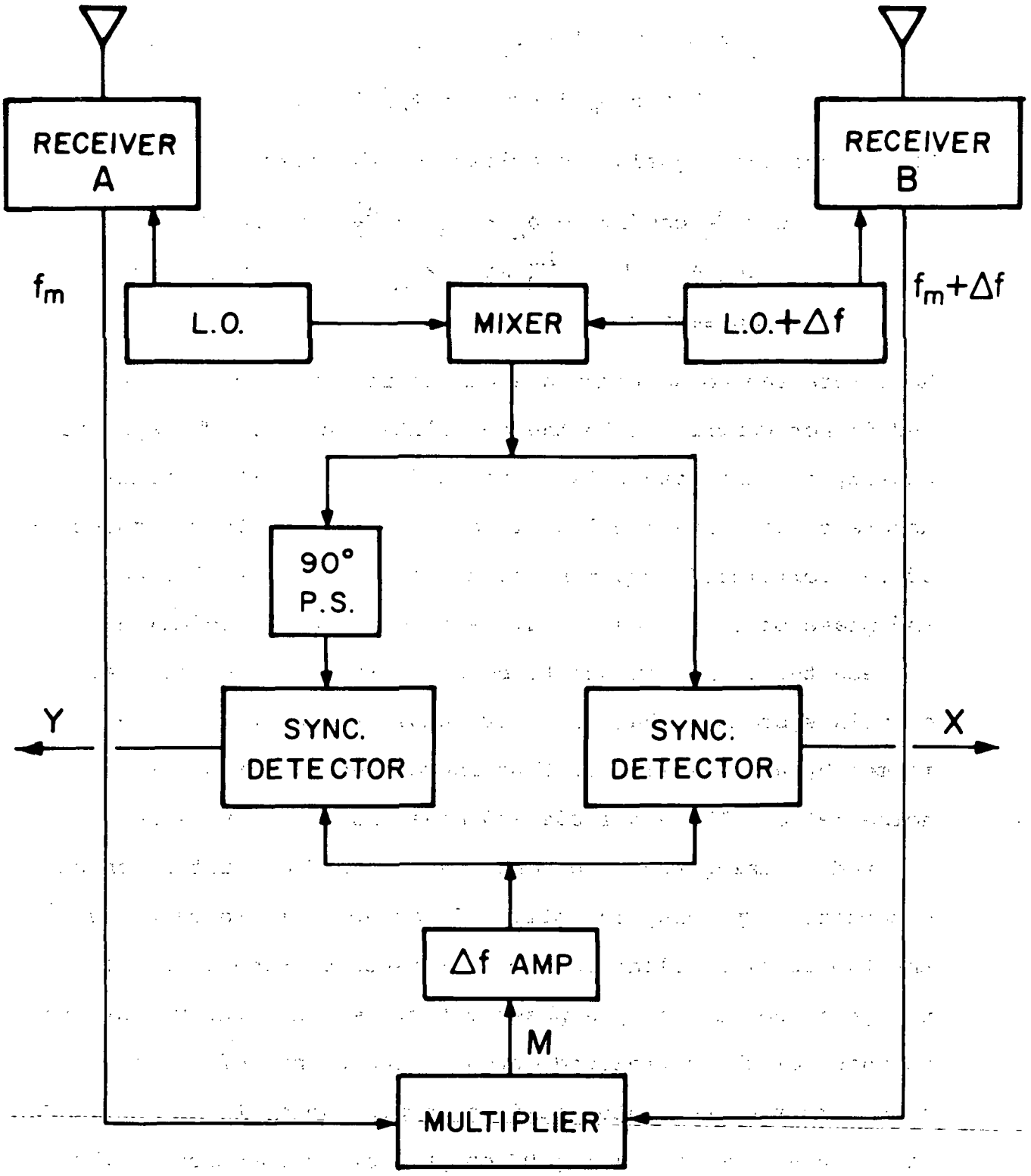

Fig. 7. Block diagram of a simple interferometer using frequency off-set and synchronous detection.

$$S_{ma} = A \sin(\omega_m t + \phi_a) + N_a(t) \qquad (16)$$

$$S_{mb} = B \sin((\omega_m + \Delta\omega) t + \phi_b) + N_b(t)$$

When these two signals are multiplied the result is

$$M = \frac{AB}{2} \cos(\Delta\omega t + \phi_a - \phi_b) - \frac{AB}{2} \cos[(2\omega_m + \Delta\omega)t \cos(\phi_a + \phi_b)] + \frac{AB}{2} \sin[(2_m + \Delta\omega)t \sin(\phi_a - \phi_b)] + \text{noise terms}$$

As before the noise terms are considered to be uncorrelated and do not contribute to the correlated output. The spectral density of this result is given in figure 8. It is readily apparent that this local oscillator offset shifts the spectrum of the correlated output by an amount Δf. The amplitude and phase of the signal at Δf represents the correlation between the signal inputs to both receivers. The advantage of this system is that selective amplication can be performed by a Δf amplifier, thus increasing the signal to noise ratio. The amplitude and phase information is recovered by using two synchronously switched quadrature phase detectors. By using the offset frequency difference between the two local oscillators as a reference driving signal to the phase detectors, the phase detectors track the variations in phase of the correlated output. The output of the phase detectors are then integrated to remove the switching transients. The resulting DC outputs are a function of the phase shift between the incoming signals to the two receivers. They are also a function of the phase angle between the

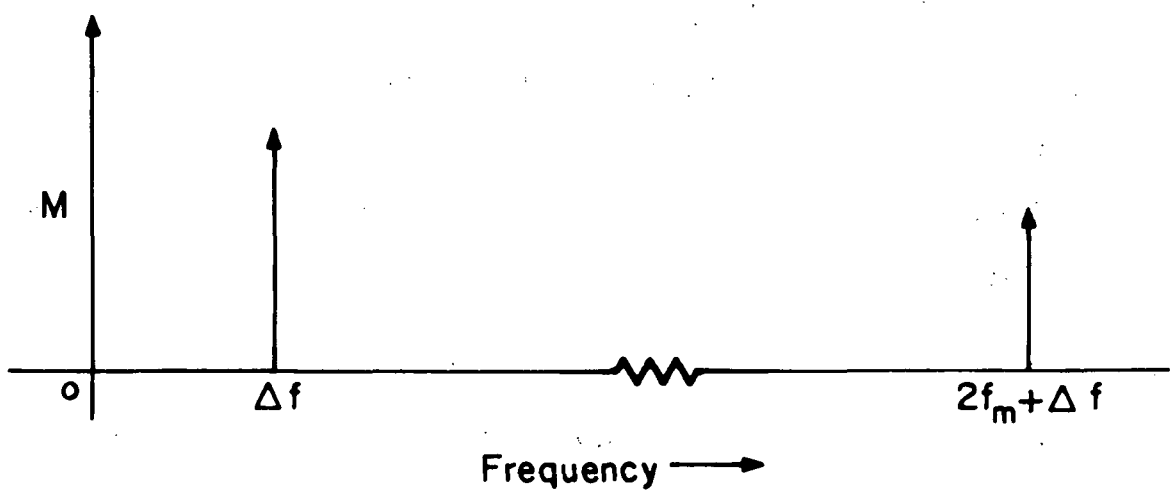

Fig. 8. Frequency spectrum of the multiplier output using off-set frequency.

reference Δf and the correlated components, and the product of the amplitudes of S_{ma} and S_{mb}. If ϕ_D is the phase difference between the Δf reference and the correlated Δf, then the output of one of the phase detectors can be represented by:

$$D = \frac{AB}{2} \cos \phi_D \tag{17}$$

If A equals B, D is proportional to the power of the received signal.

When the reference Δf is shifted by 90°, it adds directly to ϕ_D so that

$$D = \frac{AB}{2} \cos(\phi_D + 90) = \frac{AB}{2} \sin(\phi_D) \tag{18}$$

The X and Y outputs of the quadrature phase detectors shown in figure 7 represent the sine and cosine components of the correlated signal [Clark and Frost, 1969a].

3. APPLICATIONS

Interferometers have found extensive use in the field of radio astronomy in determining the size and locations of radio sources in space. They have also been used to investigate disturbances in the ionosphere. The introduction of synchronous satellites has enhanced the usefulness of the interferometer, because they represent a known, fixed source. An ideal synchronous satellite presents a relatively stationary RF source, so that fringing is due to a change in ray path length rather than a change in the satellite position. This difference in ray path length can be related to the difference in the electron content in the ionosphere. Thus disturbances in the electron content of the ionosphere are detected as fringing by the interferometer [Sherrill, 1971]. The actual geostationary satellite does move slightly during the day and repeats itself every 24 hours. This slow movement causes a slow fringe rate which is predictable and can be eliminated from the data.

The short baseline system described in the following section was specifically designed to detect ionospheric disturbances by monitoring the telemetry signal frequencies of the Application Technology Satellite (ATS) series satellites.

4. SHORT BASELINE SYSTEM

The block diagram of the base station configuration is shown in figure 9. Two IF conversions are performed on the 137.35 MHz incoming signal. The first IF down conversion is to 32 MHz. This is accomplished by generating a first local oscillator signal of 105.35 MHz. A phase-locked loop which is locked to the system synthesizer output is used in order to maintain frequency coherence and spectral purity of the local oscillator within the bandwidth of the receivers. The frequency synthesizer output is multiplied by four to approximately 35 MHz. This is phase compared with the 35 MHz from the voltage controlled oscillator (VCO). The output from the phase detector acts as a DC control voltage to lock the VCO to the synthesizer. The subsequent multiplication by 3 to 105.35 MHz does not generate harmonics within the receiver bandwidth.

The second IF down conversion is to 2 MHz. This is accomplished by generating a 30 MHz local oscillator. Since the system uses the principle of frequency off-set, as discussed previously in this work, the second local oscillator (LO) for the base station is off-set by 1 KHz. Therefore the actual second LO for the base station is 30.001 MHz, and the second LO for the out station is 30 MHz. The synthesizer has a coherent 30 MHz output, and this is used directly for the out station, however, the base station second LO must be generated. This is again accomplished through the use of

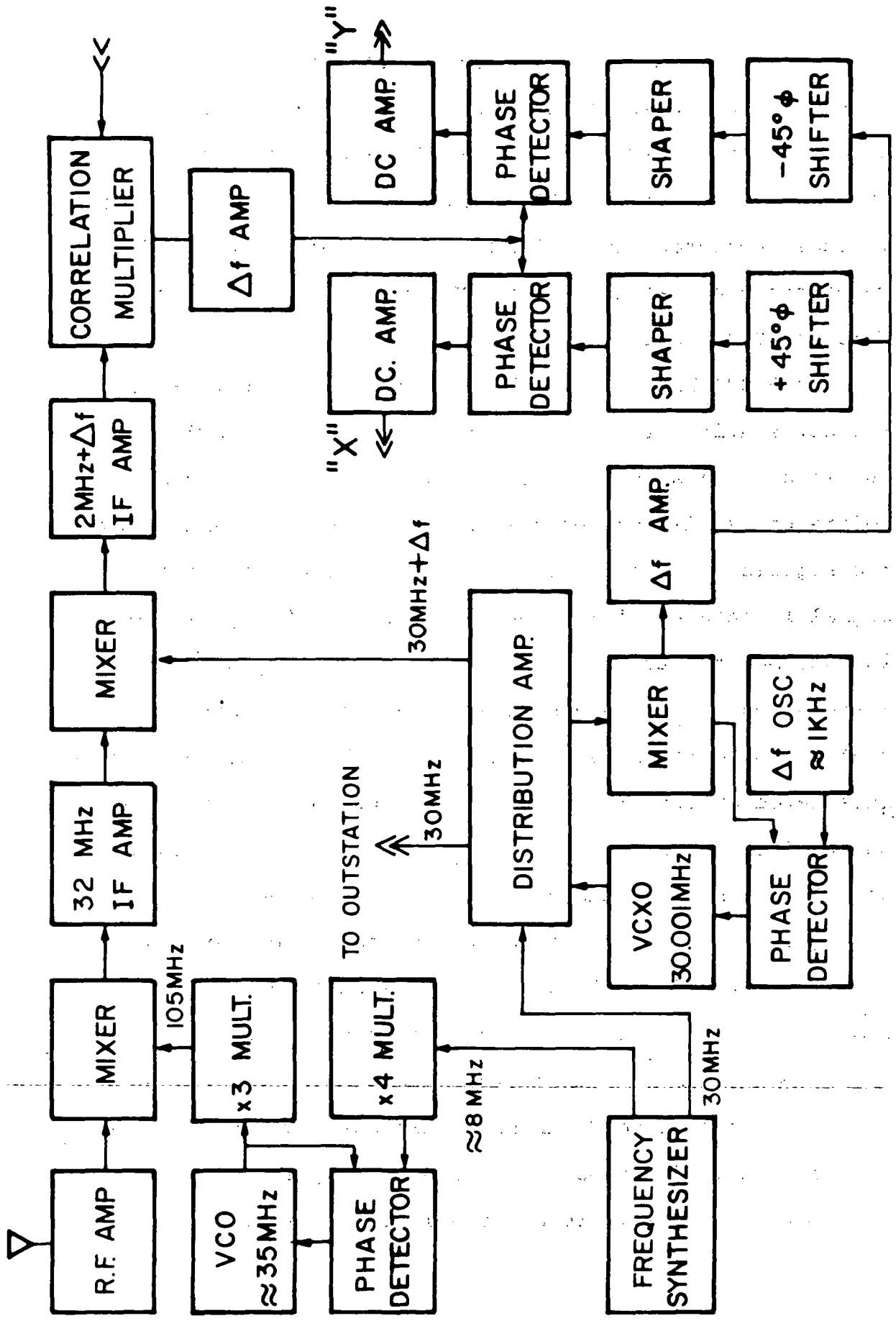

Fig. 9. Block diagram for the base station of the short baseline interferometer.

a phase locked loop in order to maintain system coherence. A voltage controlled crytal oscillator (VCXO) running at 30.001 MHz is mixed with the 30 MHz reference from the frequency synthesizer. The resulting 1 KHz from the mixer is phase compared with a 1 KHz signal from a stable Δf reference oscillator, and the DC output is used to lock the VCXO to 30.001 MHz.

The 2.001 MHz from the base station and the 2 MHz from the out station are cross-correlated, and the resulting output is a 1 KHz signal whose phase with respect to the Δf reference oscillator represents the phase difference between the signals arriving at the two spaced receiver sites. This signal is then amplified and processed. A 90° phase splitter is incorporated to separate the correlated outputs by 90°. Shapers convert the sinusoidal 1 KHz signal to square waves that are used to drive the quadrature phase detectors. The integrated output of the phase detectors have a linear DC output from 0° to 360°. The DC outputs of the two phase detectors represent the phase difference between the incoming signals at the two antenna sites. Two channels of output separated by 90° are incorporated to alleviate the problem of dead time in the phase detectors. Phase detector dead time will not occur at the same time in both channels thus the output record can be continuous. These two phase detector outputs are passed through DC amplifiers, and the outputs of DC amplifiers are available for suitable recording.

The out station shown in figure 10 is similar to the base station. The receivers are identical and the first LO generation is identical. Since the second LO has no offset, it is fed directly from the 30 MHz distribution amplifier.

The initial set up of the system will be short baseline and both receivers will be situated at the same location, so there is no problem maintaining coherence between the two stations. If at some future time the baseline is extended and there is a need to separate the base station and out station receivers, then it will be necessary to lock the local oscillators to a common source or lock them via a microwave link.

4.1 Synthesizer and Receivers

The interferometer system is designed around a Hewlett Packard 5103A frequency synthesizer as our frequency standard. This instrument can be programmed to generate frequencies from 1 KHz to 1 MHz in .1 Hz steps and from 1 MHz to 10 MHz in 1 Hz steps. There is also a 30 MHz output available at the rear panel. In this particular case the synthesizer output is selected to be 8.779166 MHz.

The RF converters and IF strips are commercially available units. The RF converters are Tapetone TC-137 Low Noise Converters. They are tuned to 137.35 MHz. This is one of the telemetry signal frequencies of the application technology Satellite (ATS) series. They have a power gain of approx-

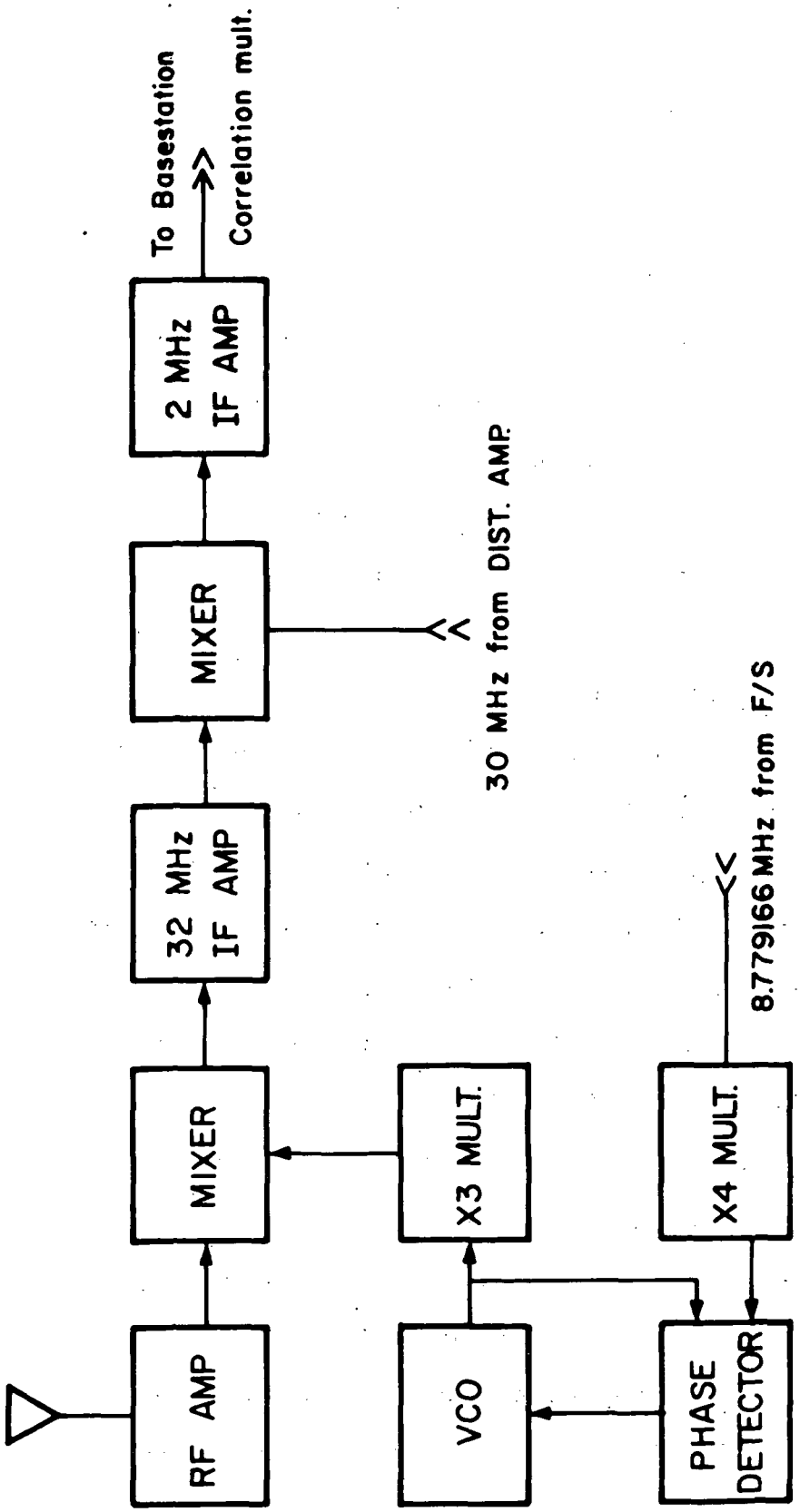

Fig. 10. Block diagram for the out station of the short baseline interferometer.

imately 35 db, and a 3 db bandwidth of 600 KC, with a noise figure of about 4db.

The first IF amplifiers are tuned to 32 MHz and are synchronously tuned units with mixers at their outputs to convert from 32 MHz to a second IF of 2 MHz. Their overall bandwidths are 250 KHz. The local oscillator injection voltages at 30 MHz of 0.4 to 0.9 volts rms required for mixing are obtained from the distribution amplifiers. The overall gain of the 32 MHz IF's is 80 db when terminated into a 50 ohm load.

The second IF amplifiers are synchronously tuned to 2 MHz and have crystal filters with bandwidths of 3.1 KHz at the -6db points. The overall gain of these IF's are 50 db. The gain of each receiver is adjusted by a manual gain control in the 32 MHz IF Amplifiers.

Identical units are used in both the base station and the out station as shown on the block diagrams. The above described units use vacuum tube devices and thus require filament (6.3 vac) and plate voltage (+150 VDC). Two separate, regulated power supplies are used for the base station and the out station.

4.2 First Local Oscillator Generation

Since the received signal is at 137.35 MHz, and the first IF is 32 MHz, the first LO to be generated is 105.35 MHz. To minimize spurious and unwanted harmonic components and still maintain phase coherence with the synthesizer,

a phase-locked oscillator was chosen. The generation of the 105.35 MHz can be subdivided into three sections, a phase-locked loop, a X4 multiplier, and a X3 multiplier as shown in figure 11.

The X4 Multiplier shown in figure 12 consists of a doubler, a buffer amplifier, and a second doubler followed by a low Q tuned amplifier. The bandwidth of the overall stage is 5 MHz to allow for changes in the synthesizer frequency. The doublers, M1 and M2, are double balanced mixers and are shown in figure 13. The oscillator section is shown in figure 14 and is a tuned gate FET oscillator [Clark and Frost, 1969b]. The gate circuit is tuned by controlling the voltage across a varactor diode. The oscillator is followed by a buffer amplifier which drives the X3 multiplier and the phase detector. The phase detector shown in figure 15 uses an N-channel FET as a chopping circuit [Clark and Frost, 1969b.] The VCO output drives the gate of the FET as a switch. The diode from gate to ground bypasses any positive excursions. The output of the X4 multiplier is applied to the source lead. Its output is filtered and the DC control voltage is applied to the varacter diode in the VCO.

The phase-locked signal generated by the VCO is also coupled to the X3 multiplier shown in figure 16. The output of the X3 multiplier is the desired first LO at 105.35 MHz. The 35.11666 MHz signal from the VCO is applied to the base-

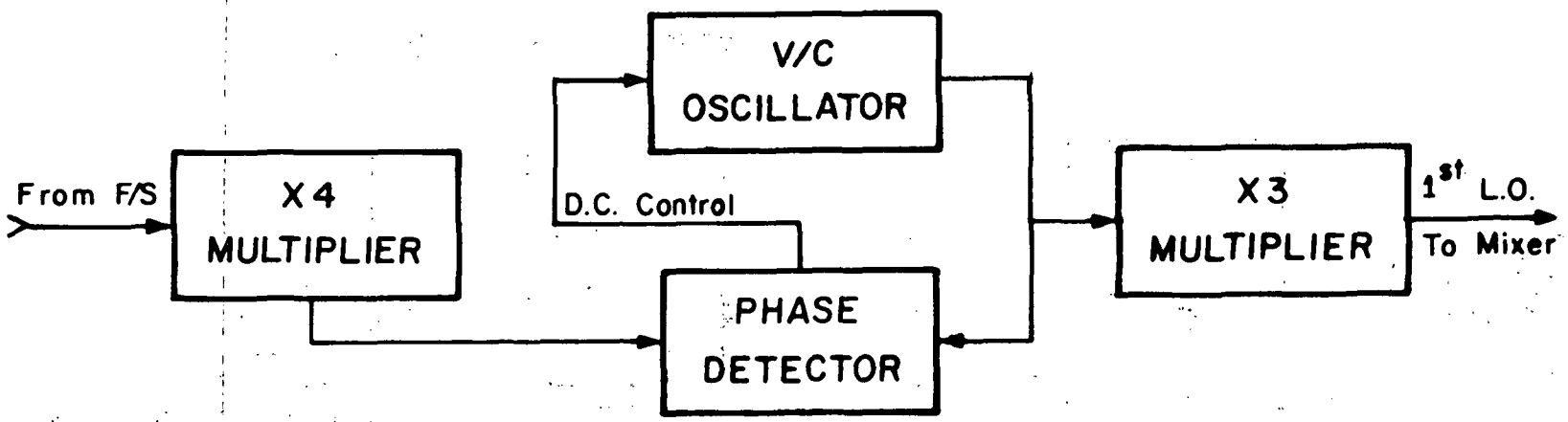

Fig. 11. Block diagram for generation of the first local oscillator.

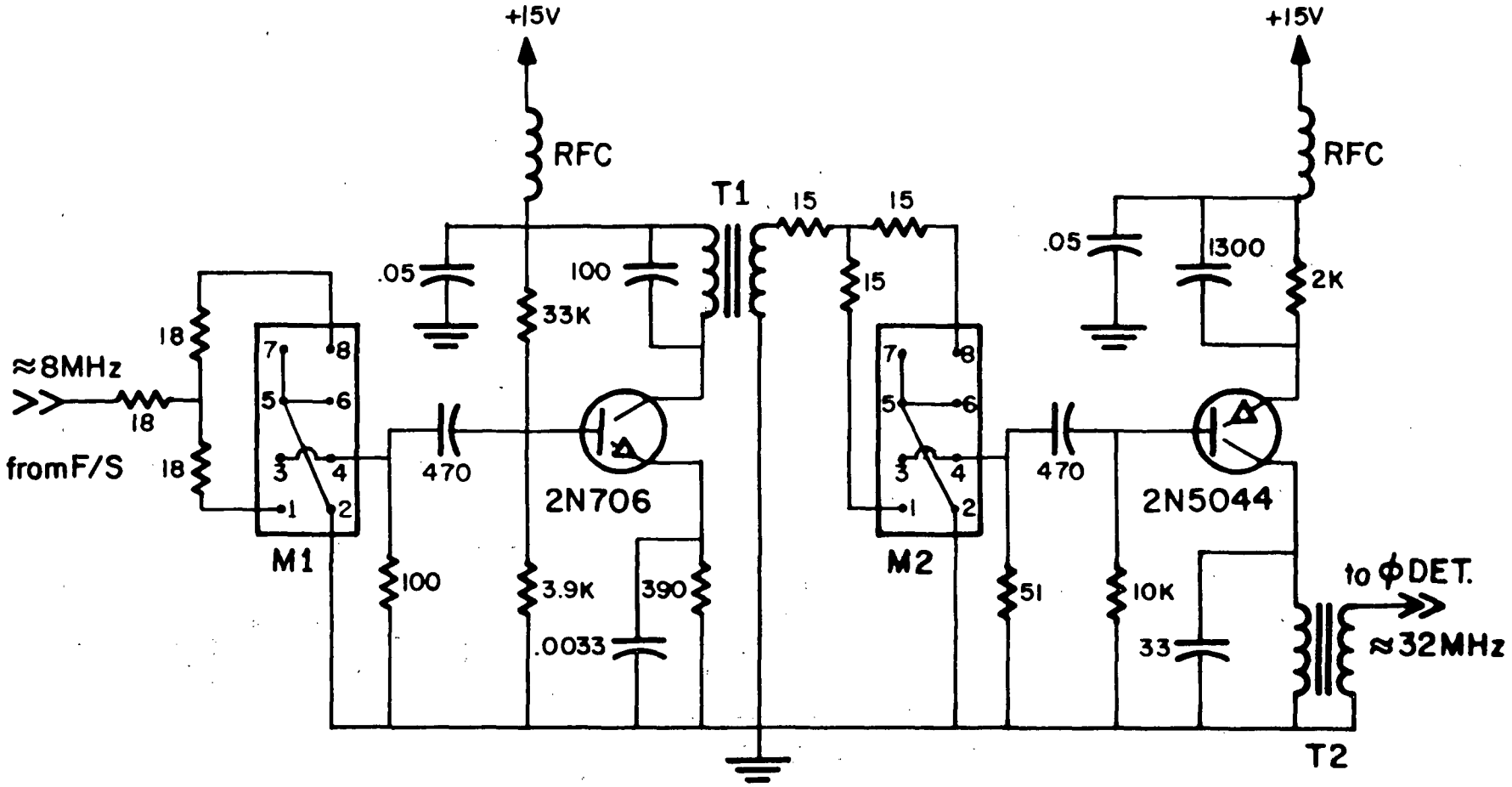

Fig. 12. Schematic diagram of the X4 multiplier.

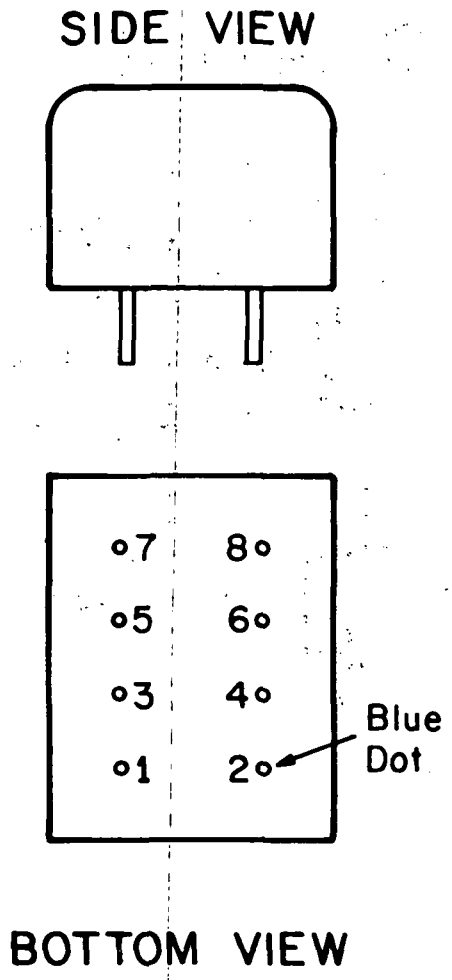

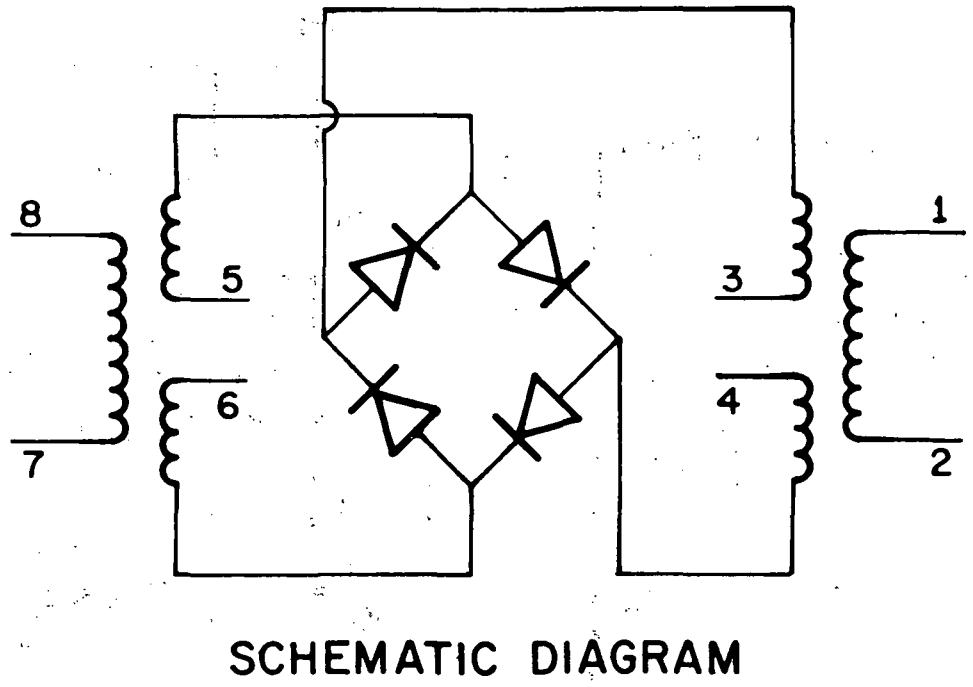

Fig. 13. MCL Model SRA-1 double balanced mixer.

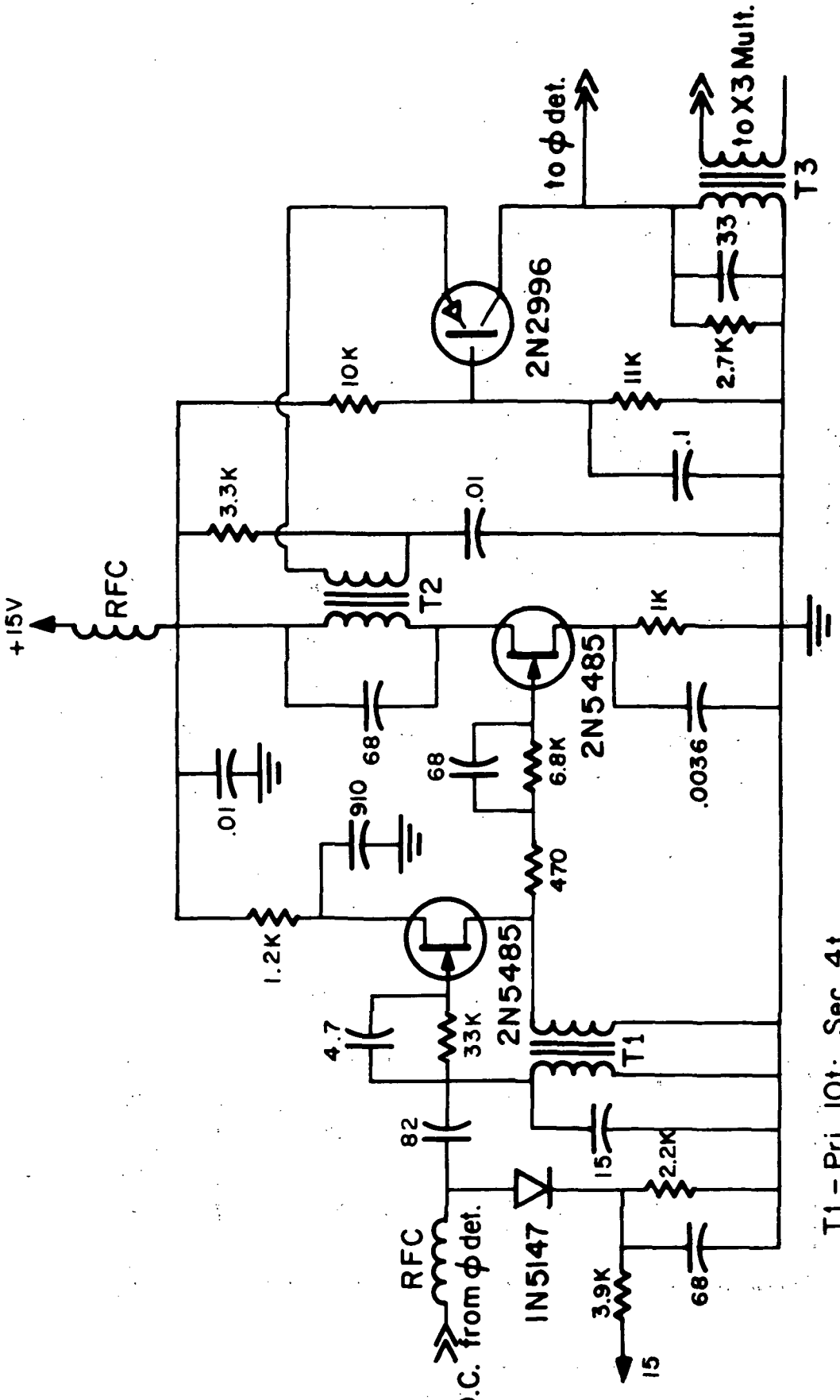

Fig. 14. First LO voltage controlled oscillator.

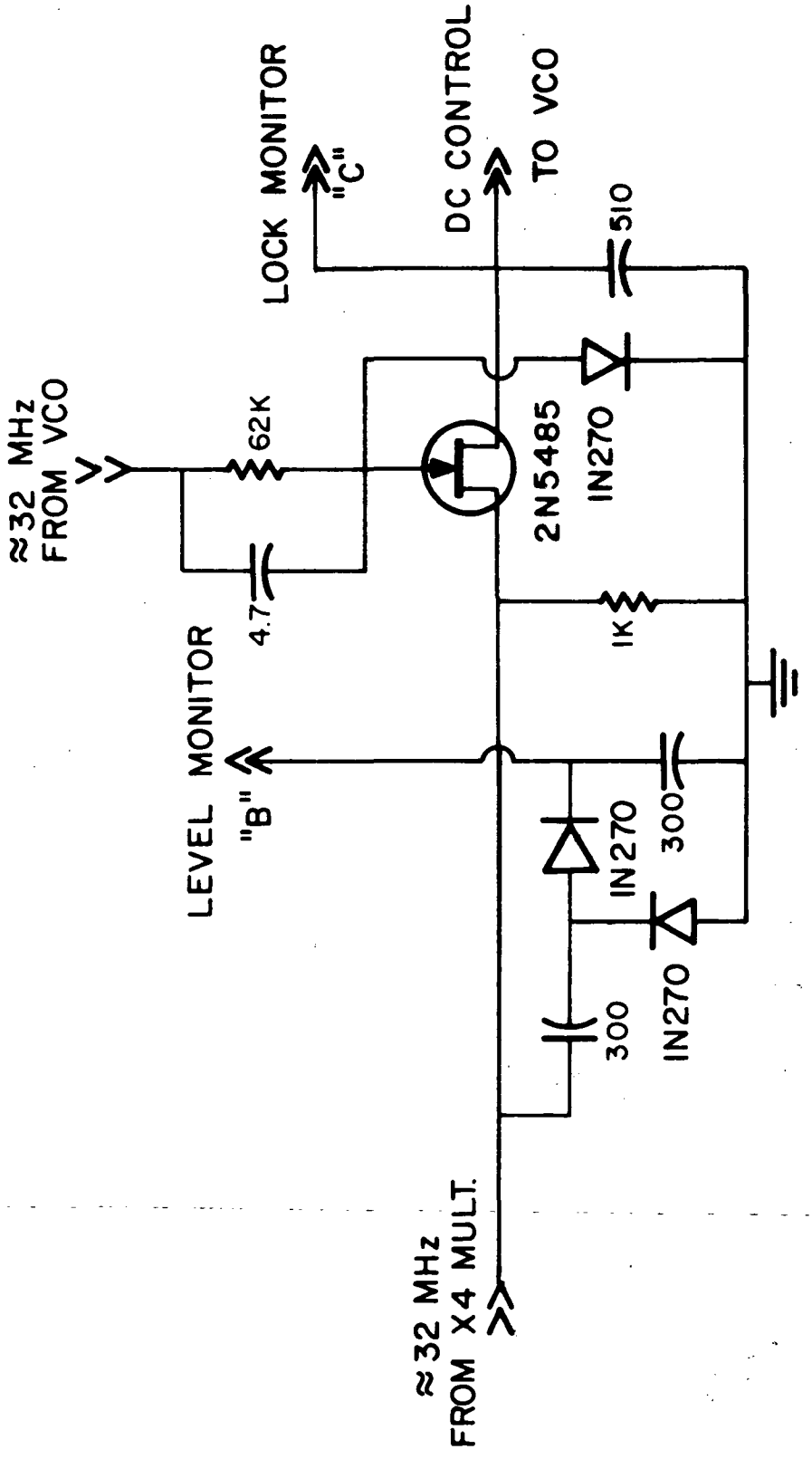

Fig. 15. Phase detector for the 1st LO phase-locked loop.

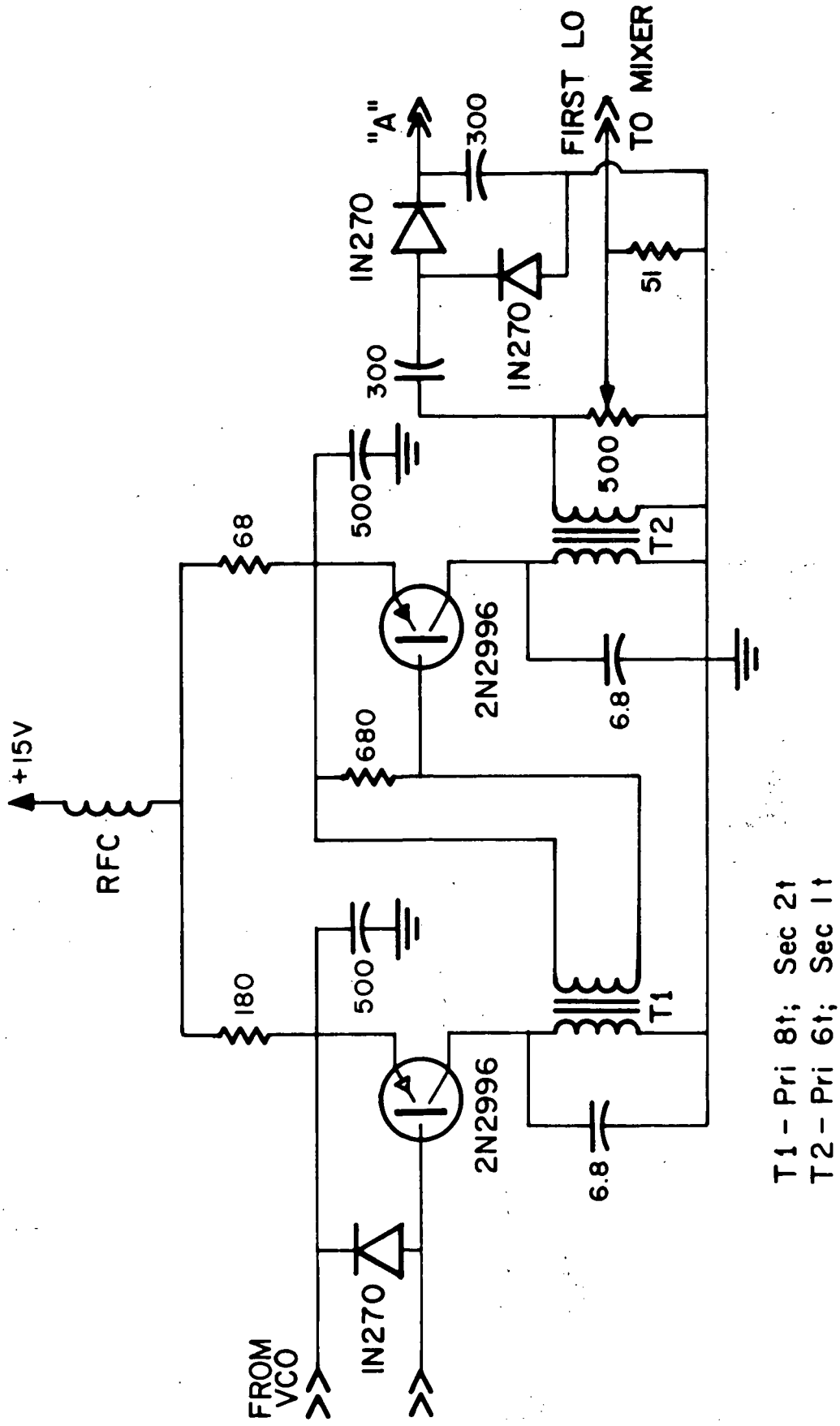

Fig. 16. X3 multiplier.

emitter junction of the transistor, which is baised in the nonlinear portion of its characteristic curve. The tank in the collector circuit is tuned to the third harmonic (105.35 MHz). A second stage of amplification follows and the output is matched to 50 ohms to match the mixer input on the RF converter. A level adjust is included at the output to set the injection level for optimum mixing. The output can be adjusted from 0 to 1.2 volts rms.

The lock range of the loop is about 500 KHz. The curve in figure 17 indicates the characteristics of the VCO. The oscillator has been tuned for a center frequency of 35.11666 MHz as shown on the curve.

The first LO can be changed quite simply to accept a wide range of input frequencies. It is a simple matter of changing the frequency setting on the front panel of the synthesizer. The LO frequency will be the synthesizer output multiplied by twelve. The LO will remain locked so long as the frequency change is within the 500 KHz lock range of the loop. If it is desired to move the LO outside this lock range, it can be accomplished by retuning the VCO, so that the center frequency of the lock range is at the new desired LO. This is realized by setting the synthesizer frequency to the desired setting and then varying the tuning slug of T1 of the VCO for a zero DC control voltage. The PLL still retains its 500 KHz lock range about the new center frequency. This first LO unit is supplied by a regulated

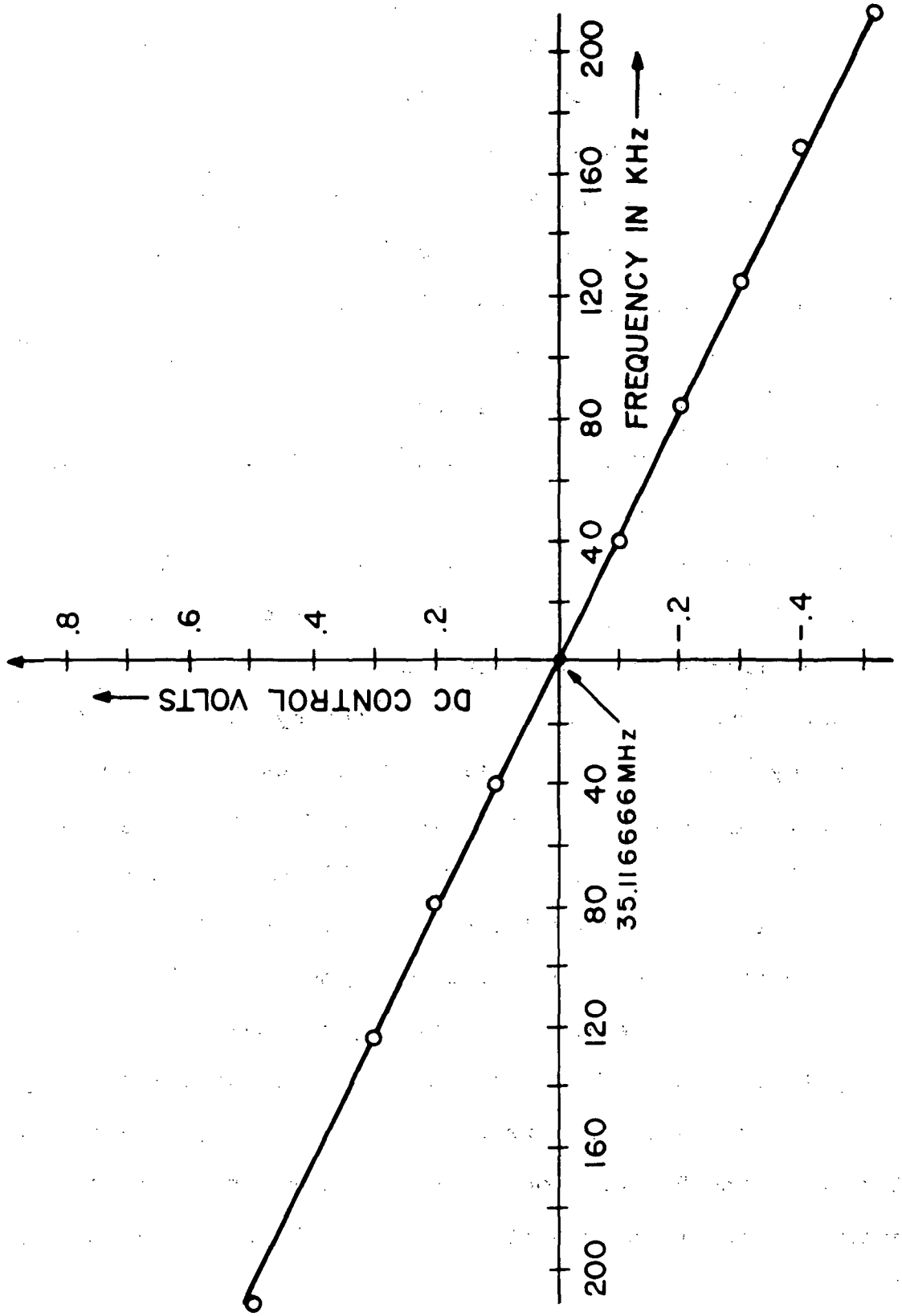

Fig. 17. DC control vs. frequency for the VCO.

+15 volt power supply.

To facilitate operational and maintenance checks, a metering circuit is provided to check the RF level from the X4 multiplier and the X3 multiplier. A metering check for an unlocked condition is also provided for this unit. The metering schematic is shown in figure 18.

4.3 Second Local Oscillator Generation

The second IF conversion is from 32 MHz down to 2 MHz. The block diagram for the generation of the second local oscillator is given in figure 19. The second conversion like the first, just maintain frequency and phase coherence with the overall system. The HP-5103A frequency synthesizer has a 30 MHz output on the rear panel of the instrument. For the out station no further signal processing is needed and the 30 MHz is fed directly to the out station via the distribution amplifier for use as the second local oscillator.

The afore discussed offset frequency (Δf) is injected into the system by offsetting the second LO at the base station by 1000 Hz with respect to the out station. This is accomplished by again using a phase-locked loop configuration.

The VCXO used in the loop, shown in figure 20 is a common base configuration and utilizes crystal controlled feedback on the emitter. A varactor diode in series with the crystal is used to control the frequency of the oscil-

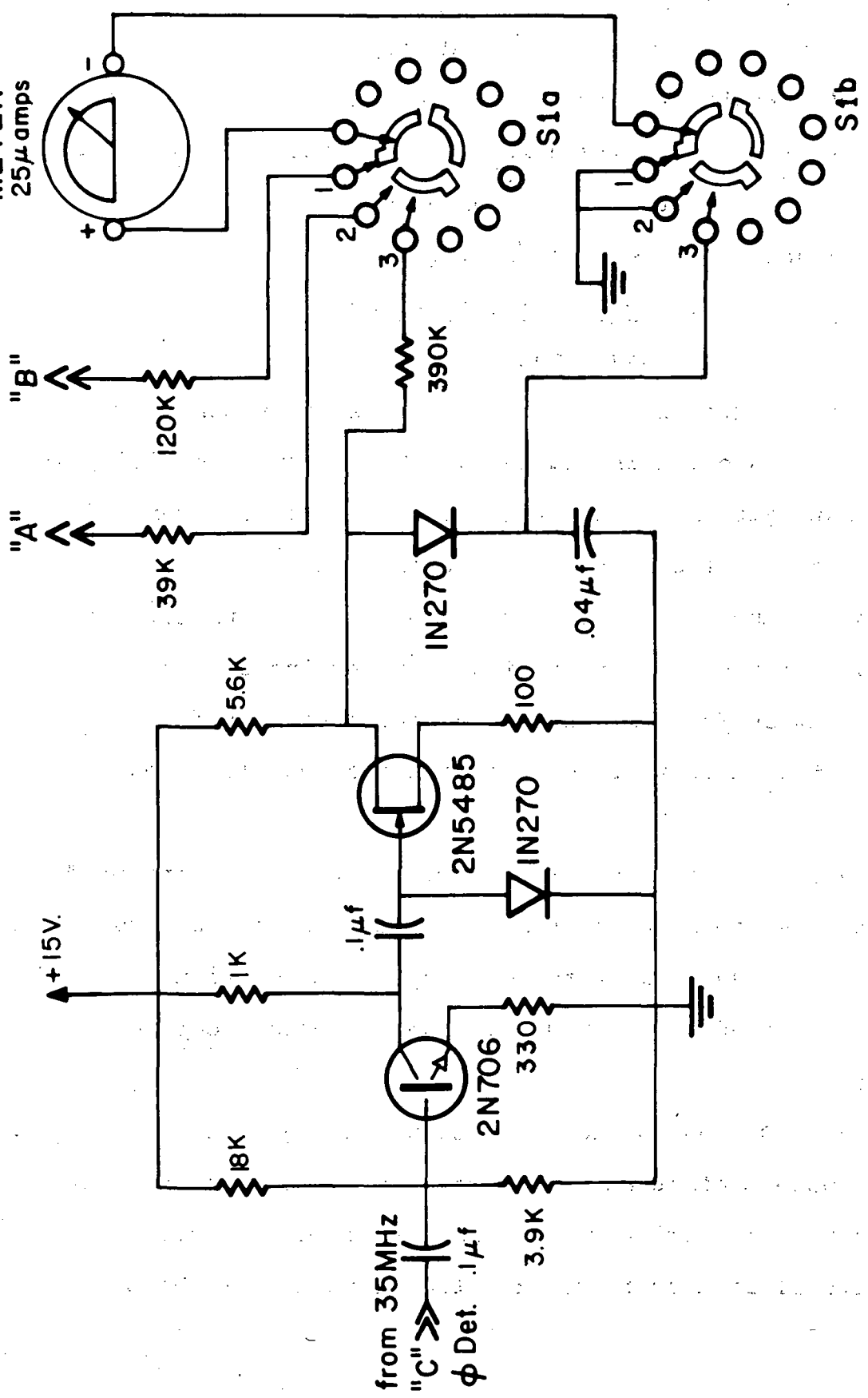

Fig. 18. Monitoring schematic diagram.

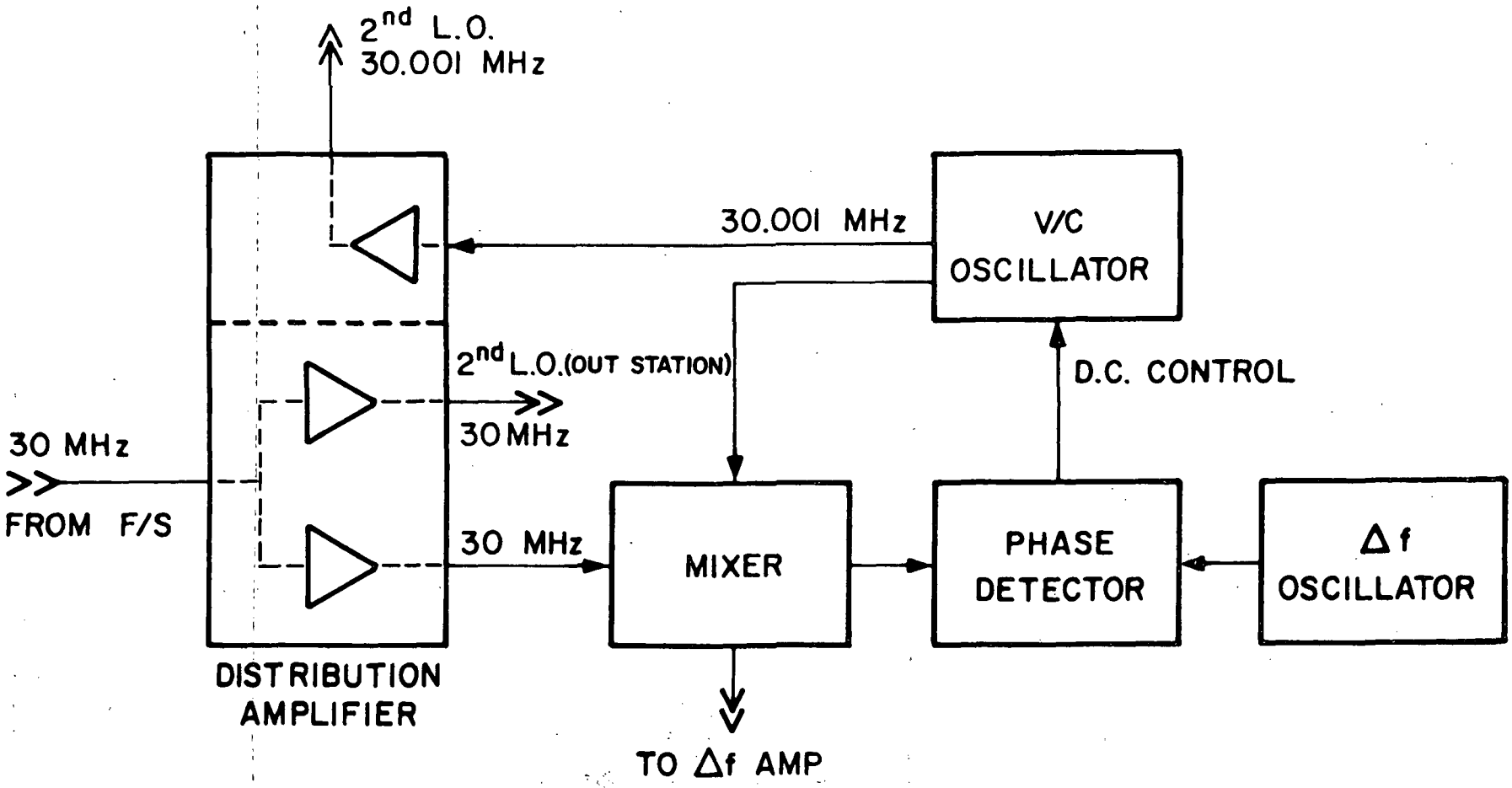

Fig. 19. Block diagram for the second local oscillator generation.

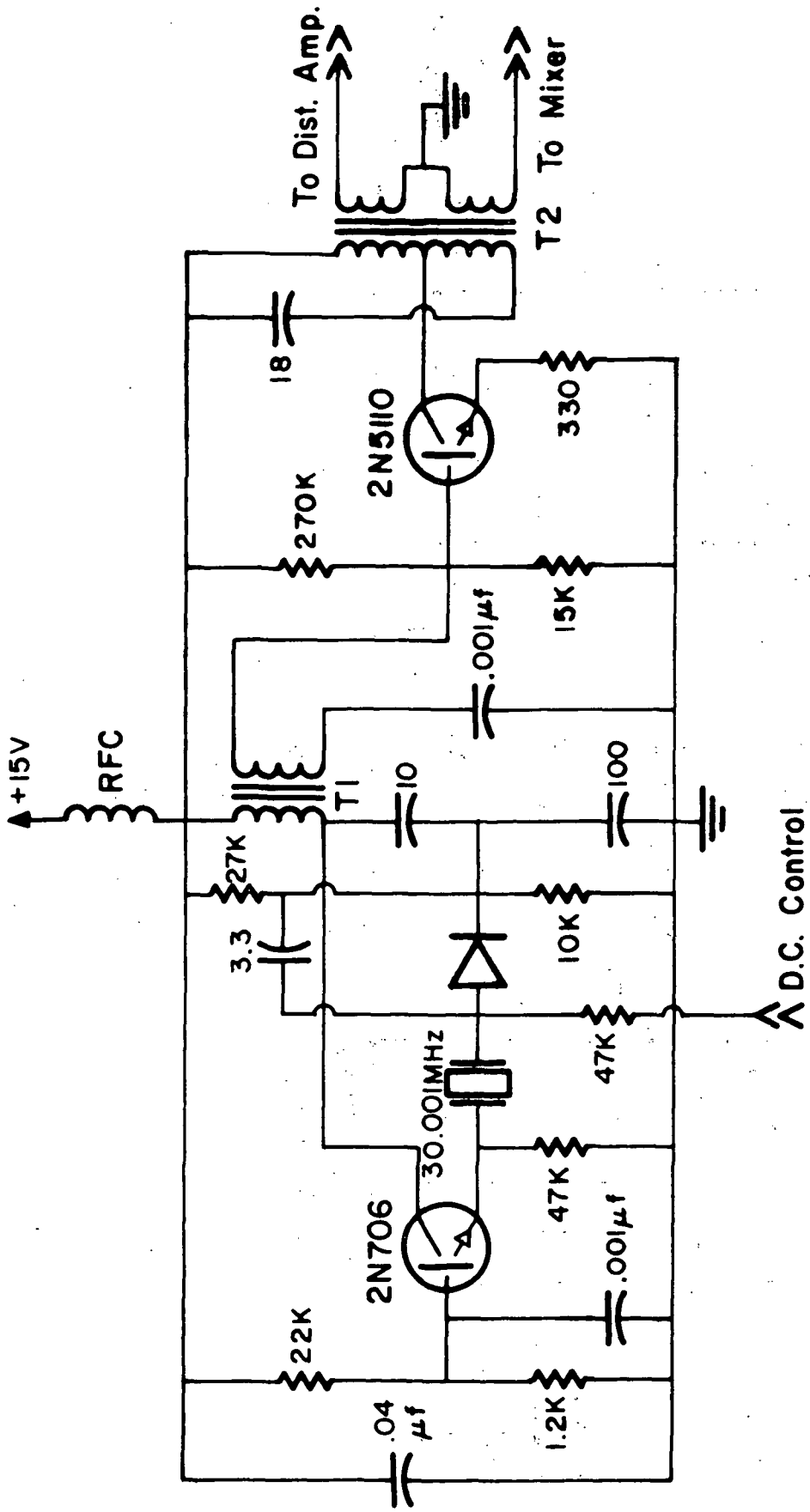

Fig. 20. 30.001 voltage controlled crystal oscillator (VCXO).

lator. The output of the oscillator is given one stage of amplification. One output is coupled to the distribution amplifier where it is buffered for use as the second LO signal. A second output is mixed with 30 MHz from the frequency synthesizer and used for phase comparison. The frequency versus DC control voltage characteristics for the VCXO are given in figure 21. The lock range is only about ±50 Hz about the center frequency. This narrow range poses no problem because the drift of the Δf oscillator is less than .1% of the operating frequency of 1000 Hz.

The Δf oscillator shown in figure 22 is tuned to the offset frequency of 1000 Hz. The configuration using complimentary FET's provides the necessary high stability needed by the VCXO and by the narrow bandwidth filters in the correlator.

The mixer shown in figure 23, mixes the 30 MHz from the frequency synthesizer and the 30.001 MHz from the VCXO. The output is used for phase comparison with the Δf oscillator. It is also used as the reference input to the quadrature detectors in the correlator. The mixer itself uses standard diode mixing followed by a high frequency trap allowing only the 1000 Hz signal to pass. This is followed by a standard biased common emitter amplifier.

The phase detector shown in figure 24 compares the 1 KHz from the mixer with the 1 KHz from the Δf oscillator [Clark and Frost, 1969b]. The resulting DC control voltage locks

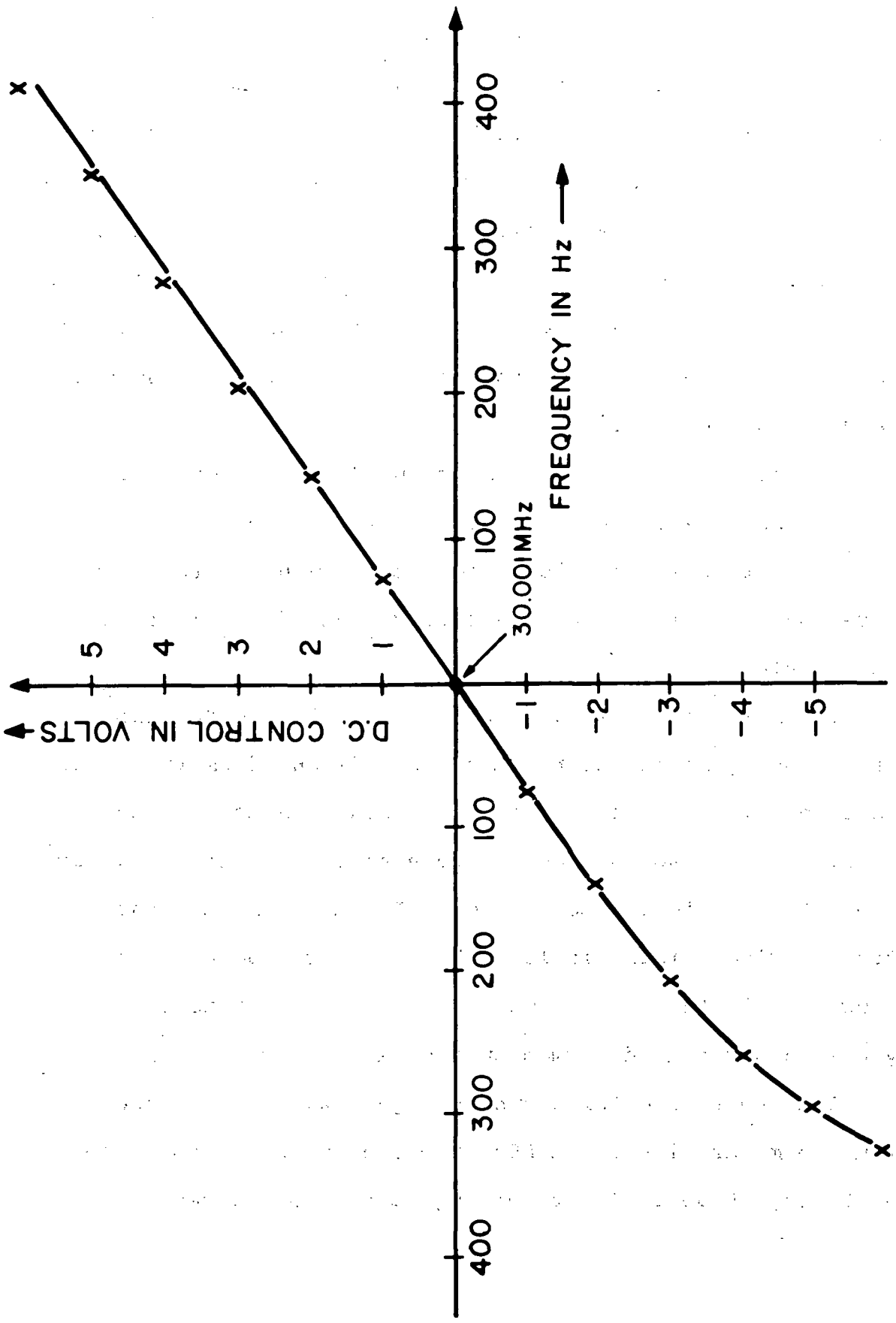

Fig. 21. D.C. control vs. frequency for the 30.001 MHz VCXO.

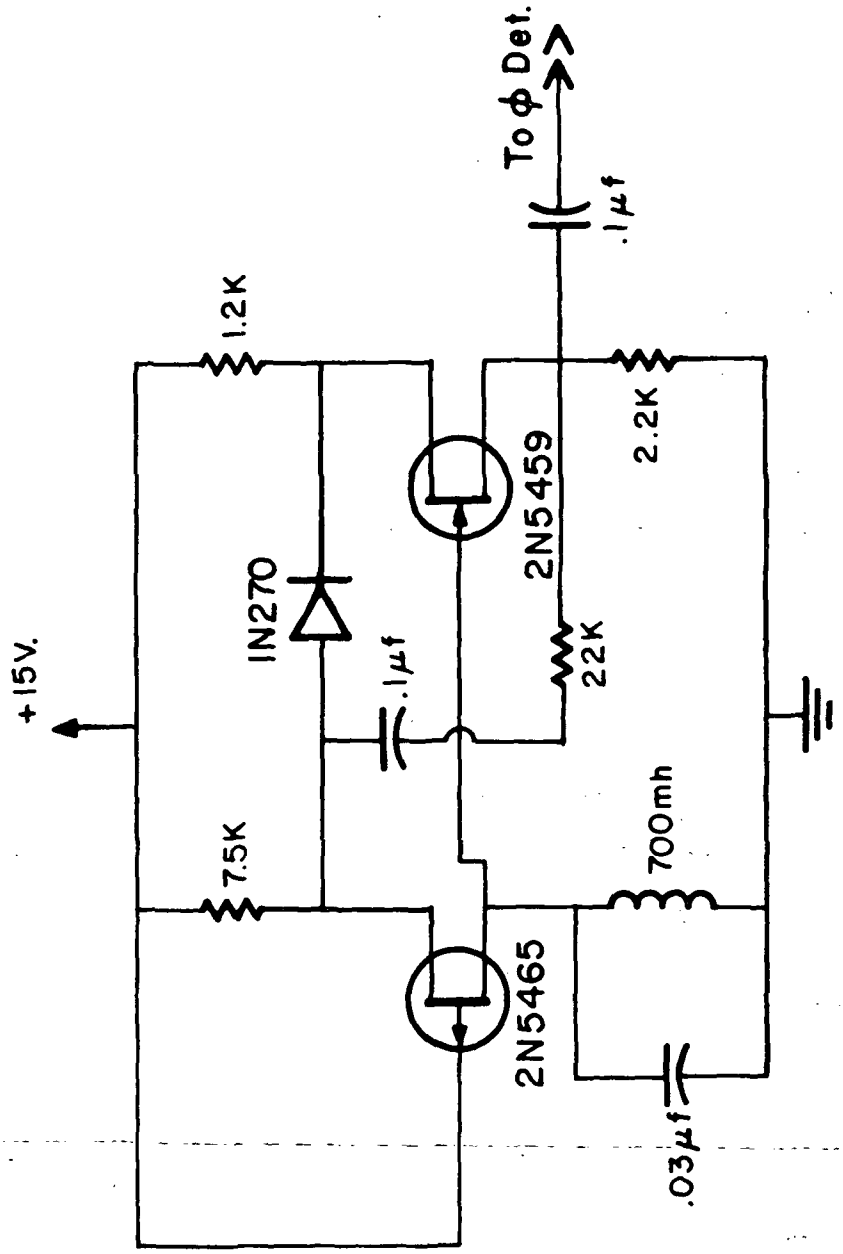

Fig. 22. 1 KHz reference oscillator

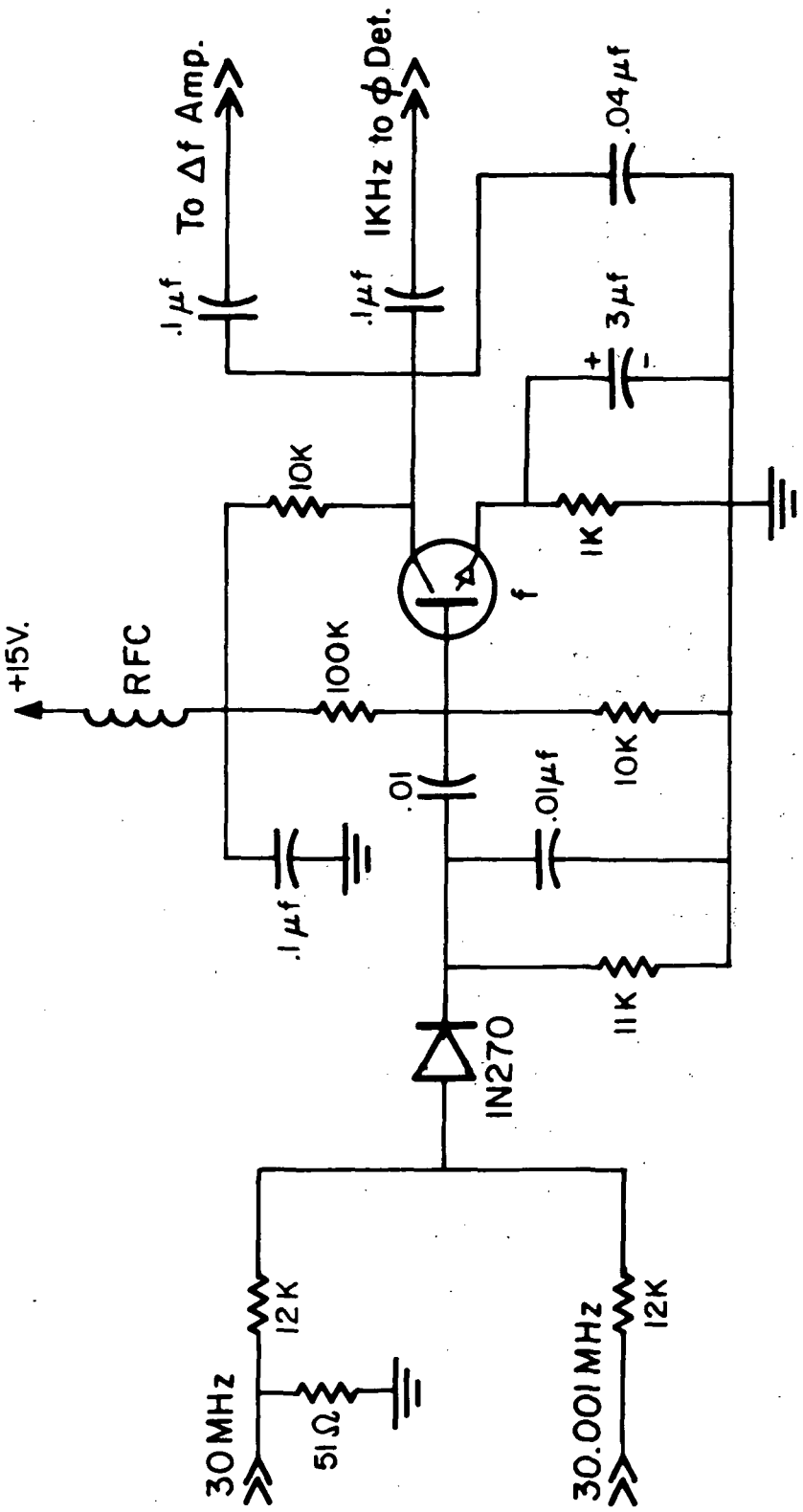
To Δf Amp.
1KHz to φ Det.
.1μf
.1μf
.04μf
3μf
10K
1K
+15V.
RFC
100K
10K
.01
.01μf
.1μf
11K
IN270
30 MHz
12K
51Ω
30.001 MHz
12K

Fig. 23. Mixer.

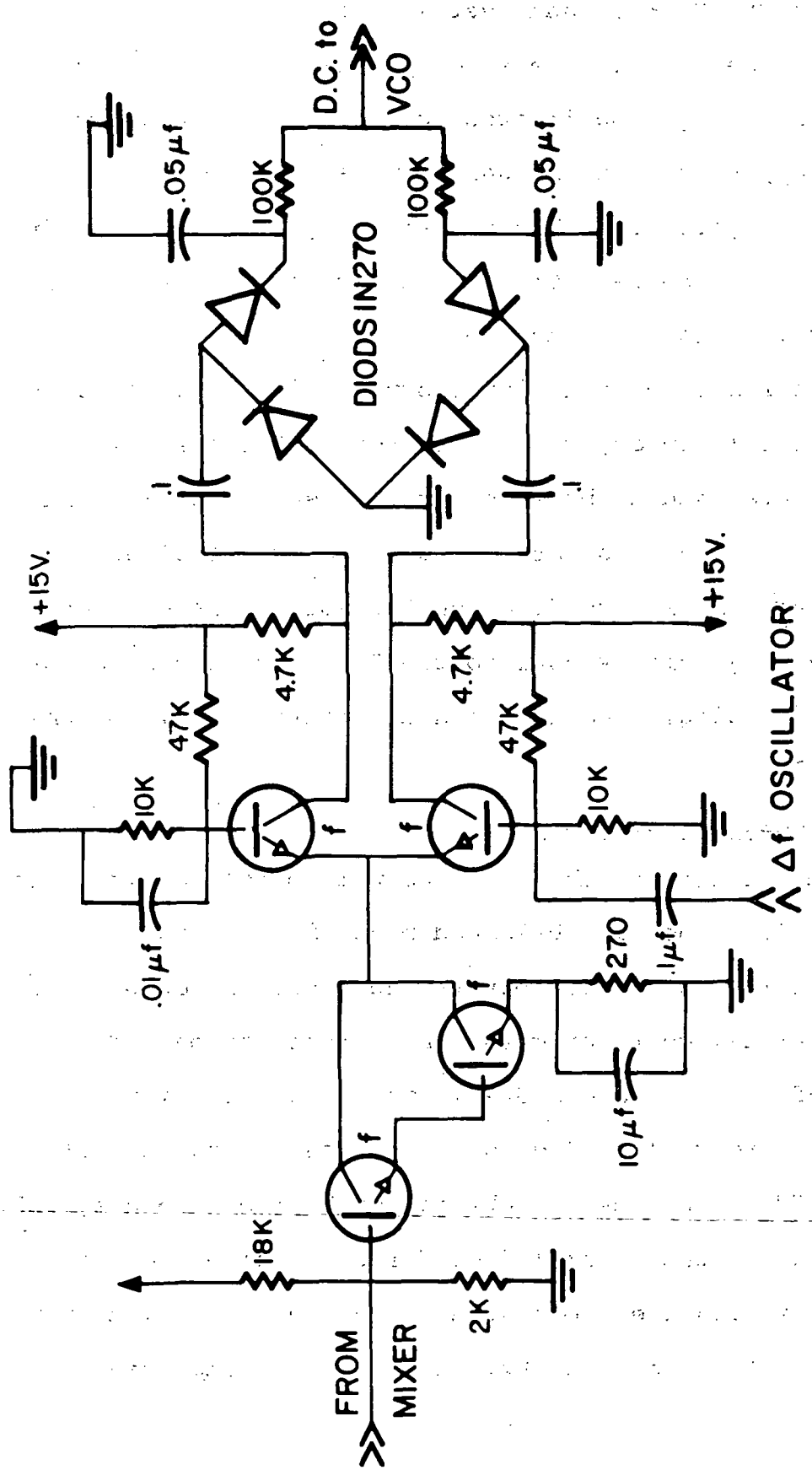

Fig. 24. 1 KHz phase detector.

the VCXO to 30 MHz + Δf and system coherence is maintained. The circuit uses the low level output from the mixer and amplifies it using a Darlington Pair configuration. This feeds a chopping circuit in which two switching transistors are driven in parallel. The output is applied across a full wave bridge and the resulting DC output is filtered and applied as a control voltage to the VCO.

The distribution amplifier shown in figure 25 contains three identical, tuned, common emitter amplifiers. The amplifiers are used as buffers for the second local oscillators for both the base station and the out station. Variable degenerative feedback on the emitter is provided so that the injection signal to the IF strips can be adjusted for optimum mixing. The inputs and outputs are all matched to 50 ohm loads.

4.4 Dual Channel Correlation

A block diagram of the dual channel correlator is given in figure 26. A double, balanced mixer is used as the correlation multiplier to convert the second IF outputs to a 1000 Hz signal containing the phase information. The device used is a MCL-model SRA-1 double balanced mixer and is shown in figure 13. The low power conversion loss of this device is 7db. In order to obtain the best possible signal-to-noise ratio, the Δf amplifier directly following the multiplier is required to have high gain and a very narrow bandwidth centered on 1000 Hz. The twin-tee amplifier shown

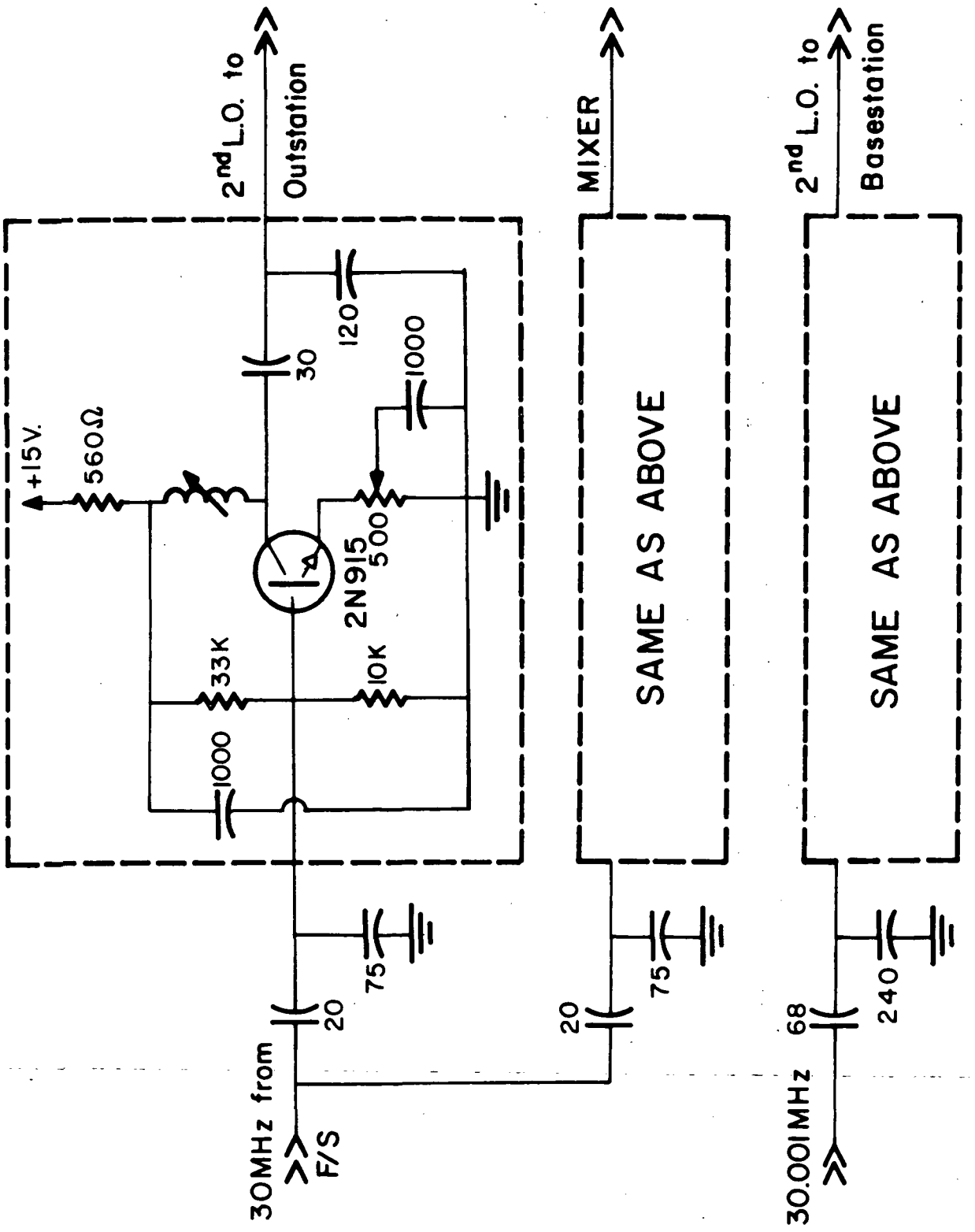

Fig. 25. Distribution amplifier.

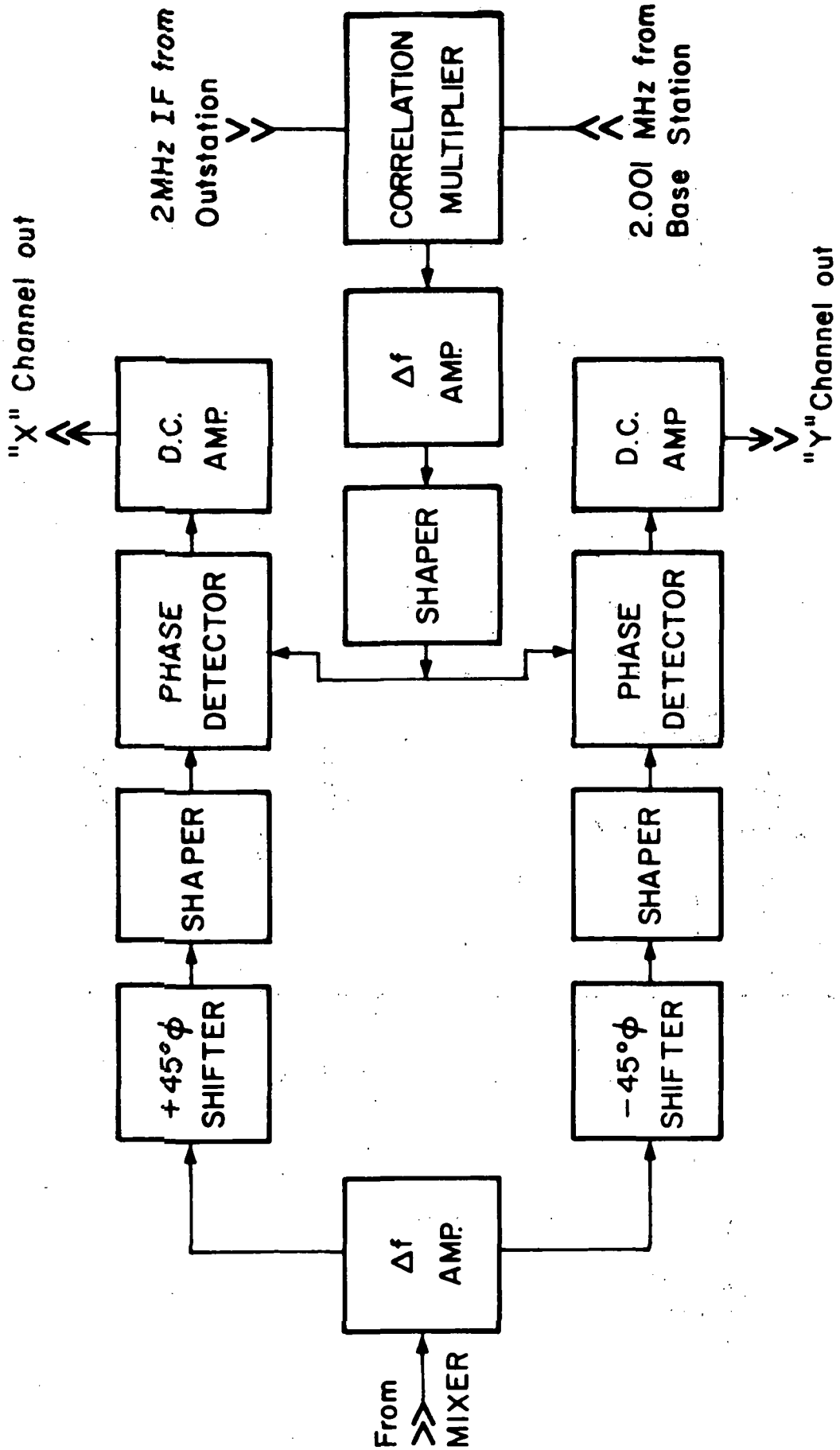

Fig. 26. Block diagram of the dual channel correlator.

in figure 27 satisfies these requirements with a gain of 33 db and a bandwidth of 10 Hz [Burr-Brown, 1963]. Unfortunately the phase shift characteristics of this amplifier give rise to 180° phase shift over the band pass. To compensate for this undesirable characteristic a second twin-tee amplifier was constructed, and the phase shift characteristics of both amplifiers were matched. The matched amplifier was used to amplify the Δf reference signal from the mixer. Thus any phase shift due to a small change in Δf will be equally felt in the reference signal and the correlated signal so that there will be no relative phase change between the two.

The Δf reference signal is taken from the mixer rather than from the Δf oscillator since there exists a small phase drift due to changes in ambient temperature between the Δf oscillator signal and the actual Δf existing between the 30 MHz from the frequency synthesizer and the 30.001 MHz from the VCO.

The reference Δf signal is next passed through a 90° phase splitter to separate the correlated output by 90°. The phase splitter shown in figure 28 is a RC op-amp circuit that synthesizes a fourth-order 90° phase difference network [Lloyd, 1971]. It has an operating bandwidth of 250 Hz to 2,500 Hz and a phase tolerance of ±1° over the bandwidth.

Both the correlated Δf signal and the Δf reference signal must be shaped into square pulses in order to trigger the

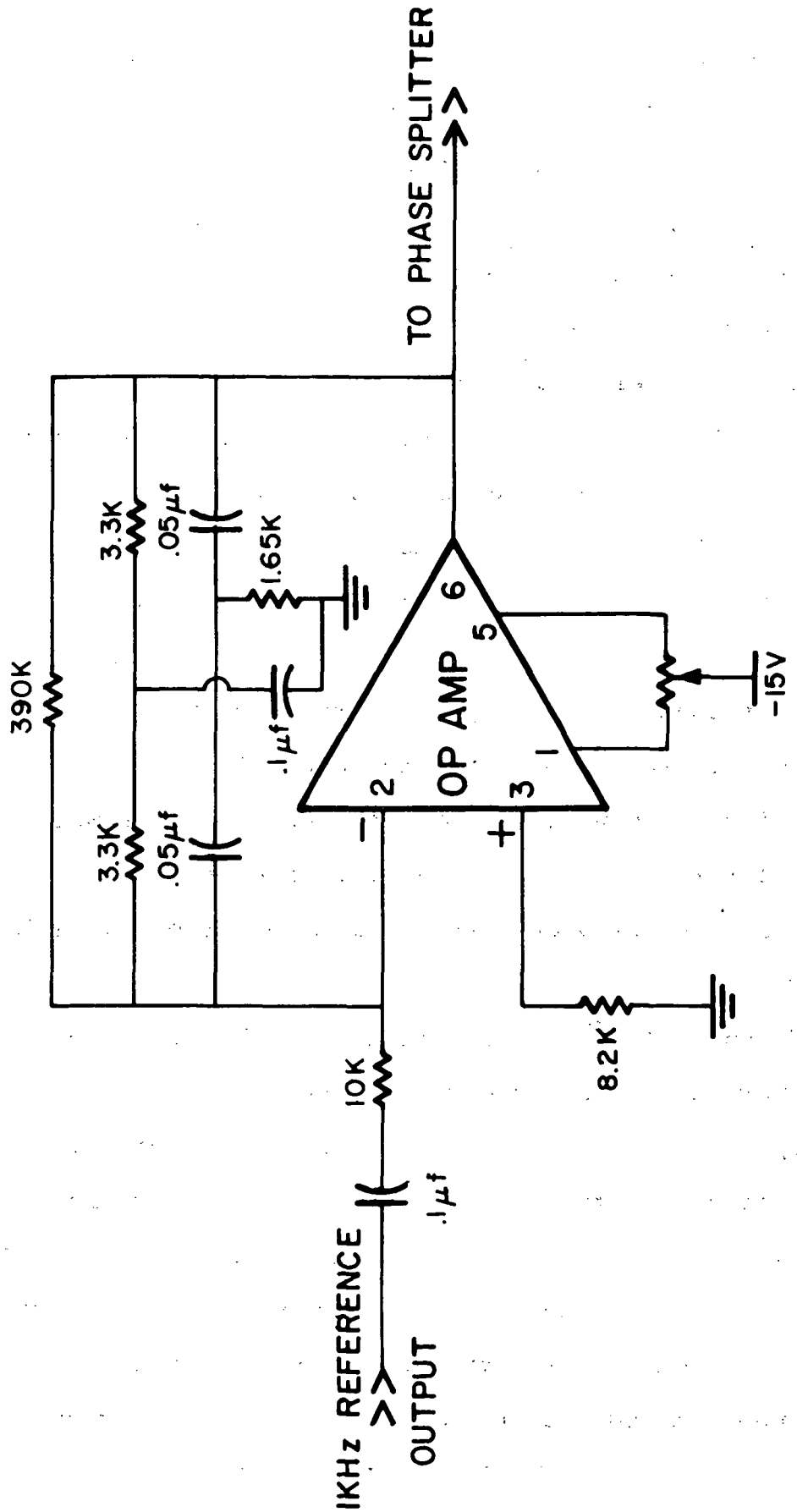

Fig. 27. 1 KHz twin-tee amplifier.

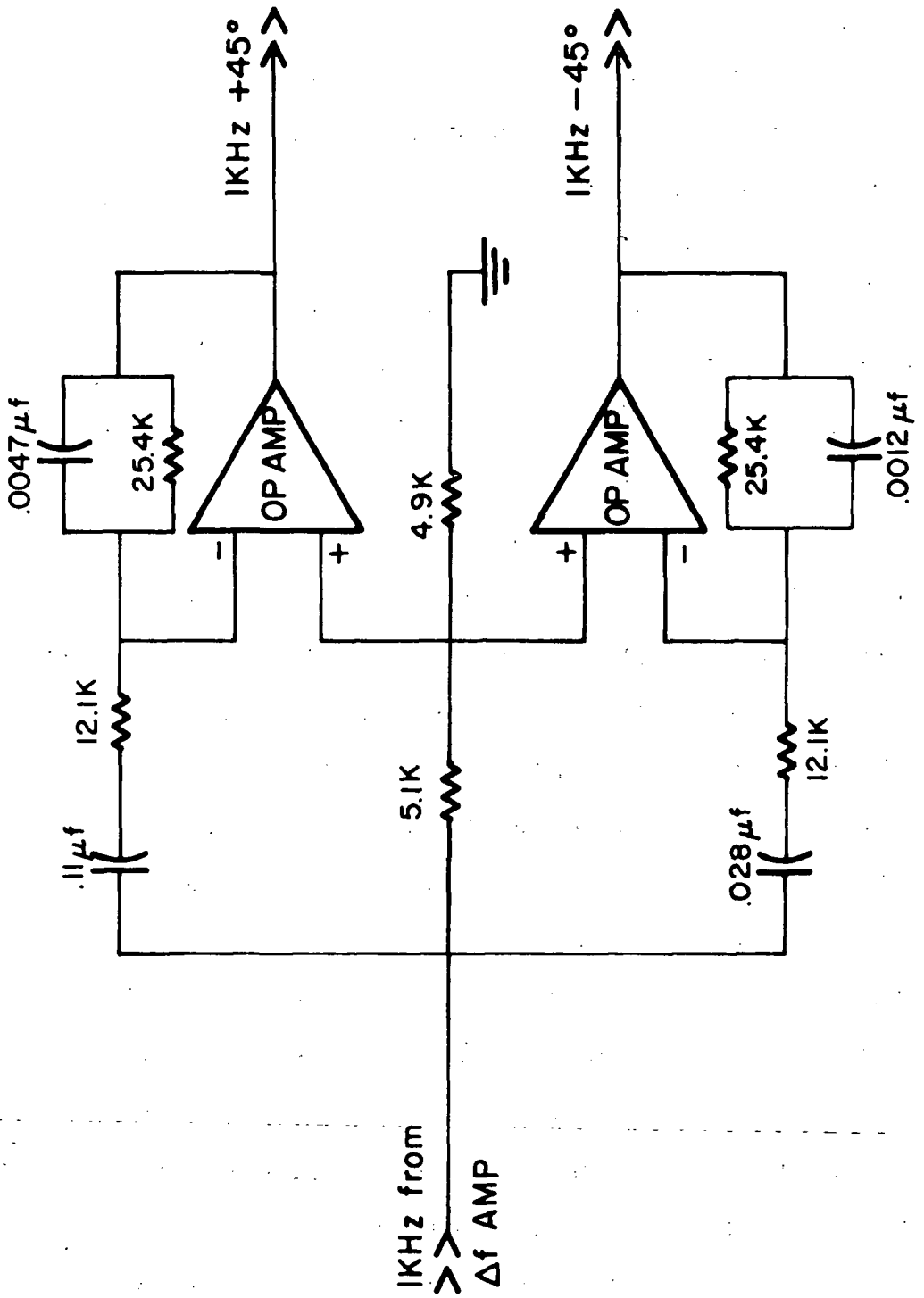

Fig. 28. 90° phase splitter schematic.

digital phase detector. The shaping circuit is shown in figure 29 [Manco, 1971]. It uses a high speed switching transistor which is normally cut off with no signal applied. This applies +5 volts on both inputs of the nand gate so the output remains at 0 volts. As the input signal swings positive, the transistor turns on quickly forcing the collector to about 0 volts. This in turn forces the nand gate output to +5 volts, resulting in a clean, fast rise time square pulse. The pulses are differentiated at the input to the phase detectors shown in figure 30. The resulting input to the phase detectors are 5 μsec. positive spikes.

The phase detector consists of a SN 7400 IC which contains four nand gates. The nand gates are cross-connected as shown to implement a R-S flip-flop. The logic for this flip flop is given in figure 30 as is the integrated output of the phase detector. It can be seen from the logic table that when both inputs are in phase an undefined or race condition exists. This causes a small dead time in an interval about the 0° phase difference point. Since the input pulses are only 5 μsec in duration, the race condition only produces ±1.8° of dead time about the 0° condition. The outputs of both phase detectors are integrated, and then directly coupled to DC amplifiers with unity gain. The correlator unit requires a reguires a regulated +15 volt and -15 volt power supply for the operational amplifiers. The SN 7400 IC's require +5 volts. This is accomplished by dropping the +15 volt supply to +5 volts using a zener diode.

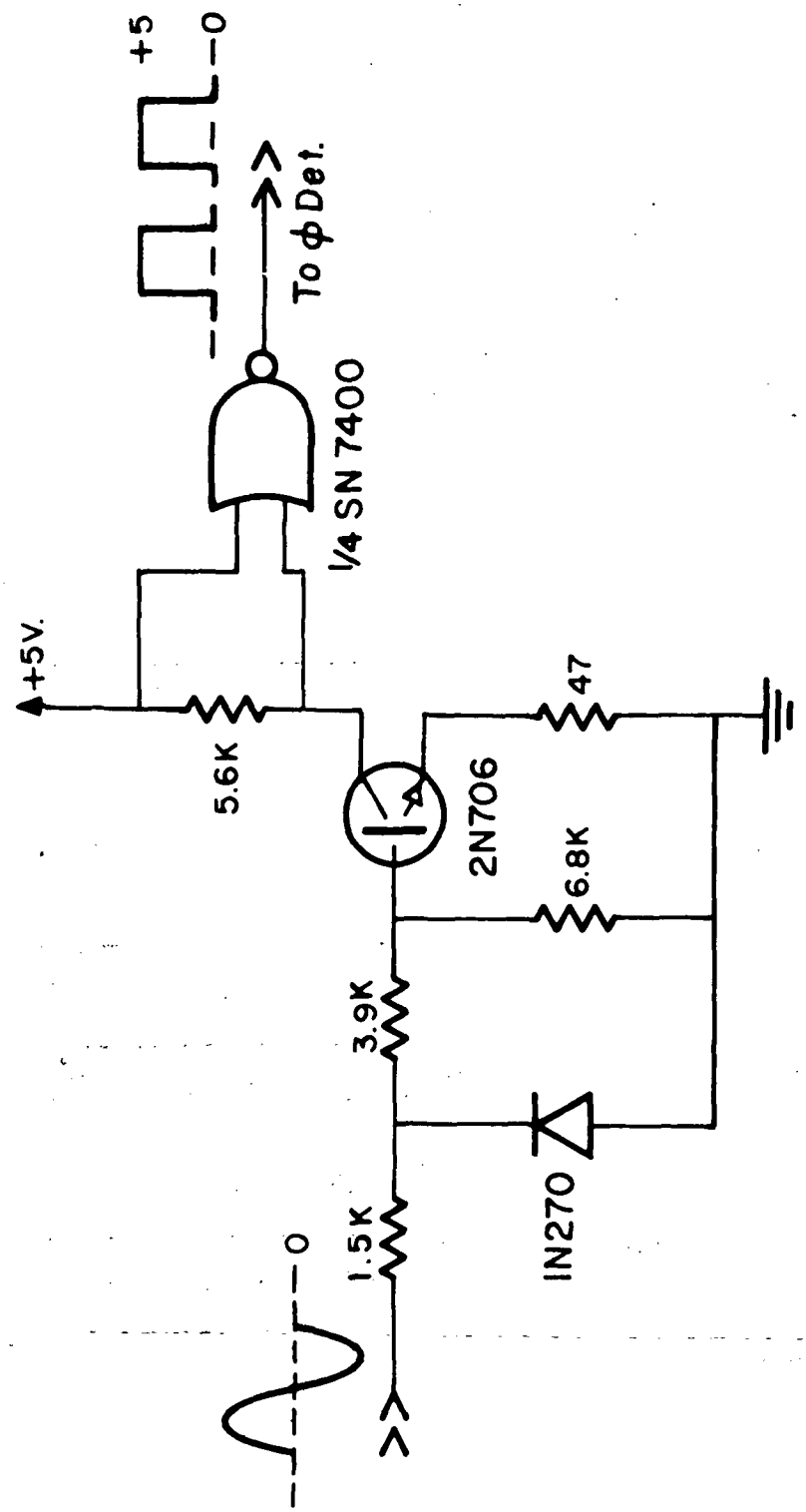

Fig. 29. Shaping circuit schematic.

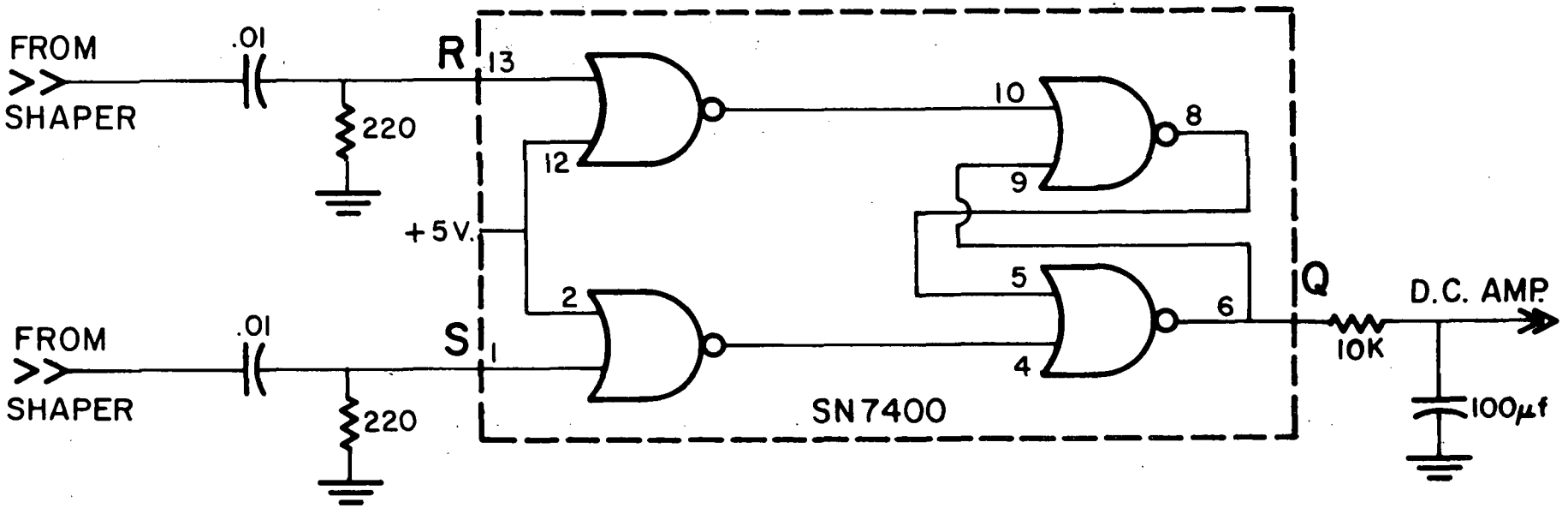

LOGIC TABLE

R	S	Q	Q
0	0	0	0
0	1	0	1
1	0	0	0
0	0	1	1
0	1	1	1
1	0	1	0
1	1	undefined	

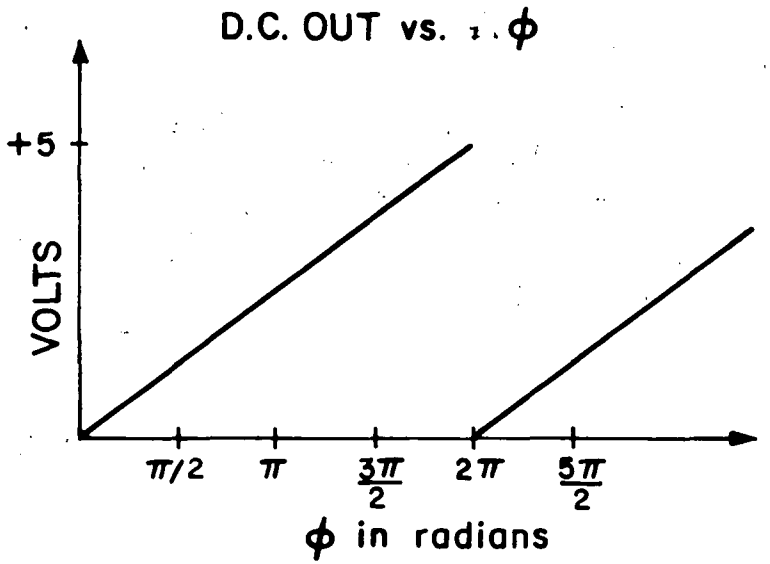

Fig. 30. Phase detector.

5. CONCLUSIONS AND RESULTS

5.1 Installation

The interferometer system described in this paper has been built, and an evaluation of the system is presently being performed.

The initial configuration uses a north-south baseline, and the site separation is 142 meters or about 65 wavelengths at 137.35 MHz. The source being monitored is the ATS-III geostationary satellite. The antenna used for the base station is a twenty eight foot parabolic dish and the outstation uses a Yagi antenna. Since the initial setup has a relatively short baseline, both receivers are located in the same building and coaxial cable is used for lead in from the antennas.

5.2 Phase Detectors

Two types of phase detectors are incorporated into the final interferometric design. The digital phase detector mentioned in the previous section is the first type. Both inputs to this detector are a string of 5μ sec. pulses. These pulses are obtained from the zero crossings of the Δf reference signal and the correlated output signal. Hence, this detector responds only to the phase variations of the received signal and not to amplitude variations. The output of this detector is very useful for studying traveling ionospheric disturbances (TID's).

Since one of the main uses of the interferometer will be to study ionospheric scintillation, in phase and amplitude, a second type of detector was built. These we call quadrature component detectors, and they are shown schematically in figure 31. Since they are identical detectors operating in phase quadrature, only one will be described. The sine wave output from the reference Δf phase splitter is converted to a symmetric square wave by the first operational amplifier. This square wave is then shaped, and it is used to drive a field effect transistor (FET) 2N5485. This FET acts as a switch on the non-inverting input of a second operational amplifier with unity gain. (It switches the non-inverting input from ground to essentially an open circuit). The inverting input to the operational amplifier is driven by the correlated signal. It can be shown that for equal input frequencies this second operational amplifier and FET act together as a synchronous detector. As long as the correlated signal amplifier is not allowed to limit its signal, the integrated outputs of these quadrature component detectors are given by

$$x = K \sin \phi, \quad y = K \cos \phi,$$

where K is proportional to the amplitude of the input signal and ϕ is proportional to its phase angle. The amplitude K and phase ϕ can then be separated by the data

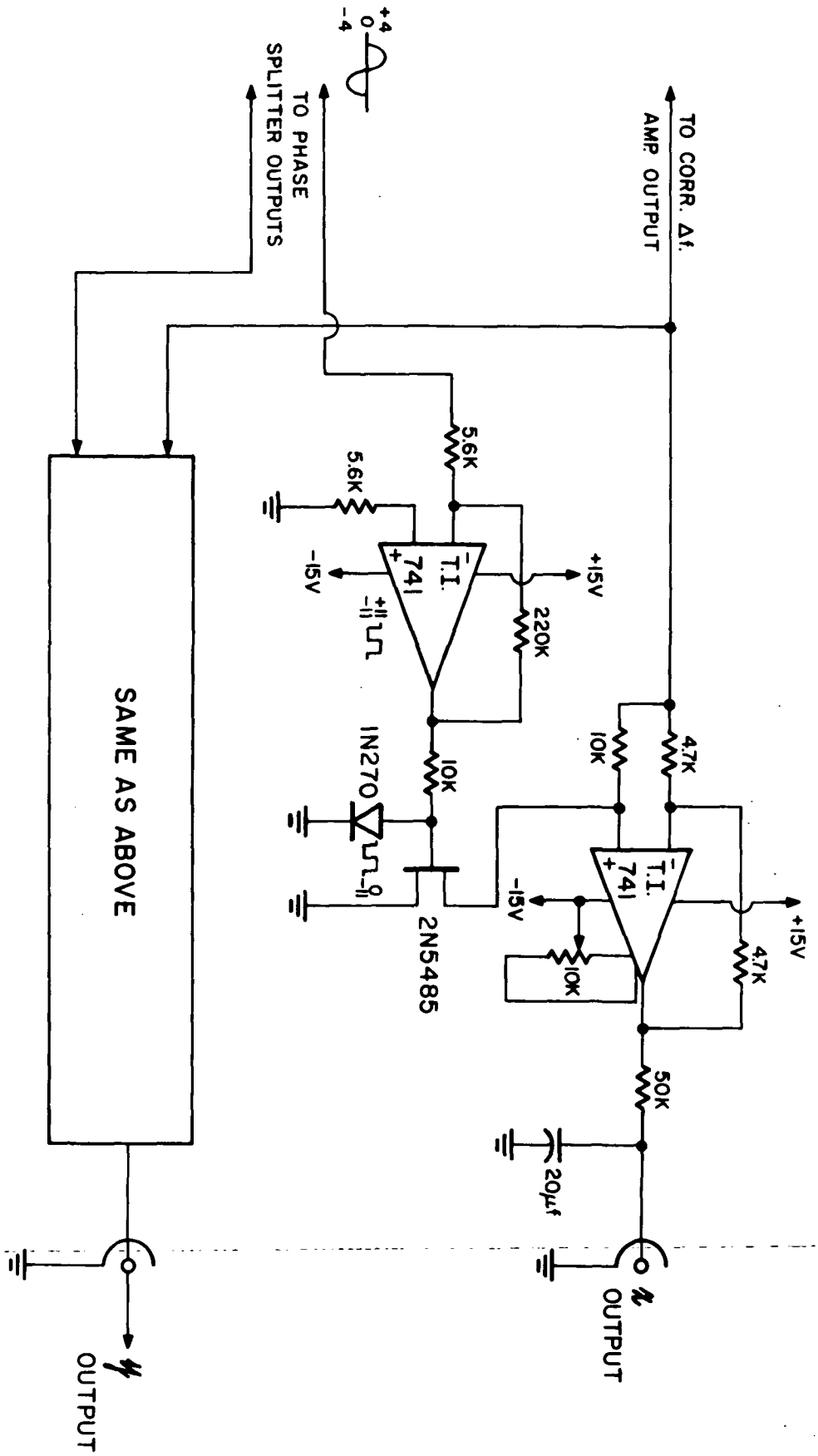

Fig. 31. Quadrature component detectors

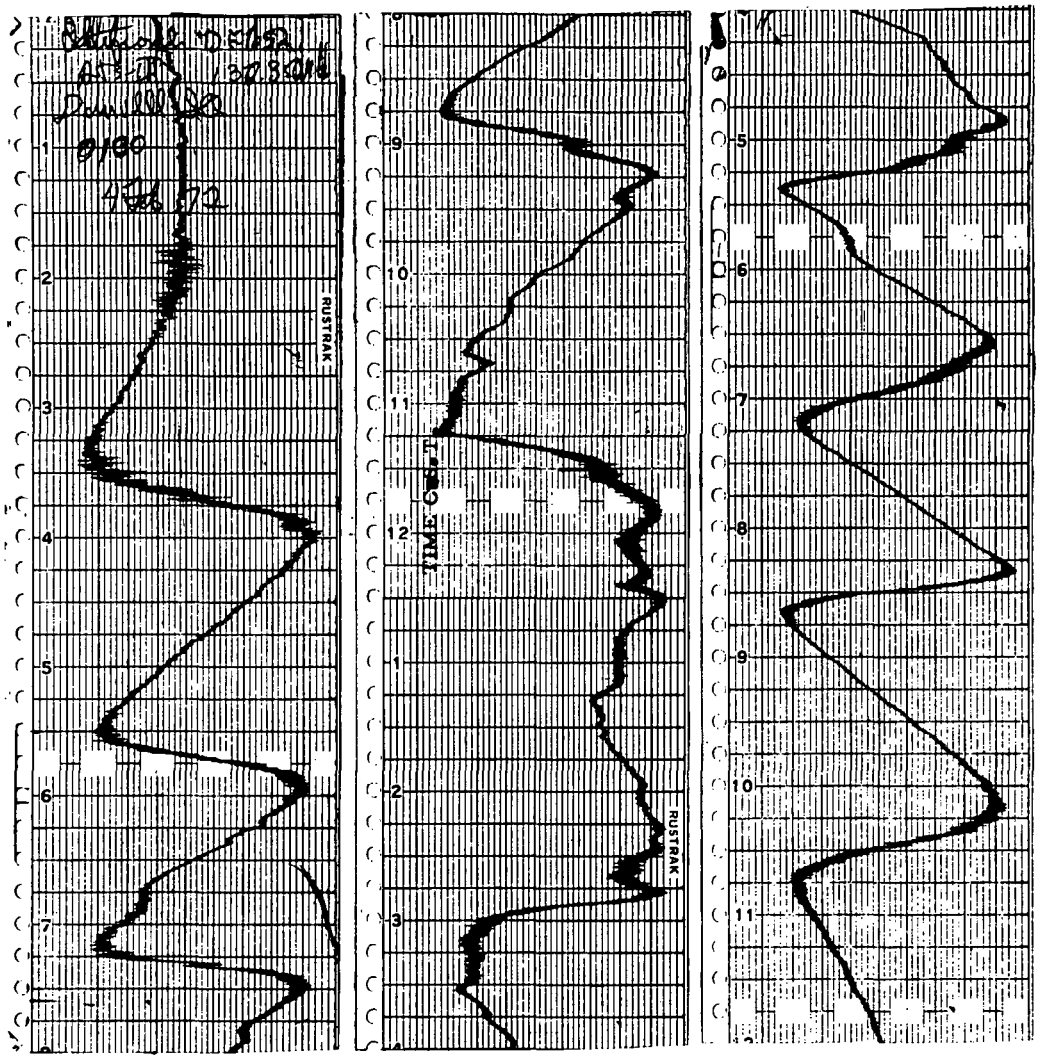

Fig. 32. Section of strip chart showing the fringe pattern due to satellite motion over a twenty four hour period. 0000 hours is at top left and 2400 hours is at bottom right.

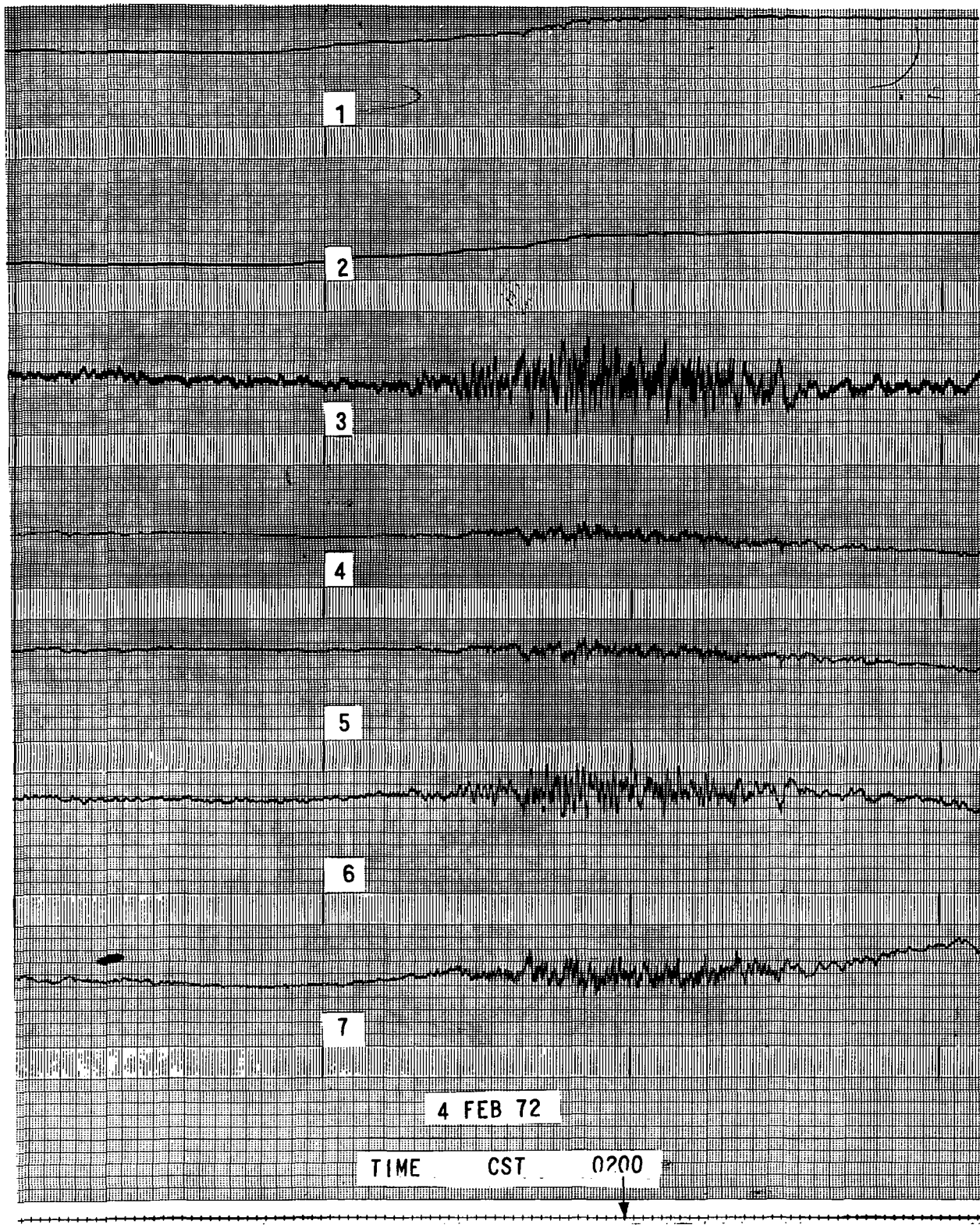

Fig. 33. High speed recording of an isolated patch of scintillation. Polarimeter is on channels 1 to 3 and the 65λ interferometer is on channels 4 to 7. Time advances to the right, and the marks are every minute.

reduction process.

5.3 Results

Although the satellite being observed, the ATS-III, is geostationary, it is not strictly stationary. It has a slight periodic movement with a period of twenty-four hours. This slow movement is detected as fringing by the interferometer. The fringe pattern associated with the satellite movement over a twenty four hour period is shown in figure 32. (Each fringe in the figure represents 360° of phase rotation). This phase detector data was recroded on 4 February 1972 at Danville, Illinois at an antenna spacing of 65 wavelengths. Superimposed on the regular fringe pattern are irregular fluctuations caused perhaps by TID's (Note particularly between 0915 and 1800 cst).

VHF waves passing through the ionosphere can also be subject to scintillation caused by ionospheric disturbances. An isolated patch of scintillation can be seen in figure 32 between 0145 and 0230. A higher speed recording of this data, the x and y quadrature component detector outputs, and the outputs from a polarimeter are shown in figure 33. The time marks at the bottom are in one minute increments, and time is increasing to the right. Channels 1 and 2 are the Faraday rotation channels from the polarimeter. Channel 3 is the polarimeter amplitude channel on which medium amplitude scintillation is present.

The interferometer outputs are on channels 4 to 7. Channels 4 and 5 are the phase detectors, and 6 and 7 are the x and y outputs. Note the small fluctuation on the phase channels compared to the x and y outputs. This appears to indicate that the scintillation is mainly in amplitude. To verify this, the K and ϕ components will have to be reduced from the data. As of this writing we have not done this. A record similar to figure 32 is shown in figure 33. The data channels on this record are the same as figure 32, but in this data the scintillation is stronger and lasting for a longer period of time. Again it appears to be more in amplitude than in phase.

The interferometer performs well within its design specifications at the test spacing of sixty-five wavelengths. We are now preparing to build the few minor components necessary to make the outstation protable. When this is finished we will then make measurements at various spacings and directions.

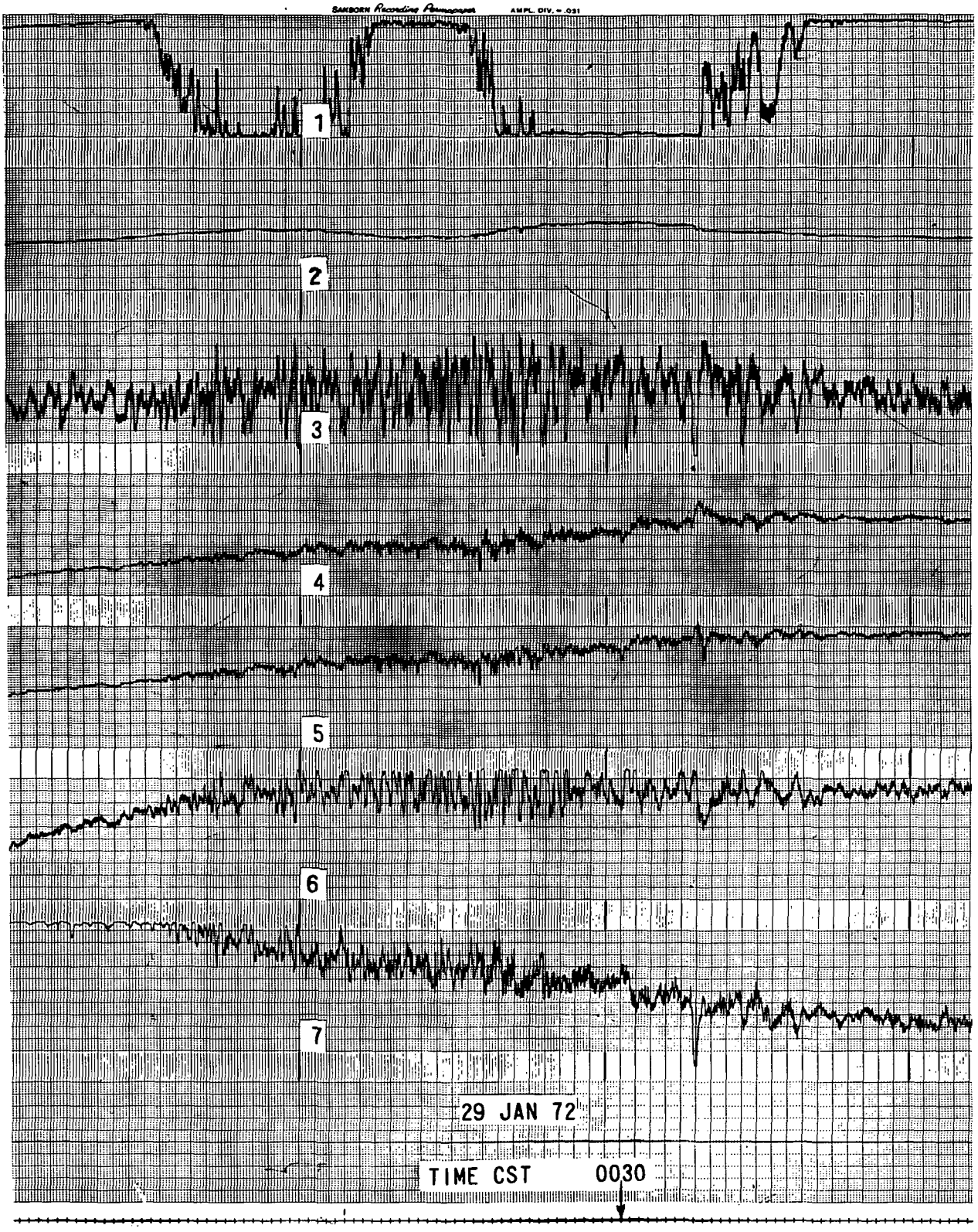

Fig. 34. High speed recording of a prolonged period of strong scintillation channels are the same as figure 33.

LIST OF REFERENCES

Clark, R. R. and Frost, A. D., The Radio Interferometer, Scientific Report No. 1, December 20, 1967, Contract No. AF19 (628)-5837.

Clark, R. R. and Frost, A. D., Coordinate Conversion Techniques for use with a Correlation Radio Interferometer, Scientific Report No. 2, July 15, 1969a, Contract No. AF19 (628)-5837.

Clark, R. R. and Frost, A. D., A Long Baseline Radio Interferometer for Ionospheric Scintillation Measurements, Final Report, September 15, 1969b, Contract No. AF19 (628-5837.

Handbook of Operational Amplifier Applications, Burr-Brown Research Corporation, p. 72, (1963).

Lathi, B. P., An Introduction to Random Signals and Communication Theory, International Textbook Company, (1968).

Lloyd, A. G., A 90° Phase-difference Network, Electronic Design, Vol. 15, p. 78, July 22, 1971.

Manco, R. J., One-shot Makes Fast Trigger out of Slow Input Pulse, Electronic Design, Vol. 44, p. 60, September 27, 1967.

Sherill, W. M., A Survey of HF Interferometry for Ionospheric Propagation Research, Radio Science, Vol. 6, No. 5, pp. 549-566, May 1971.

Thomas, J. B., An Introduction to Statistical Communication Theory, John Wiley & Sons, (1969).

DETERMINATION OF CHANGES IN EXOSPHERIC ELECTRON CONTENT BY A COMPARISON OF GROUP DELAY AND FARADAY ROTATION

by

Richard E. DuBroff

March 1972

Sponsored by

National Aeronautics and Space Administration

NGR 14-005-002

Technical Report No. 45-2

Ionosphere Radio Laboratory

ELECTRICAL ENGINEERING RESEARCH LABORATORY
ENGINEERING EXPERIMENT STATION
UNIVERSITY OF ILLINOIS
URBANA, ILLINOIS 61801

ABSTRACT

A proposed technique of obtaining the exospheric electron content is by subtracting the ionospheric electron content obtained from Faraday rotation measurements of VHF signals from a geostationary satellite, from the electron content obtained simultaneously from group delay measurements of the same signals. In this study, this technique is evaluated by using Faraday rotation data and group delay data simulated by ray tracing for a Chapman layer model extending from the ground to a height h_B, and an exosphere model extending from h_B to the satellite. The effect of varying the boundary height, h_B, is considered and it is shown that the Faraday rotation measurement is not significantly affected by the exospheric region, as expected in view of the rapidly decreasing geomagnetic field in that region. The group delay measurement is then considered in order to determine the size of the errors which would be involved if the electron content were obtained by approximating the group delay as a linear function of the electron content. Based upon the results of the simulation it is found that the accuracy of the technique is sufficient for providng only the changes in the exospheric electron content, but not necessarily the instantaneous values of the exospheric electron content.

ACKNOWLEDGMENT

The suggestions and comments made by Dr. N. Narayana Rao and Dr. K. C. Yeh, throughout the course of this work, proved to be very valuable. The subroutines which were written for this research were used in connection with the ESSA three dimensional ray tracing program (Jones, 1966). This work was supported by the National Aeronautics and Space Administration, Grant No. NGR 14-005-002.

TABLE OF CONTENTS

LIST OF TABLES

LIST OF FIGURES

1. INTRODUCTION

This study is concerned with the measurement of ionospheric and exospheric electron contents by observing radio signals at 40, 140, and 360 MHz from a geostationary satellite. By observing the radio signals sent from a satellite located in the exosphere, it is desired to determine how much of the electron content is contributed by the ionosphere and how much is contributed by the exosphere.

The relative contributions from each region may vary, for example, during the course of one day. Cislunar radar measurements (Yoh, 1965) have, in fact indicated that there may be a diurnal flux of ionization between the two regions. Park (1970) has shown that the magnetospheric electron content in a field tube may change considerably following magnetic storms.

At first glance, it appears that it may be possible to determine the contribution to the electron content by comparing simultaneous measurements of the group delay time, and the Faraday rotation angle. The Faraday rotation angle (Ω) can be measured experimentally, and is related to the electron content in the following way:

$$\Omega \cong \frac{K}{f^2} \int_{\text{ray path}} H_0 N_e \cos\theta \, ds \qquad (1)$$

where K is a constant of proportionality and is equal to 2.97×10^{-2} in international units. In practice, the

following approximation is commonly used:

$$\Omega \cong \frac{\bar{M}K}{f^2} \int N_e dh = \frac{\bar{M}KN_T}{f^2} \qquad (2)$$

where $\bar{M}$ includes the weighted mean effect of the magnetic field. Because of the magnetic field dependence in equation (1), the Faraday rotation angle is not believed to be indicative of electron content from regions in which the magnetic field is relatively weak (most of the exosphere).

The differential group delay measurement, in contrast, does not depend on the magnetic field. The group delay time is the time required for a signal travelling at the group velocity to go from the satellite to the Earth. The differential group delay, therefore, is the difference in the times of arrival of two different signals, each travelling at its own group velocity. The differential group delay, then, for two different frequencies is related to the electron content in the following way:

$$\Delta T = \frac{80.5 \times 10^{-6}}{2c} \left(\frac{1}{f_1^2} - \frac{1}{f_2^2} \right) \int N_e \, ds \qquad (3)$$

and does not depend upon the magnetic field.

Therefore, it would seem that the exospheric electron content (N_{TE}) could be found from:

$$N_{TE} = N_T \underset{\text{group delay}}{} - N_T \underset{\text{Faraday rotation}}{} \qquad (4)$$

The approach which has been outlined above, however, is contingent upon a few assumptions which need to be

examined, in order to ensure that any errors which may be inherent in this type of analysis will not be large enough to cause a significant degree of uncertainty in the determination of the exospheric electron content.

2. METHOD

The method employed to investigate the uncertainties in the determination of the exospheric electron content is a computer simulation of the transmission of radio waves from a satellite, through the exosphere and the ionosphere to a receiver on the ground. By specifying the electron density and the magnetic field, it is possible to determine how a ray from the satellite will be refracted by the exosphere and the ionosphere and, therefore, by using a ray tracing program it is possible to determine the path of the ray. In addition, it is possible to determine the Faraday rotation and group delay for the ray. The ray tracing program used is an adaption of the ESSA 3-D ray tracing program (Jones, 1966). The details of the determination of the electron content from the results of the ray tracing program are discussed in the following sections.

The rays are traced through several different models of the ionosphere and of the exosphere. The Chapman layer is used for the ionosphere and the model of Angerami and Thomas (1964) is used to simulate the exosphere. The electron density at the base of the exosphere is set equal to the electron density at the top of the ionosphere, so that the electron density will vary continuously with height, although the gradients might not match at the base of the exosphere. The magnetic field is modeled by an Earth centered dipole.

Since rays of different frequencies and different modes (ordinary and extraordinary) have to be traced, it is necessary to ensure, in the simulation, that the rays will all land very nearly at the same location on the ground. For this reason, several rays of the same frequency and mode have to be traced iteratively until the ray comes sufficiently close (0.5 meters) to the desired landing point. After a ray has been homed (i.e. landed within 0.5 meters of the target), another ray with a different frequency and/or a different mode can be traced. The method of homing which is used is shown in Figure (1).

The choice of 0.5 meters as the homing criterion should not introduce any significant amount of error in the simulation. Based upon the results which were obtained in the simulation the maximum uncertainty which could occur in the determination of the electron content as a result of the homing criterion is ±.14% of the electron content. In many cases the uncertainty would be a few thousandths of a percent. In addition, the size of most practical antennas which would be used at the frequencies of interest would be greater than .5 meters.

In the case of Faraday rotation the difference between the ordinary and extraordinary phase paths is several hundred meters for the ionosphere models considered in this study. Consequently, the errors which are introduced into the Faraday rotation measurement by the homing criterion

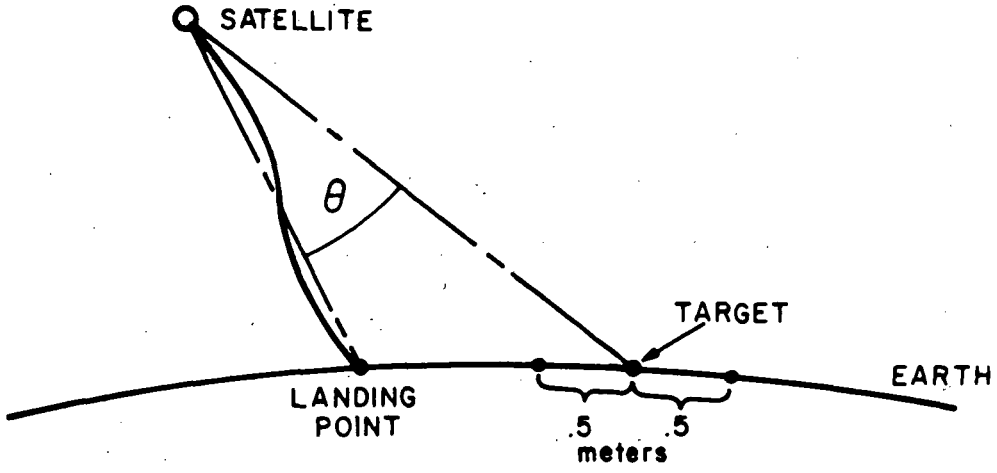

Figure 1. Method of homing the ray.

are no greater than a few tenths of a percent for a rotation measurement at 40 MHz.

This method of homing can only be used when the target and the actual landing point of the ray are nearly on the same geographic longitude, because of the way in which the homing computations are performed by the computer. This presents no problems for the ionosphere and exosphere models used in the ray tracing simulation, since the azimuth deviations of the rays are very small. In order to achieve the homing, the elevation angle of the ray is changed by a fraction of $\theta(\frac{3}{4}$ seems to be the best choice) until the landing point of the ray is within 0.5 meters of the target. Figure (2) shows the geometry of the simulation.

Using this procedure, simulated Faraday rotation and group delay data are obtained and used in an effort to resolve some of the problems; and to illustrate the limitations of the method of determining exospheric electron content.

The particular values ξ and γ were chosen in order to place the satellite on the equator and on the same longitude (approximately) as Urbana, Illinois. The path shown in Figure (2) is a straight line between Urbana and the satellite.

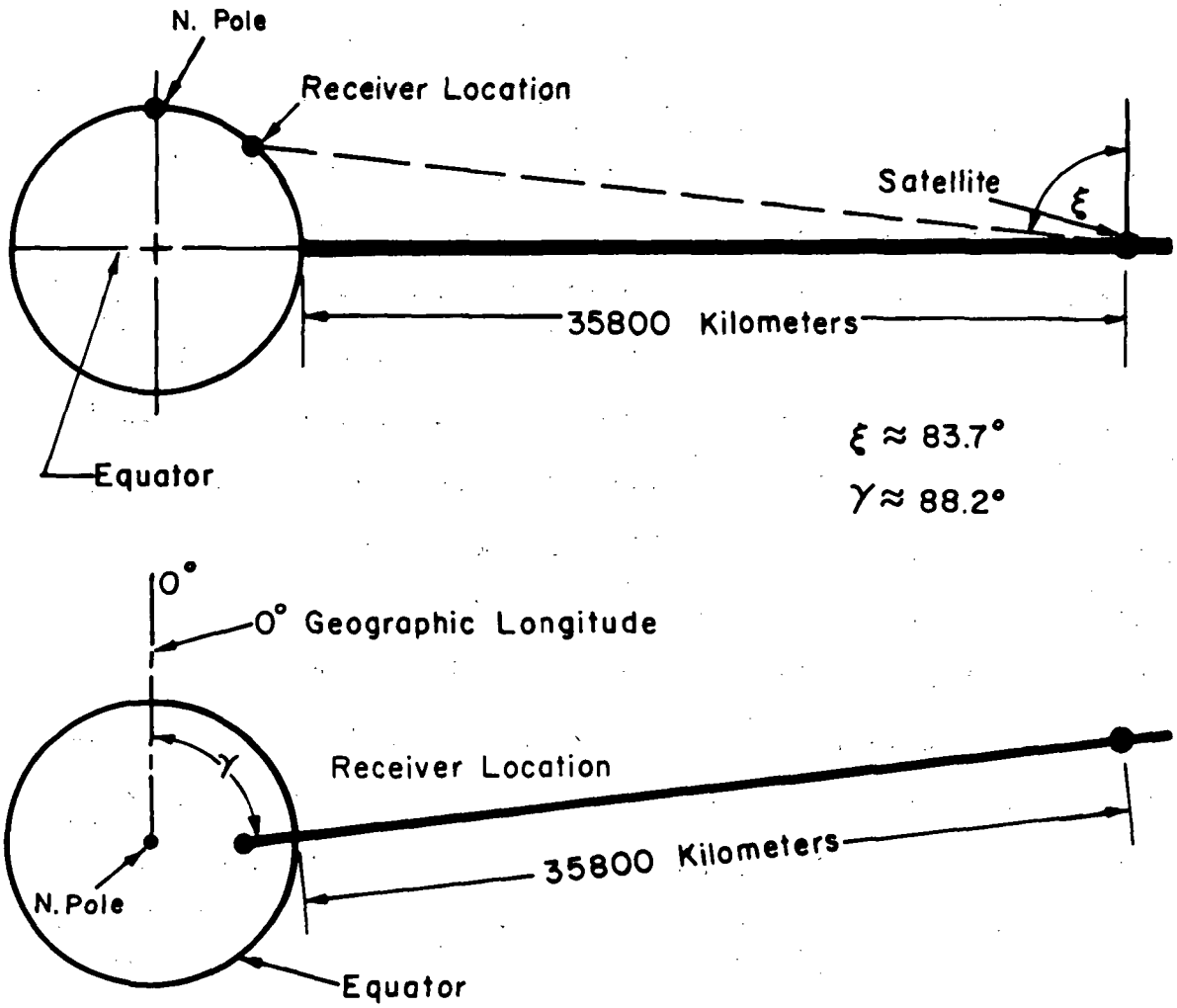

Figure 2. Geometry of the simulation.

3. SIMULATED FARADAY ROTATION IN A CHAPMAN LAYER

There are several models which describe the electron density as a function of height. In this study the Chapman layer is used to simulate the electron density as a function of altitude in the ionosphere. The electron density is given by:

$$Ne = \frac{f_c^2}{80.5 \times 10^{-6}} \exp\left[0.5(1 - z - \varepsilon^{-z})\right] \qquad (5)$$

where

$$z = \frac{h - h_{max}}{H}$$

In an ionosphere which is formed from a single ionized constituent, $H = \frac{kT_i}{m_i g}$ where T_i and m_i are the temperature and mass of the ionized constituent. Also, h is the height, h_{max} is the height at which the maximum value of electron density occurs, and f_c is the plasma frequency which corresponds to the maximum value of electron density. In the simulation, H was chosen to be 60 km and h_{max} was chosen to be 350 km.

The total electron content, N_T, can be obtained by integrating equation (5).

$$N_T = \int_0^\infty N_e \, dh \qquad (6)$$

It is, however, not necessary to integrate to infinity as is shown in Figure (3) which is a graph of $\int_0^\beta Ne \, dh$ as

a function of β in km. In fact, for the Chapman model which is used in the simulation, Figure (3) suggests that it may only be necessary to integrate up to a few thousand km, since the electron density above 2000 km is too small to contribute to the electron content.

An experimental technique for determining the electron content is Faraday rotation. The Faraday rotation measurement deduces the electron content from the polarization twist of a linearly polarized radio signal as it traverses the ionosphere. If we denote the polarization twist by Ω, the relation between Ω and the electron density is given by the following well known equation:

$$\Omega \simeq \frac{2.97 \times 10^{-2}}{f^2} \int N_e H_0 \cos\theta \, ds \qquad (1)$$

From equation (1) it can be seen that when H_0 (the magnetic field) becomes small, the polarization will change very little even though N_e might not be small. However, when the Chapman layer is used to simulate the ionosphere, the electron density above 1000 km is so minute that it tends to obscure the effect of the diminishing magnetic field. The situation is depicted graphically in Figure (4) which shows $\Omega = \frac{2.97 \times 10^{-2}}{f^2} \int_0^{\beta} N_e H_0 \cos\theta \, ds$ as a function of the height of β in thousands of km. The value of Ω was obtained by integrating equation (1) numerically and using an Earth centered dipole magnetic field model. Figures (3) and (4) both were obtained by integrating along a

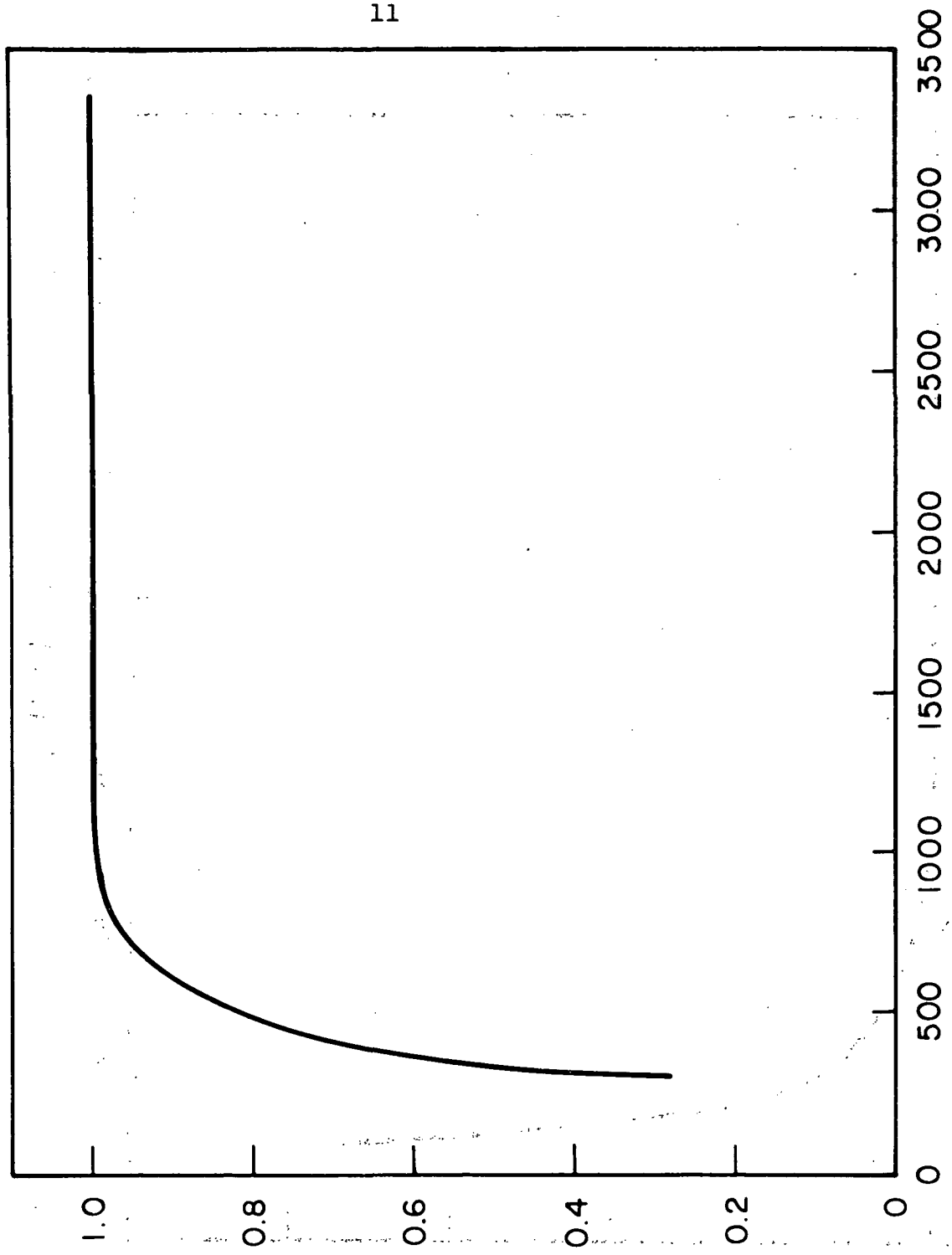

Figure 3. Normalized electron content integrated to a height shown as the abcissa.

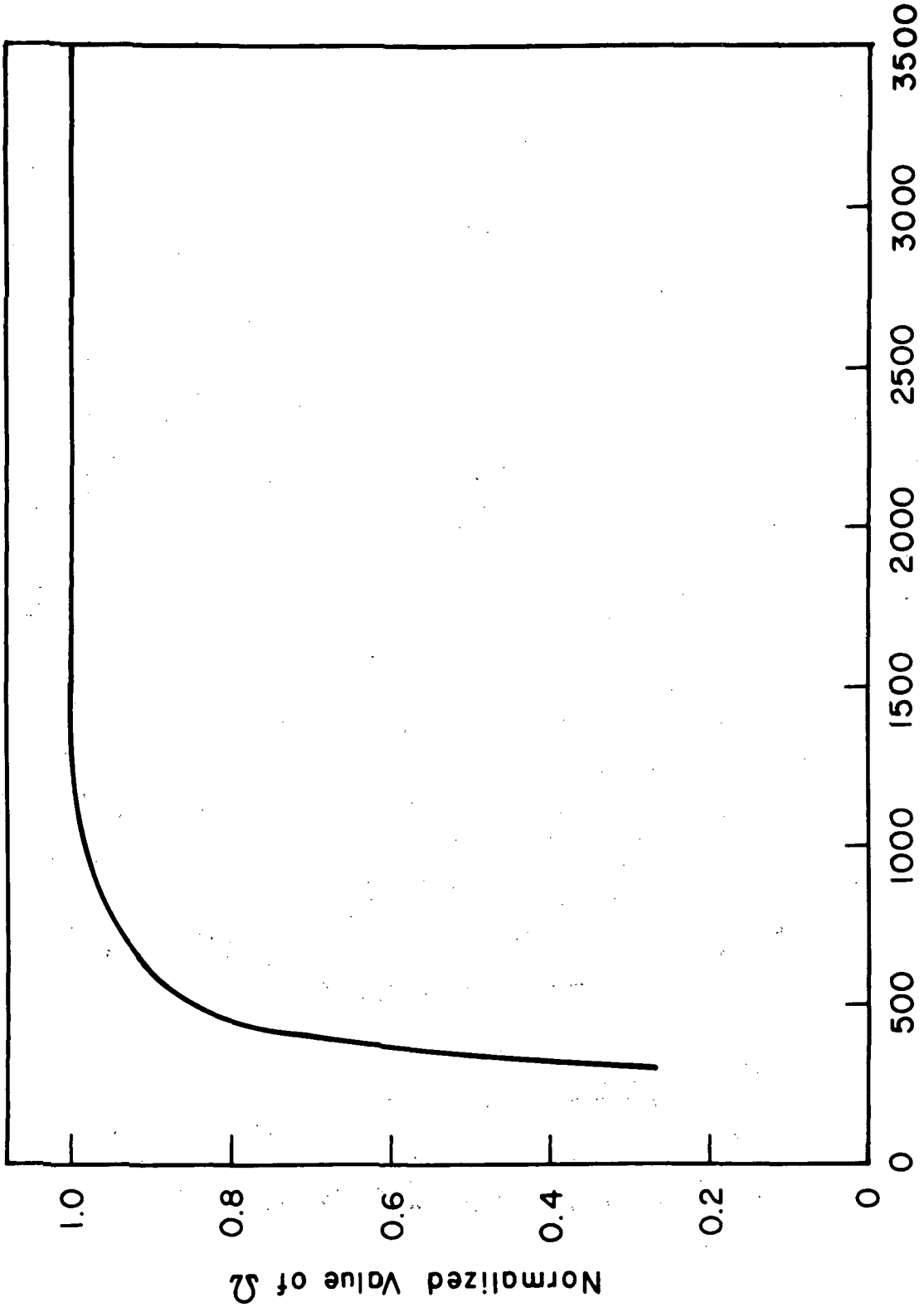

Figure 4. Normalized Ω integrated to a height shown as the abcissa.

vertical path.

A comparison between Figure (3) and Figure (4) illustrates that the electron content varies almost linearly with the rotation, Ω. The expression relating Ω and the integral of the electron density can be simplified by replacing ds by sec x dh and replacing $H_0 \cos\theta \sec x$ with a constant, $\bar{M}$, which can subsequently be taken from under the integral sign. The angle, x, is the zenith angle of the ray. Therefore, the approximate expression for Ω becomes:

$$\Omega \cong \frac{2.97 \times 10^{-2} \bar{M}}{f^2} \int N_e \, dh \qquad (2)$$

if the integration over the path, s, in equation (1) is nearly a straight line. The close similarity between Figure (3) and Figure (4) will break down if a model in which the electron density in the exosphere is substantially larger than that given by equation (5) is used to simulate N_e. This will be demonstrated in the next section.

4. SIMULATED FARADAY ROTATION IN A MODEL IONOSPHERE CONSISTING OF A CHAPMAN LAYER AND A MODEL EXOSPHERE

4.1 Distribution of Electron Density in the Model Exosphere

The Chapman model of the ionosphere is not well suited for the simulation of exospheric electron density for several reasons. The scale height is not apt to remain constant over the wide extent of the exosphere (from about 1000 to 35800 km for the purpose of this simulation). In addition, the Chapman model does not include the effect of the curved geomagnetic field lines upon the distribution of the ions.

A more realistic alternative would be to use a Chapman model to simulate the electron density up to around 1000 km, and then to use an additional model (Angerami and Thomas, 1964) to simulate the region from the upper boundary of the Chapman layer to the satellite. Any subsequent mention of the ionosphere should, then, be construed loosely--i.e., the simulated ionosphere will include both the Chapman layer and the exospheric model, unless otherwise noted.

In the exospheric model, it is assumed that the electron and ion temperatures are equal at any point on the upper boundary of the Chapman layer, and that the temperature distribution along each magnetic field line is isothermal. The expression for the geopotential height z along a given field line is given as:

$$z(\Phi_0,\Phi) = r_0 \left\{ \left[1 - \frac{\cos^2\Phi_0}{\cos^2\Phi}\right] + \frac{\Omega_e^2 r_0}{2g_0}\left[\cos^2\Phi_0 - \frac{\cos^6\Phi}{\cos^4\Phi_0}\right] \right\} \quad (7)$$

where,

Φ_0 = geomagnetic latitude of field line at upper boundary of Chapman layer

Φ = geomagnetic latitude of point on the field line

r_0 = radius of the Earth and height of upper boundary of Chapman layer

Ω_e = angular velocity of the Earth

g_0 = gravitational acceleration at the upper boundary of Chapman layer

From equation (1) it can be seen that z varies linearly with height in the Chapman layer. In the exospheric model, however, the dependence of z upon height is not linear, as is shown in Figure (5). Also the value of z depends upon the position of the point in question. The ordinate in Figure (5) is the height along the path shown in Figure (2).

Equation (7) can be put into a more compact form for the purpose of ray tracing by utilizing the equation for a dipole field line

$$\frac{r}{r_0} = \frac{\cos^2\Phi}{\cos^2\Phi_0} \tag{8}$$

Equation (8) can be used to express $\cos^2\Phi_0$ in terms of $\cos^2\Phi$, r, and r_0 in equation (7).

$$z(r,\Phi) = r_0\left\{\frac{r - r_0}{r} + \frac{\Omega_e^2}{2g_0}\cos^2\Phi\left[\frac{r_0^2}{r} - \frac{r^2}{r_0}\right]\right\} \tag{9}$$

The form of equation (9) is still not completely satisfactory for the ray tracing program, since the ray tracing program utilizes a spherical geographic coordinate

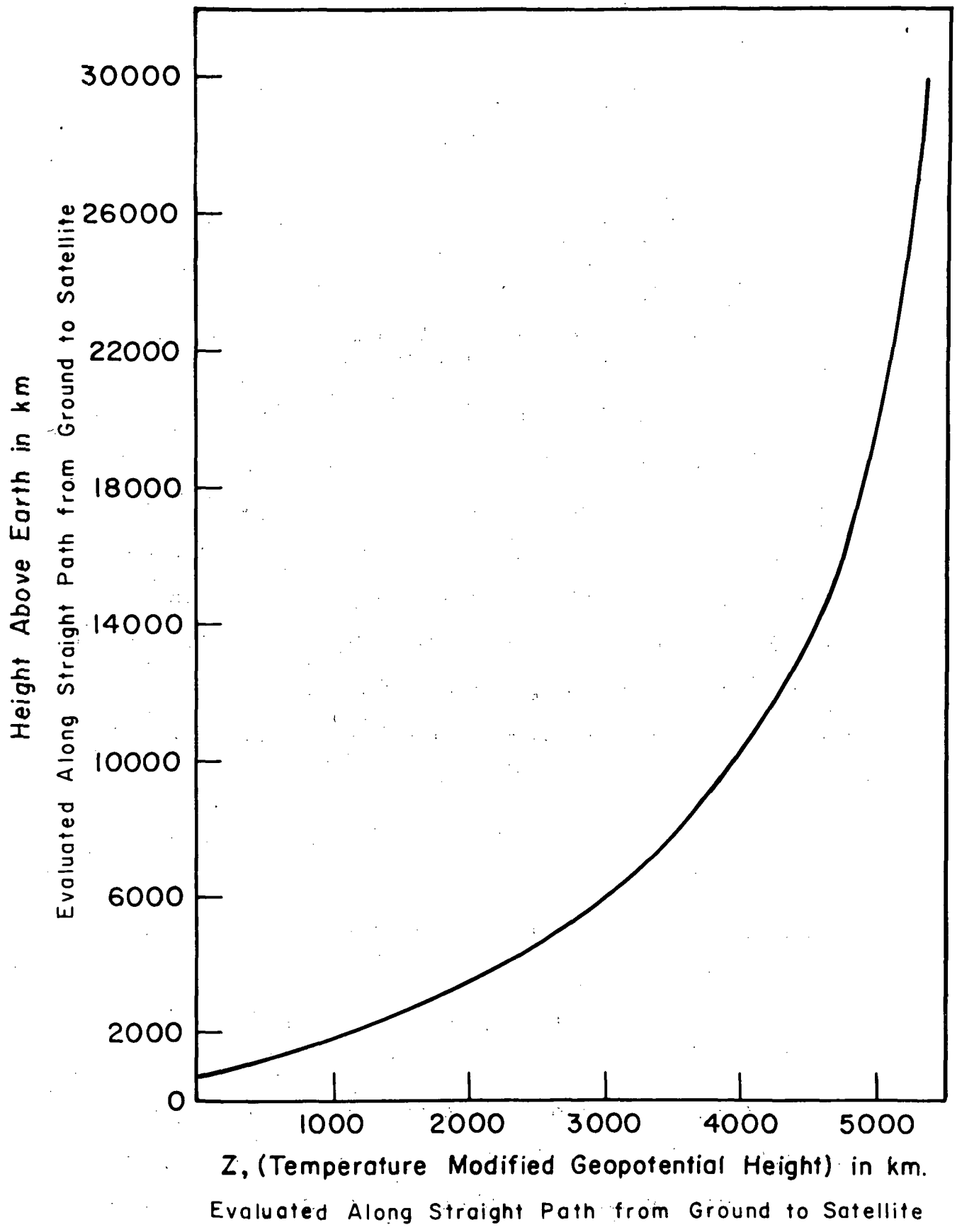

Figure 5. Variation of z in the exosphere.

system with the center of the Earth serving as the origin. The geomagnetic latitude can be written in terms of the geographic latitude (ϕ) and the geographic longitude (λ) through the following equation:

$$\sin\Phi = \sin\phi \sin\phi_1 + \cos\phi \cos\phi_1 \cos(\lambda - \lambda_1) \quad (10)$$

or

$$\cos^2\Phi = 1 - \sin^2\Phi = 1 - \sin^2\phi \sin^2\phi_1 - \cos^2\phi \cos^2\phi_1 \cos^2(\lambda - \lambda_1) - 2\sin\phi \sin\phi_1 \cos\phi \cos\phi_1 \cos(\lambda - \lambda_1) \quad (11)$$

where the subscript 1 indicates the geographic coordinates of the North magnetic pole.

Therefore, equation (9) becomes:

$$z = r_0 \left\{ \frac{r - r_0}{r} + \frac{\Omega_e^2}{2g_0} \left[\frac{r_0^3 - r^3}{r_0 r} \right] \left[1 - (\sin\phi \sin\phi_1)^2 - (\cos\phi \cos\phi_1 \cos(\lambda - \lambda_1))^2 - 2\sin\phi \cos\phi \sin\phi_1 \cos\phi_1 \cos(\lambda - \lambda_1) \right] \right\} \quad (12)$$

The electron density in this exospheric model can then be expressed as a function of z in the following way:

$$N_e = \frac{N_{eo}}{\eta^{1/2}} \sqrt{\varepsilon^{-z/H_1} + \eta_2 \varepsilon^{-z/H_2}} \quad (13)$$

where: $\eta_2 = \left. \frac{[H+]}{[O+]} \right|_{r = r_0}$

$$\eta = 1 + \eta_2 = \left. \frac{[H+] + [O+]}{[O+]} \right|_{r = r_0}$$

$N_{e0} = N_e \Big|_{r = r_0}$

H_1 = scale height of oxygen at $r = r_0$

H_2 = the scale height of hydrogen at $r = r_0$

The ray tracing program requires the specification of the gradients of N_e in the radial, longitudinal, and co-latitudinal directions--i.e., $\frac{\partial N_e}{\partial r}$, $\frac{\partial N_e}{\partial r(2)}$, and $\frac{\partial N_e}{\partial r(3)}$. Noting that $\frac{\partial N_e}{\partial z}$ is given by:

$$\frac{\partial N_e}{\partial z} = \frac{N_{e0}}{2\eta^{1/2}} \cdot \frac{\left\{ -\frac{1}{H_1} \varepsilon^{-z/H_1} - \frac{\eta_2}{H_2} \varepsilon^{-z/H_2} \right\}}{\left[\varepsilon^{-z/H_1} + \eta_2 \varepsilon^{-z/H_2} \right]^{1/2}} = \frac{N_{e0}^2}{2N_e\eta} \left\{ -\frac{1}{H_1} \varepsilon^{-z/H_1} - \frac{\eta_2}{H_2} \varepsilon^{-z/H_2} \right\} \tag{14}$$

the gradients can be written in terms of $\frac{\partial N_e}{\partial z}$.

$$\frac{\partial N_e}{\partial r(1)} = \frac{\partial N_e}{\partial z} r_0 \left\{ \frac{r_0}{r^2} - \frac{\Omega_e^2}{2g_0} \left[1 - \sin^2\phi \sin^2\phi_1 - \cos^2\phi \cos^2\phi_1 \cos^2 (\lambda - \lambda_1) - 2\sin\phi \cos\phi \sin\phi_1 \cos\phi_1 \cos(\lambda - \lambda_1) \right] \left[\frac{r_0^2}{r^2} + \frac{2r}{r_0} \right] \right\} \tag{15}$$

$$\frac{\partial N_e}{\partial r(2)} = \frac{\partial N_e}{\partial z} \frac{r_0 \Omega_e^2}{2g_0} \left[\frac{r_0^3 - r^3}{r_0 r} \right] \left[-2\sin\phi \cos\phi \sin\phi_1 + 2\cos\phi \sin\phi \cos^2\phi_1 \cos^2(\lambda - \lambda_1) - 2\cos^2\phi \sin\phi_1 \cos\phi_1 \cos(\lambda - \lambda_1) + 2\sin^2\phi \sin\phi_1 \cos\phi_1 \cos(\lambda - \lambda_1) \right] \tag{16}$$

$$\frac{\partial N_e}{\partial r(3)} = \frac{\partial N_e}{\partial z} \frac{r_0 \Omega_e^2}{2g_0} \left[\frac{r_0^3 - r^3}{r_0 r}\right][2\cos^2\phi \cos^2\phi_1 \cos(\lambda - \lambda_1) \sin$$

$$(\lambda - \lambda_1) + 2\sin\phi \cos\phi \sin\phi_1 \cos\phi_1 \sin(\lambda - \lambda_1)] \qquad (17)$$

Figure (6) is a graph of N_e as a function of height. Since N_e is not spherically symmetric, the graph of N_e vs height depends upon the path along which N_e is evaluated. In the case of Figure (6) the path is shown in Figure (2).

The discontinuity in the electron density gradient at the boundary between the ionosphere and the exosphere would be troublesome in the ray tracing program, if the step size between consecutive ray points (above and below the discontinuity) were as large as it is for the step size between other pairs of consecutive ray points. Fortunately, the step size in the vicinity of the discontinuity is several orders of magnitude smaller than the step size in the rest of the exosphere.

4.2 Faraday Rotation for Various Values of the Upper Boundary of the Chapman Layer

In general, in the model ionosphere (consisting of the Chapman model and the model exosphere) the gradient of the electron density at r_0 is discontinuous. The fact that the gradient in the model exosphere is steeper than the gradient of the Chapman model at r_0 causes the electron density to be diminished (relative to a Chapman model alone) above r_0. However, at several thousand kilometers above the surface of the Earth the electron density is enhanced. Although

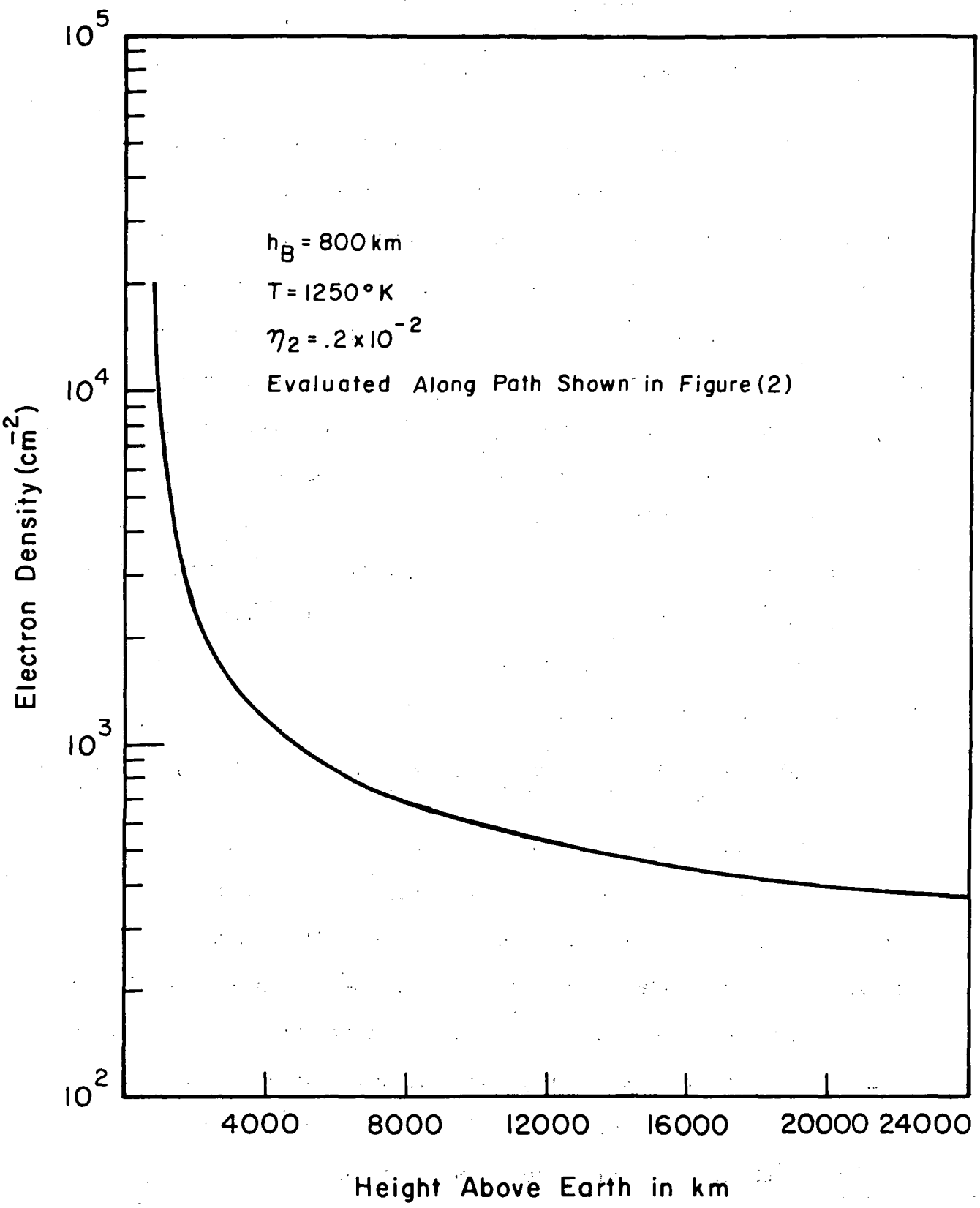

Figure 6. Exospheric electron density profile.

this situation may be somewhat artificial due to the discontinuity of the gradient, it can be thought of as a redistribution of the electron density.

By using the ray tracing program, the content of the ionosphere can be determined for several values of h_B (h_B = r_0 - the radius of the Earth), which is the height of the boundary between the Chapman model and the model exosphere, and is between 500 km and 1500 km in this study. At h_B = 1500 km, for example, the content is reduced to 78% of its value when h_B = 500 km. Presumably, that part of the content which is revealed by a Faraday rotation measurement will exhibit a less drastic change as h_B varies from 500 to 1500 km because the electron density profile is only changing in the region of the ionosphere above h_B, where the diminishing magnetic field can be expected to decrease the sensitivity of the Faraday rotation measurement. A comparison between the total electron content of the ionosphere, and the content revealed by the Faraday rotation technique is shown in Figure (7).

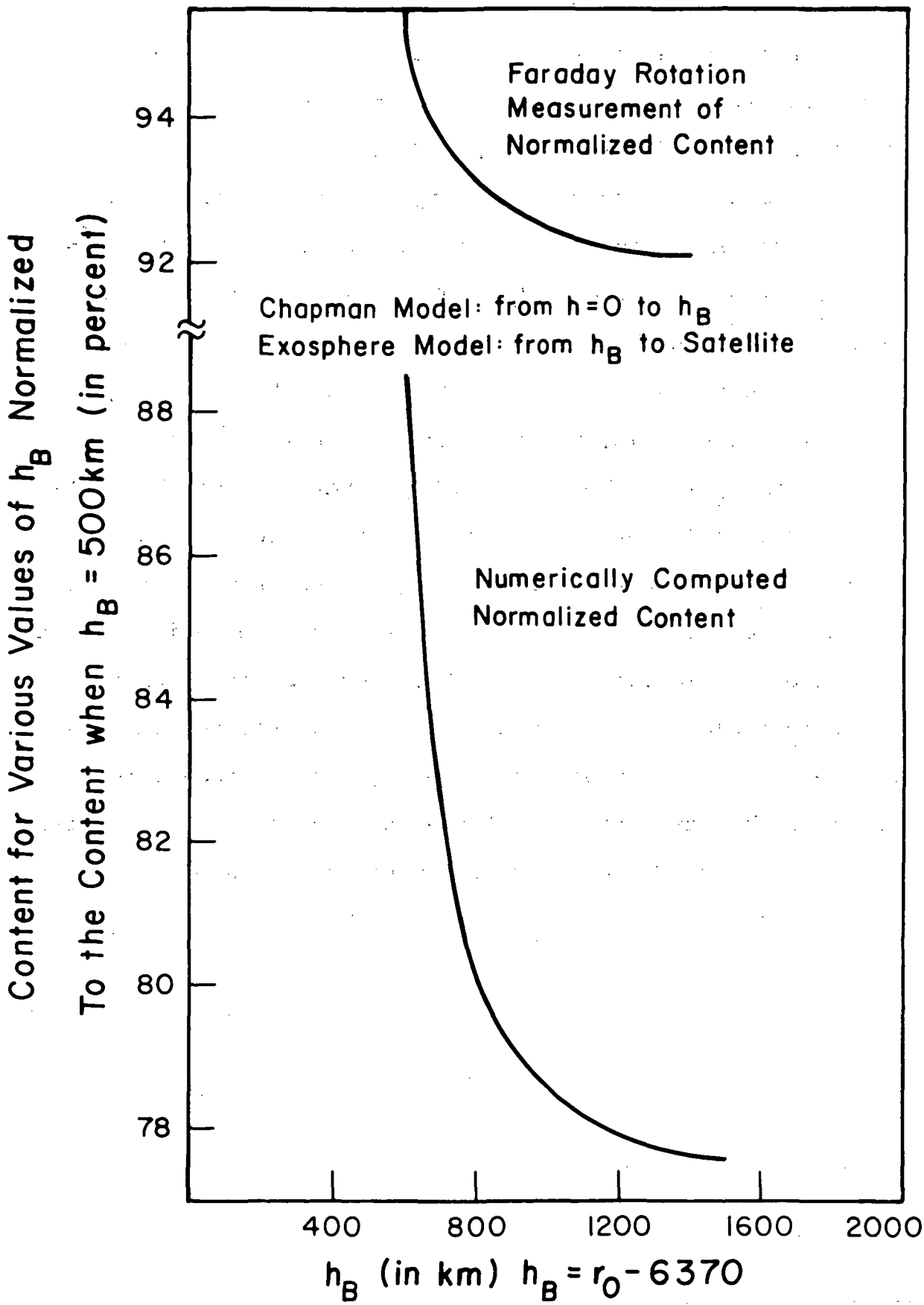

Figure 7. Comparison between numerically computed electron content and electron content deduced from simulated Faraday rotation.

5. APPROXIMATIONS IN THE ANALYSIS OF GROUP DELAY MEASUREMENTS

The group delay time, in this simulation, refers to the time required for a wave packet to travel from the satellite to the Earth. In practice, it may be difficult to determine the group delay absolutely, and, in fact, it is usually the differential group delay which is determined. At the satellite, two (or more) carrier frequencies are modulated by the same frequency. If the phase relationships between the modulation envelopes is known at the satellite, the change in the relative phases of the modulation envelopes can be determined at a station on the Earth, and therefore the differential group delay time can be determined.

The time required for a wave packet to reach the Earth from the satellite is:

$$T_i = \int_{Pi} \frac{ds}{v_{g_i}} \qquad (18)$$

where: v_{g_i} = the group velocity at the carrier frequency f_i

ds = the path element along the group ray (P_i)

T_i = group delay time at carrier frequency f_i

The group velocity for VHF propagation depends upon the electron density in the following way:

$$v_{g_i} = c\left[1 - \frac{80.5 \times 10^{-6} N_e}{f_i^2}\right]^{1/2} = c[1 - X_i]^{1/2} \qquad (19)$$

where f_i = the frequency of the carrier.

Therefore, equation (18) can be expanded in an infinite series.

$$T_i = \frac{1}{c}\int_{P_i} ds + \frac{1}{2c}\int_{P_i} X_i\, ds + \frac{3}{8c}\int_{P_i} X_i^2 ds + \frac{5}{16c}\int_{P_i} X_i^3\, ds + \ldots \quad (20)$$

since $X_i << 1$.

In the simulation, however, the group path, G_i, is computed rather than the group delay time T_i. The group path is the distance that would be traversed by a signal travelling at c for a time equal to the group delay time. Thus,

$$G_i = cT_i \quad (21)$$

Therefore,

$$G_i = \int_{P_i} ds + \frac{1}{2}\int_{P_i} X_i\, ds + \frac{3}{8}\int_{P_i} X_i^2\, ds + \frac{5}{16}\int_{P_i} X_i^3\, ds + \ldots \quad (22)$$

By measuring G_i at several different frequencies (f_i = 40, 140, and 360 MHz) it is possible to determine the differential group path between any pair of three frequencies (f_i & f_j).

$$G_i - G_j = \left[\int_{P_i} ds - \int_{P_j} ds\right] + \frac{1}{2}\left[\int_{P_i} X_i ds - \int_{P_j} X_j ds\right] + \frac{3}{8}\left[\int_{P_i} X_i^2 ds - \int_{P_j} X_j^2 ds\right] + \frac{5}{16}\left[\int_{P_i} X_i^3 ds - \int_{P_j} X_j^3 ds\right] + \ldots \quad (23)$$

Two major assumptions are necessary to determine $\int X ds$ from equation (23). They are:

(i). $P_i = P_j$, since the propagation path is nearly a straight line

(ii). since $X_i << 1$, any terms in equation (23) which involve the integral of X_i to the second or higher powers can be neglected.

By using the ray tracing program any term in equation (23) can be evaluated. Therefore, the validity of assumptions (i) and (ii) can be checked. If assumptions (i) and (ii) are valid then equation (23) can be solved for $\int N_e \, ds$, since $G_i - G_j$ then becomes:

$$G_i - G_j \cong \frac{1}{2} \int [X_i - X_j] \, ds \qquad (24)$$

$$\int N_e \, ds \cong \frac{[G_i - G_j] \, f_j^2 \, f_i^2}{40.25 \times 10^{-6} \left[f_j^2 - f_i^2\right]}$$

Usually, the validity of assumptions (i) and (ii) is not doubted. The necessity for testing these assumptions, however, arises from the nature of the problem itself. The exospheric electron content might only comprise between 10 and 20% or less of the total ionospheric electron content. If the error in allowing assumptions (i) and (ii) is enough to cause an uncertainty of 10 to 20% in the electron content, then the differential group delay method is not useful in determining the exospheric electron content.

As a shorthand way of refering to the terms in equation (23) the following notation is used:

$$ {}^{j}_{i}\Delta_0 = \int_{P_i} ds - \int_{P_j} ds $$

$$ {}^{j}_{i}\Delta_1 = \frac{1}{2}\left[\int_{P_i} X_i \, ds - \int_{P_j} X_j \, ds\right] $$

$$ {}^{j}_{i}\Delta_2 = \frac{3}{8}\left[\int_{P_i} X_i^2 \, ds - \int_{P_j} X_j^2 \, ds\right] $$

$$ {}^{j}_{i}\Delta_3 = \frac{5}{16}\left[\int_{P_i} X_i^3 \, ds - \int_{P_j} X_j^3 \, ds\right] $$

5.1 Validity of the Approximations for a Simulation of Group Delay Measurements in a Chapman Layer.

Using this short hand notation, assumptions (i) and (ii) can be written as ${}^{j}_{i}\Delta_0 << {}^{j}_{i}\Delta_1$ and ${}^{j}_{i}\Delta_2 << {}^{j}_{i}\Delta_1$. Oestensibly, it would seem that this condition could be satisfied more readily when i and j correspond to the pair of highest frequencies (140 and 360 MHz) and the electron density in the ionosphere is low. For a Chapman model, the maximum value of plasma frequency, fc and the height of the maximum electron density are fixed. The next three graphs (Figures (8), (9), and (10)) illustrate the dependence of ${}^{j}_{i}\Delta_k / {}^{j}_{i}\Delta_1$ upon fc for i = 40, 140, and 360 MHz and j = 140 and 360 MHz so that j>i.

It can also be seen, especially from Figure (10) that the second order term can easily approach 10% of the first order term for large values of the critical frequency, fc.

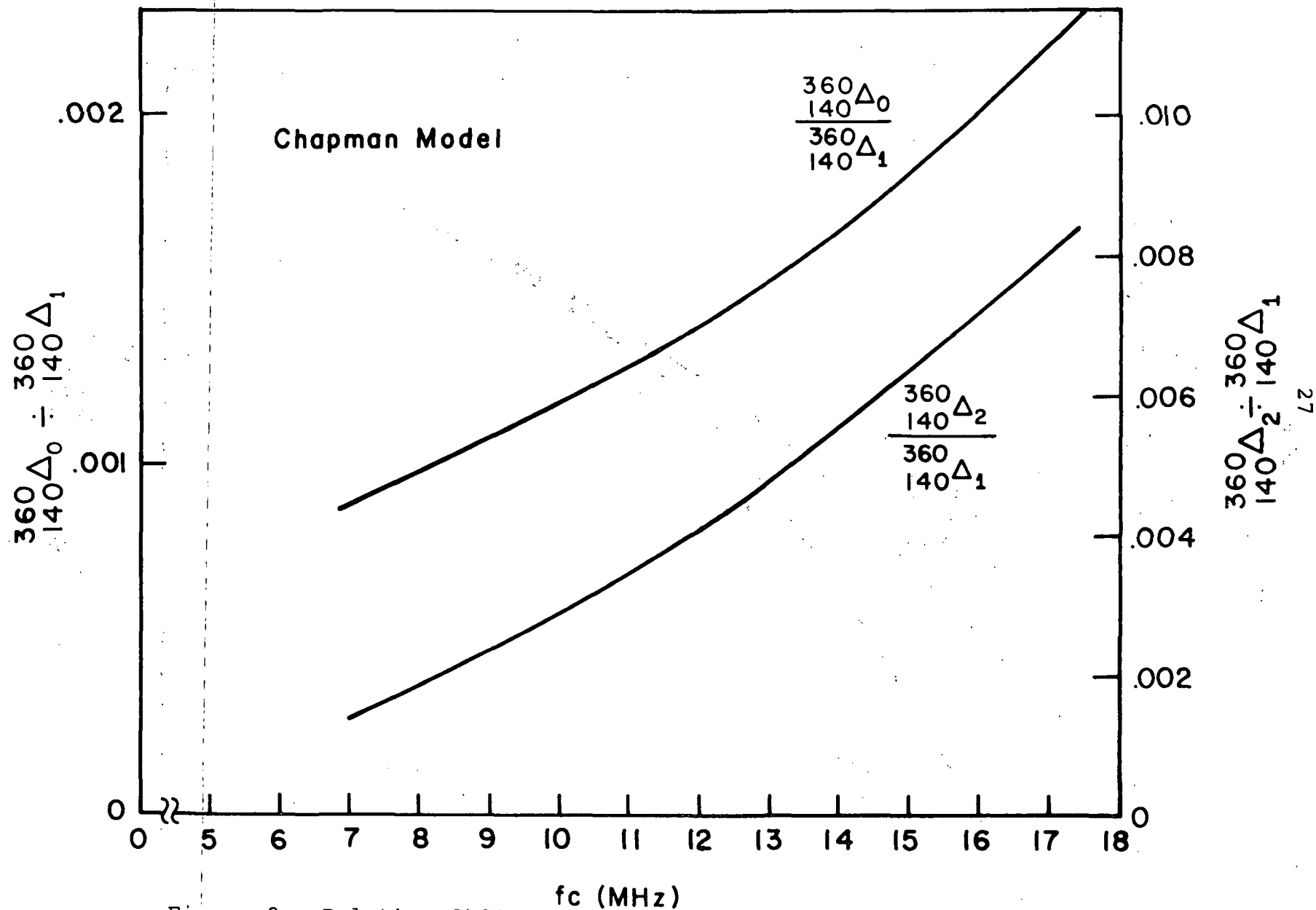

Figure 8. Relative differences in 0 and 2nd order expansion terms for group path (f_i = 360 MHz, f_j = 140 MHz).

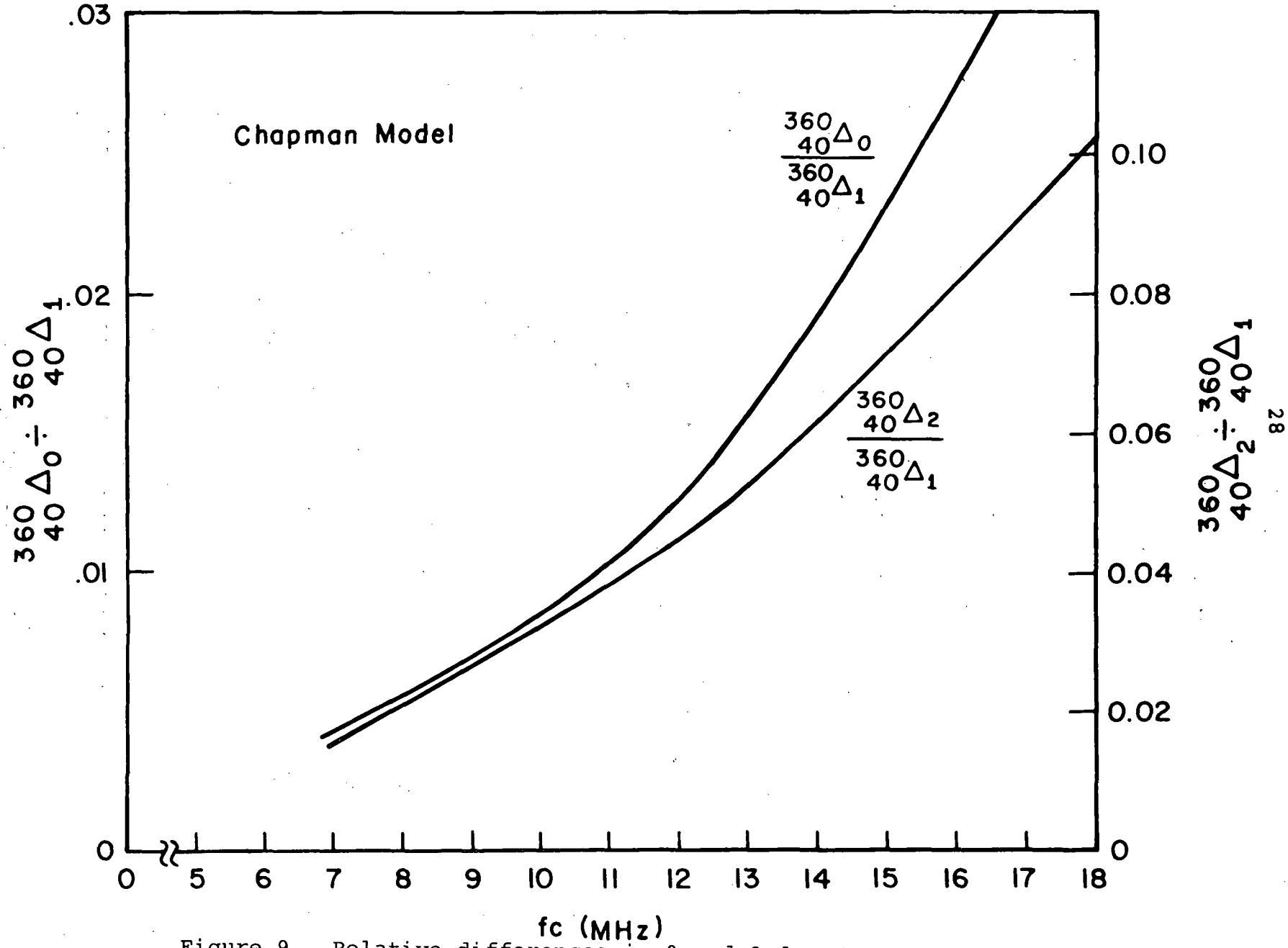

Figure 9. Relative differences in 0 and 2nd order expansion terms for group path (f_i = 360 MHz, f_j = 40 MHz).

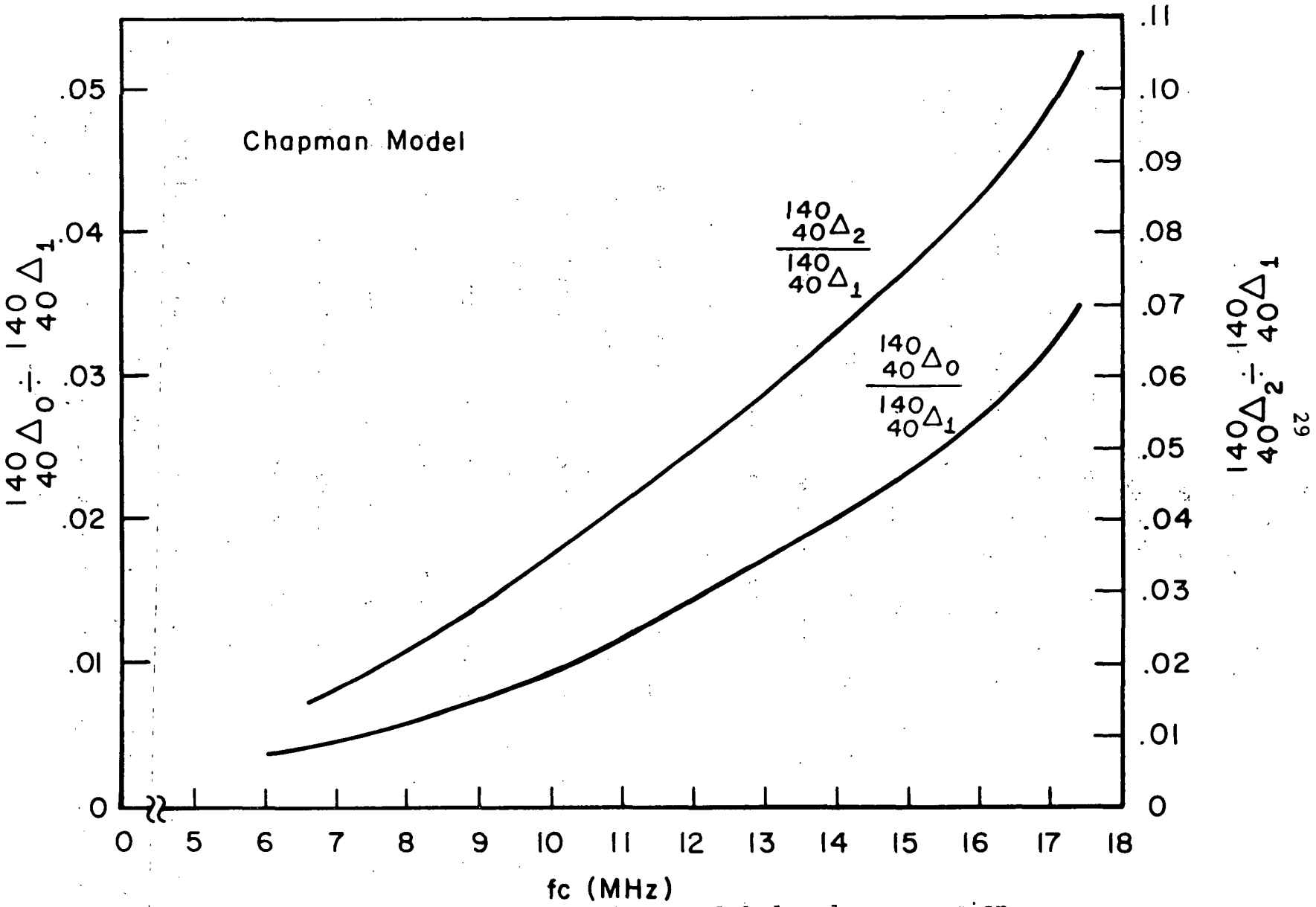

Figure 10. Relative differences in 0 and 2nd order expansion terms for group path (f_i = 140 MHz, f_j = 40 MHz).

5.2 The Effect of Adding the Model Exosphere

In view of the preceeding discussion, errors of this magnitude (about 10%) would appear to prevent the determination of exospheric electron content. However, in the case of a model ionosphere consisting of both a Chapman model and the model exosphere, it is still possible that changes in the electron density in the exosphere might be reflected only in the Δ_1 term. This assumes that since the electron density is small in the exosphere, the deviation of the ray from a straight line path is negligible, as is the integral of X^2, along the part of the path which is contained in the exosphere. Consequently, by adding the model exosphere to the Chapman layer, the Δ_0 and Δ_2 terms would not be expected to change very much from the values they would have if there were no model exosphere. Also, it might be expected that if the electron density in the actual exosphere changed, the errors in the group delay measurement which are due to the Δ_0 and Δ_2 terms would not change as much as the changes in Δ_1 as long as the electron density in the model exosphere was always much less than the electron density in the Chapman model.

Tables (1), (2), and (3) confirm these expectations. Each table uses a different value of f_c in the Chapman model. For each value of f_c, and for each pair of f_i and f_j, three different ionospheric models are used. The first model assumes that h_B = 500 km. The second model assumes that

h_B = 800 km which reduces the exospheric electron content considerably in comparison to the first model. The third model assumes that there is no exosphere--there is only the Chapman model. The third model is denoted by an asterisk in the "exosph. ht." column. For each of these combinations, the Δ_0 and Δ_2 terms are computed and it can be seen that if the only varying parameter is the height, h_B, Δ_0 and Δ_2 do not change very much. The parenthetical quantities appearing in each of the three columns (Δ_0, Δ_1, Δ_2) are the ratios

$$\left[{}^{j}_{i}\Delta_{k}\Big|_{\text{exosphere + Chapman model}}\right] \div \left[{}^{j}_{i}\Delta_{k}\Big|_{\text{Chapman model}}\right]$$

TABLE 1

The Δ_0 and Δ_2 differential group delay terms for 3 different model ionospheres (f_c = 14)

EXOSPH. HT.	f_c	f_i	f_j	Δ_0		Δ_2		Δ_1	
500	14	40	140	0.38982	(.987)	1.3348	(1.023)	25.1506	(1.275)
800	14	40	140	0.39355	(.996)	1.3037	(1.000)	20.2598	(1.027)
*	14	40	140	0.39504	(1)	1.3043	(1)	19.7280	(1)
500	14	40	360	0.39217	(.987)	1.3432	(1.023)	26.9976	(1.276)
800	14	40	360	0.39590	(.996)	1.3119	(1.000)	21.7373	(1.027)
*	14	40	360	0.39740	(1)	1.3125	(1)	21.1650	(1)
500	14	140	360	0.23460×10^{-2}	(.996)	0.84156×10^{-2}	(1.026)	1.8471	(1.285)
800	14	140	360	0.23423×10^{-2}	(.994)	0.82031×10^{-2}	(1.000)	1.4776	(1.028)
*	14	140	360	0.23565×10^{-2}	(1)	0.82046×10^{-2}	(1)	1.4374	(1)

TABLE 2

The Δ_0 and Δ_2 differential group delay terms for 3 different model ionospheres ($f_c = 10$)

EXOSPH. HT.	f_c	f_i	f_j	Δ_0		Δ_2		Δ_1	
500	10	40	140	.090042	(.992)	.34007	(1.026)	12.6428	(1.282)
800	10	40	140	.090903	(1.002)	.33168	(1.000)	10.1427	(1.028)
*	10	40	140	.090752	(1)	.33156	(1)	9.8616	(1)
500	10	40	360	.090975	(.992)	.34226	(1.026)	13.5840	(1.282)
800	10	40	360	.091803	(1.001)	.33381	(1.000)	10.8956	(1.028)
*	10	40	360	.091671	(1)	.33369	(1)	10.5940	(1)
500	10	140	360	$.9328\times10^{-3}$	(1.015)	$.21872\times10^{-2}$	(1.026)	.94128	(1.285)
800	10	140	360	$.9081\times10^{-3}$	(.988)	$.21320\times10^{-2}$	(1.000)	.75302	(1.028)
*	10	140	360	$.9189\times10^{-3}$	(1)	$.21322\times10^{-2}$	(1)	.73229	(1)

TABLE 3

The differential group delay terms for 3 different model ionospheres (f_c = 7)

EXOPH. HT.	f_c	f_i	f_j	Δ_0		Δ_2		Δ_1	
500	7	40	140	.020383	(.985)	.080766	(1.025)	6.1479	(1.283)
800	7	40	140	.020482	(.990)	.078752	(1.000)	4.9244	(1.028)
*	7	40	140	.020685	(1)	.078760	(1)	4.7906	(1)
500	7	40	360	.020697	(.986)	.081290	(1.026)	6.6089	(1.284)
800	7	40	360	.020784	(.990)	.079262	(1.000)	5.2930	(1.028)
*	7	40	360	.020992	(1)	.079264	(1)	5.1491	(1)
500	7	140	360	$.03141\times10^{-2}$	(1.024)	$.052741\times10^{-2}$	(1.047)	.46095	(1.286)
800	7	140	360	$.03021\times10^{-2}$	(.985)	$.051146\times10^{-2}$	(1.015)	.36866	(1.028)
*	7	140	360	$.03068\times10^{-2}$	(1)	$.050383\times10^{-2}$	(1)	.35854	(1)

Based on the results of tables (1), (2), and (3) it would seem that the Δ_0 and Δ_2 terms for the ionosphere should have almost the same dependence upon f_c as the Δ_0 and Δ_2 terms for the Chapman model alone. Figures (11) and (12) show the dependence of Δ_0 and Δ_2 upon f_c for the Chapman model. A set of curves similar to those shown in Figures (11) and (12) could be used to estimate the size of the Δ_0 and Δ_2 terms resulting from an actual group delay measurement.

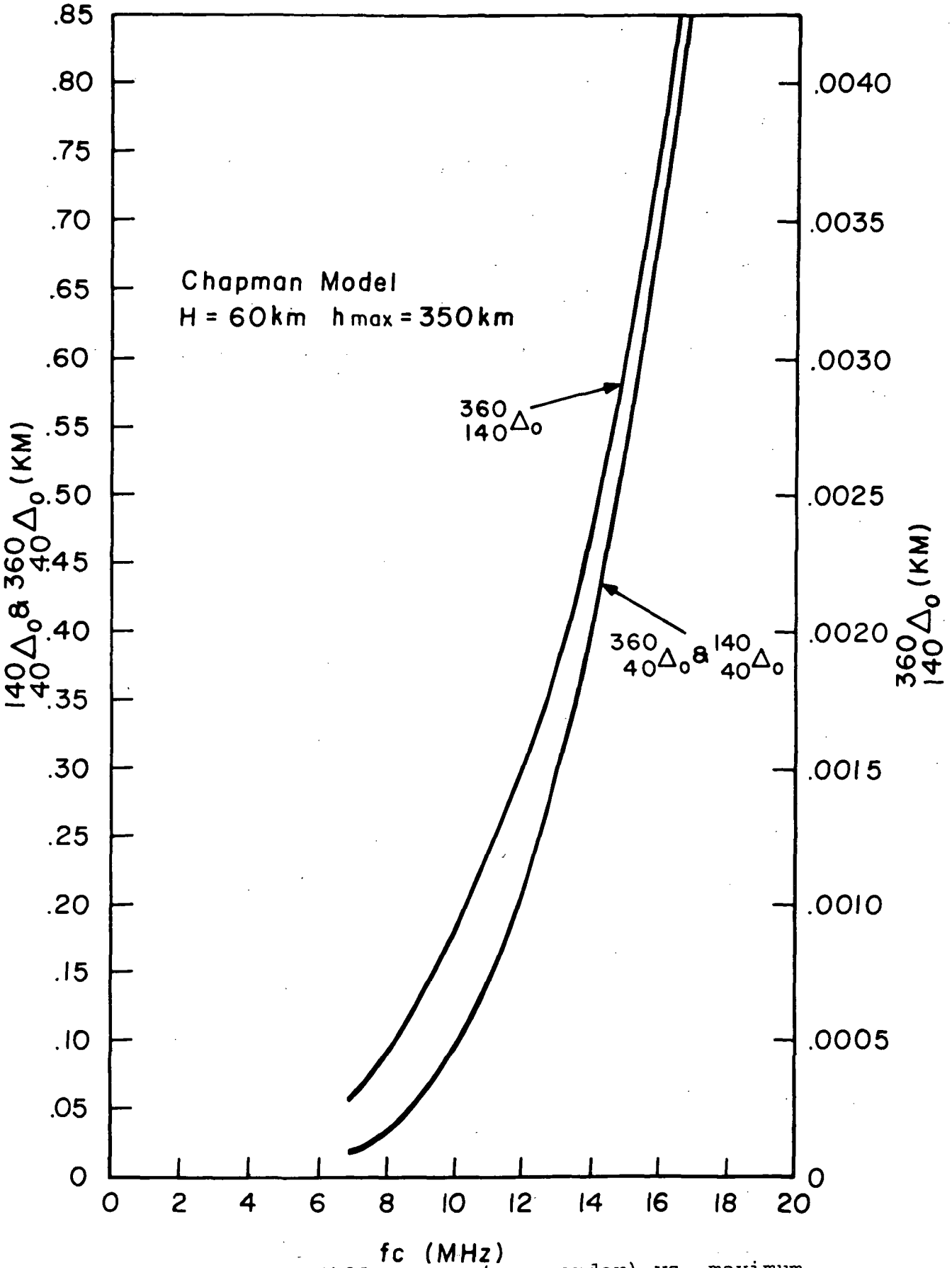

Figure 11. Absolute differences (zero order) vs. maximum plasma frequency without exosphere.

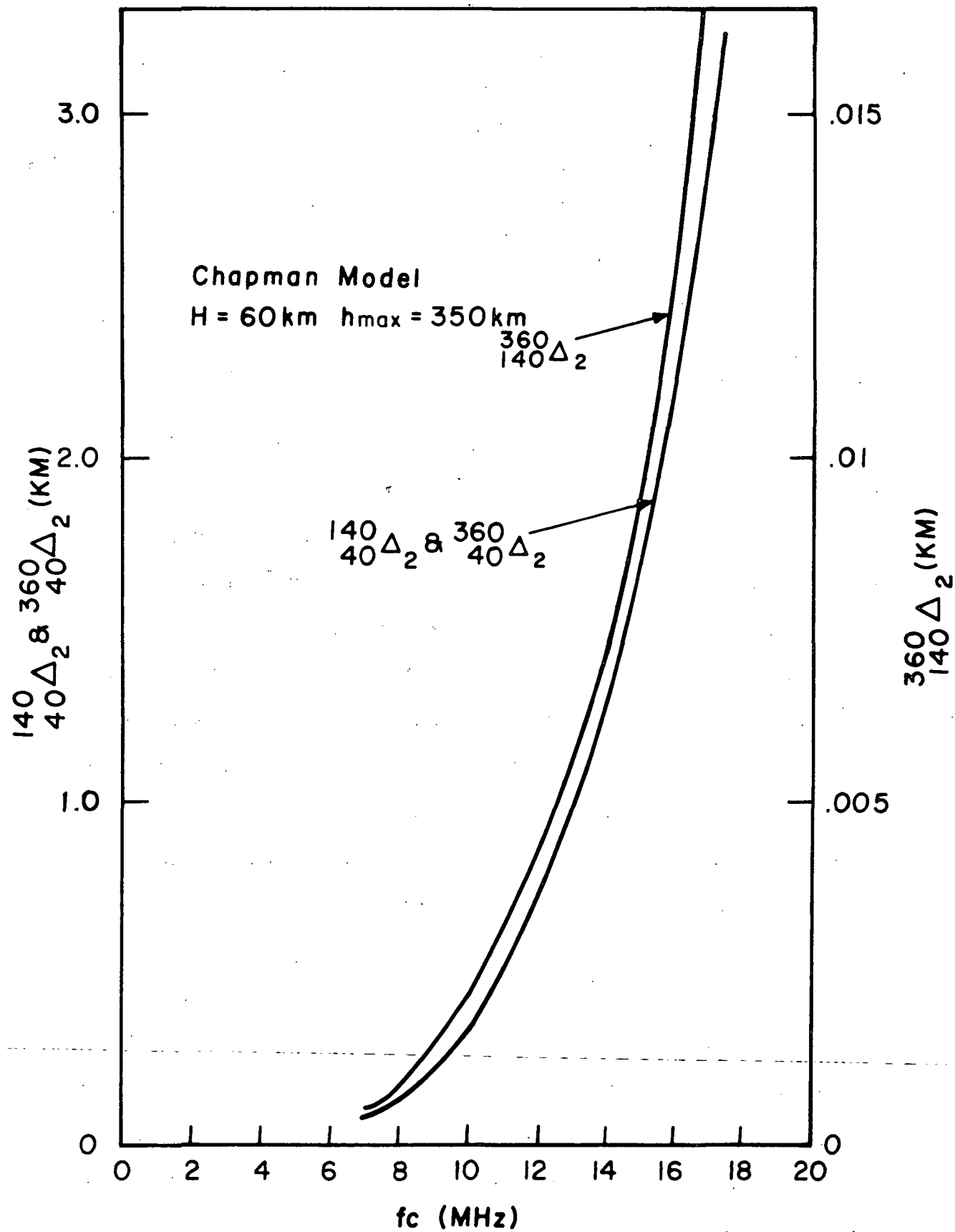

Figure 12. Absolute differences (second order) vs. maximum plasma frequency without exosphere.

6. SUMMARY AND DISCUSSION

From the results obtained, it can be confirmed that the Faraday rotation technique used by itself is not likely to provide a good indication of the total ionospheric electron content. Figure (7) in particular shows that the changes in the ionospheric electron content due to changes in the electron density profile in the exosphere do not cause proportional changes in the electron content indicated by Faraday rotation.

In addition, an amount of uncertainty appears in the Faraday rotation measurement of electron content because of the uncertainty in $\overline{M}$. This is illustrated in Figure (13) which shows the range of possible values of $\overline{M}$, and the corresponding range of values for electron content due to uncertainty in the subionospheric height. In the case of an unusually low exospheric content it is even possible for the electron content deduced from the Faraday rotation measurement to exceed the electron content deduced from group delay measurements, causing the exosphere to appear to have a negative electron content, if $\overline{M}$ is not carefully chosen.

The group delay measurement, also, might not be a good indication of the total ionospheric electron content when it is used by itself because of the errors (Δ_0 and Δ_1 terms) which are introduced in using equation (23). However, from Tables (1), (2), and (3) it can be concluded that the

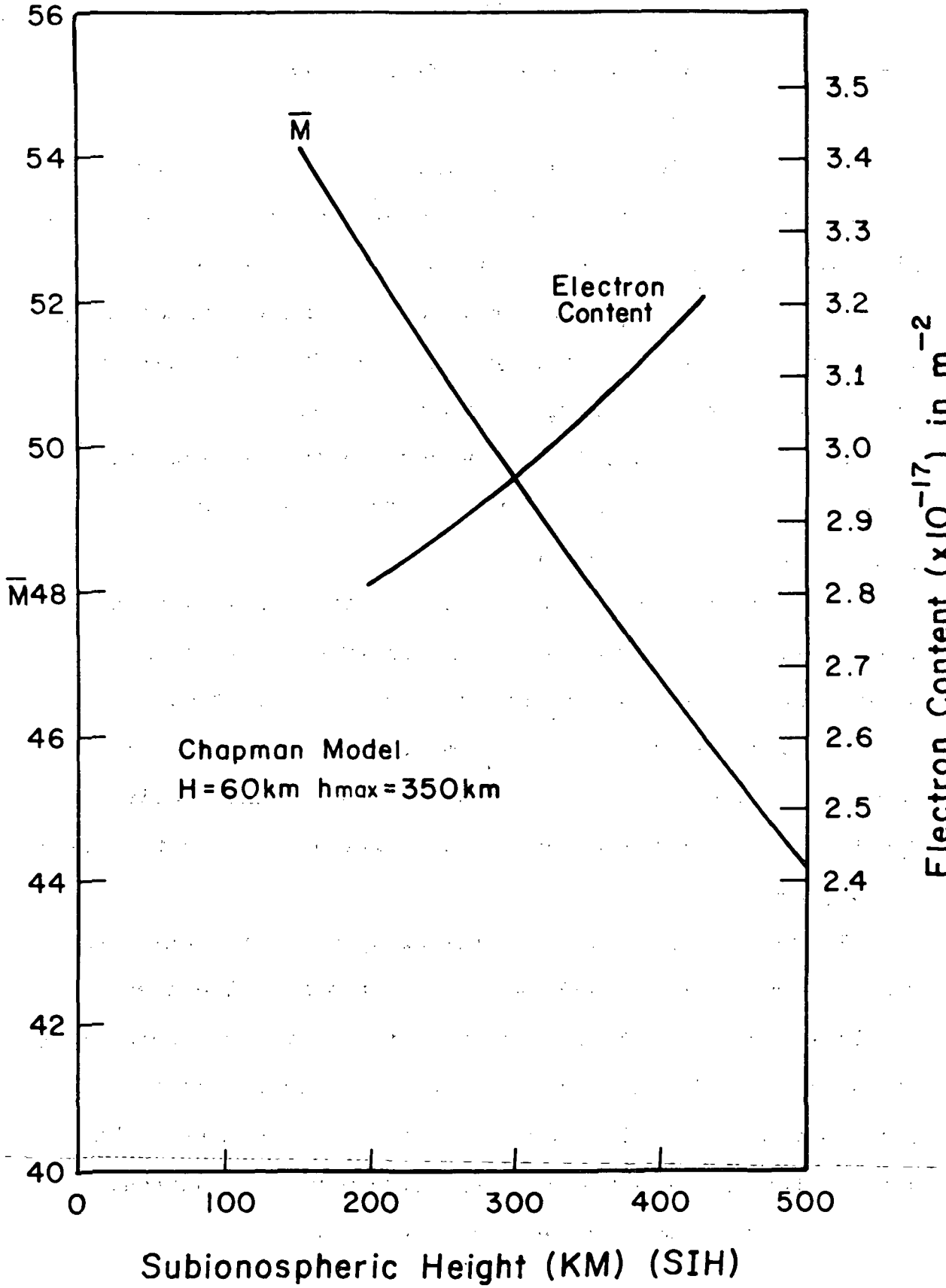

Figure 13. Uncertainty in electron content due to uncertainty in subionospheric height.

group delay measurement corresponding to the exospheric portion is accurate.

Because of the errors and limitations of these two methods it would be difficult to determine the exospheric electron content by comparing them. The errors in the group delay measurement can approach 10% and the uncertainty in the electron content deduced from the Faraday rotation method only serves to make the matter worse.

Despite these problems, however, changes in the exospheric electron content seem to be detectable from a comparison of these two techniques.

Also, small motions of the satellite in relation to the receiver on the ground will probably not affect the measurement. A change in the value of the height of the satellite was simulated (from 35800 to 36000 km) with no adverse effects on the Δ_0 and Δ_2 terms. This result was anticipated since N_e near the position of the satellite is very small.

In general, the differential group delay measurements made by comparing 360 and 140 MHz signals have the least (smallest) error. It would seem that reliable determinations of exospheric electron content could be made at these frequencies. The following table serves to summarize the size of the errors (in per cent) which would be inherent in a group delay measurement of this sort.

TABLE 4

A summary illustrating the relative size (in percent) of $^{360}_{140}\Delta_0$ and $^{360}_{140}\Delta_2$ for all the model ionospheres which were considered

h_B (KM)	f_c (MHz)	$\frac{^{360}_{140}\Delta_0}{^{360}_{140}\Delta_1}$ (%)	$\frac{^{360}_{140}\Delta_2}{^{360}_{140}\Delta_1}$ (%)
500	14	.127	.456
800	14	.158	.555
*	14	.160	.555
500	10	.099	.232
800	10	.122	.283
*	10	.125	.291
500	7	.068	.113
800	7	.082	.138
*	7	.086	.140

APPENDIX

The first subroutine is used for homing and the second subroutine is used to determine the electron density distribution for the combined model (the Chapman layer and the exosphere model) of the ionosphere.

```
      SUBROUTINE EVERY(LLL,IOK,JAM,KZ)
      IMPLICIT REAL*8(A-H,O-Z,$),INTEGER(I-N)
      COMMON W(331),PI,HFPI,TENLOG,DUM,ARE(75),TITLE(75),UNITS(75),
     1WHY(32,2),SPACE,E1MAX,E1MIN,E2MAX,E2MIN,FACT,END,CLOSE,C,PADIT1,
     2PYPR(3,3),ZERO,POPP,SL,RO,R(20),GG(7,7),HH(7,7),
     3ID(16),NN,MODE,KKA,NWHY(7),JG(2),KKK,NW(331)
C     THIS VERSION OF EVERY GOES WITH BUG-A AND IS A HOMING SUBROUTINE
C     FOR 3 DIFFERENT FREQUENCIES
      ERROR=DABS(W(100)-W(323))
      IF (ERROR.LT.(.0005)) GO TO 1
      HERE=DATAN(W(100)/W(20))
      THERE=DATAN(W(323)/W(20))
      DIFF=3.*(HERE-THERE)/4.
      W(324)=W(17)-DIFF
      W(73)=0
      RETURN
    1 PRINT 2,W(3),ERROR
      IF (W(258).EQ.360.) KZ=10
      W(73)=0
      IF (W(258).GT.130.) GO TO 3
    2 FORMAT (' ','ERROR AT',F5.1,1X,'MHZ IS',F8.5,'KM')
      W(258)=140.0
      W(259)=140.0
      RETURN
    3 W(258)=360.0
      W(259)=360.0
      RETURN
      END
```

```
      SUBROUTINE ELECTD(X,PXPR,PXPT,NTRY)
      IMPLICIT REAL*8(A-H,O-Z,$),INTEGER(I-N)
C
C     CHAPMAN LAYER WITH TILTS AND TRAVELING DISTURBANCE
C
      DIMENSION PXPR(3)
      COMMON W(331),PI,HFPI,TENLOG,DUM,ARE(75),TITLE(75),UNITS(75),
     1WHY(32,2),SPACE,E1MAX,E1MIN,E2MAX,E2MIN,FACT,END,CLOSE,C,PADIT1,
     2PYPR(3,3),ZERO,POPP,SL,RO,R(20),GG(7,7),HH(7,7),
     3ID(16),NN,MODE,KKA,NWHY(7),J(2),KKK,NW(331),MLINE
      EQUIVALENCE (EARTHR,W(19)), (F,W(3)), (READFN,W(200)),
     1(FCO,W(201)),(HM,W(202)),(SCALEH,W(203)),(DELTAM,W(204)),
     2(HT,W(205)),(HN,W(206)),(DAR,W(207)),(DAT,W(208)),(DAP,W(209)),
     3(THETAO,W(213)),(PHIO,W(214)),(ETHO,W(215)),(EPHO,W(216)),
     4(ETCO,W(217)),(EPCO,W(218)),(EKTHO,W(219)),(EKPHO,W(220)),
     5(EKTCO,W(221)),(EKPCO,W(222)),(PERIOD,W(211)),(T,W(21)),
     5(CENTRC,W(264)),(HMAX,W(284)),(TRAVEL,W(225)),(N,NW(299))
C
C
C     W(201)=CRITICAL FREQUENCY AT REFERENCE POINT
C     W(202)=LAYER PEAK HEIGHT AT REFERENCE POINT
C     W(203)=SCALE HEIGHT OF THE LAYER
C     W(204)=PEAK PERTURBATION
C     W(205)=HEIGHT OF PEAK PERTURBATION
C     W(206)=THICKNESS PARAMETER OF THE PERTURBATION
C     W(207)=WAVELENGTH IN THE R DIRECTION
C     W(208)=WAVELENGTH IN THE THETA DIRECTION
C     W(209)=WAVELENGTH IN THE PHI DIRECTION
C     W(211)=PERIOD OF THE TRAVELING DISTURBANCE
C     W(212)=TIME INCREMENT FOR TRACING RAYS
C     W(213)=VALUE OF THETA AT REFERENCE POINT
C     W(214)=VALUE OF PHI AT REFERENCE POINT
C     W(215)=GRADIENT OF PEAK HEIGHT IN THE THETA DIRECTION
C     W(216)=GRADIENT OF PEAK HEIGHT IN THE PHI DIRECTION
C     W(217)=GRADIENT OF FC IN THE THETA DIRECTION
C     W(218)=GRADIENT OF FC IN THE PHI DIRECTION
C     W(225) EQUAL TO NONZERO DISREGARDS THE TRAVELING DISTURBANCE
      CALL ERRSET(208,500,-1,1)
      GO TO ( 11, 11, 13, 14, 15 ), NTRY
   11 ONLY=0
      MONLY=0
   13 IF (R(1).GT.9999.9) GO TO 16
      IF (R(1).GT.RB) GO TO 16
      H=R(1)-EARTHR
      E2MAX=30.0
      R2=R(2)-THETAO
      R3=R(3)-PHIO
      ETC=ETCO+EKTCO*T
      EPC=EPCO+EKPCO*T
      ETH=ETHO+EKTHO*T
      EPH=EPHO+EKPHO*T
      TERMCO=R2*ETC+R3*EPC
      TERMO=R2*ETH+R3*EPH
```

```
      HMAX=HM+TERM0
      FC=FCC+TERM00
      TPI=2.*PI
      F2=F*F
      PXPR(1)=0
      PXPR(2)=0
      PXPR(3)=0
      PXPT=0
      FC2=FC*FC
      RN=HT+EARTHR
      Z=(H-HMAX)/SCALEH
      TERM6=DEXP (.5*(1.-Z-DEXP (-Z)))
      TERM7=.5*(-1.+DEXP (-Z))
  999 IF (TRAVEL) 25,26,25
   25 DELTA=0
      GO TO 30
   26 TERM1=(R(1)-RN)/HN
      TERM2=DEXP (-TERM1*TERM1)
      TERM3=TPI*(T/PERIOD+RN*R2/DAT+(R(1)-RN)/DAR+RN*DSIN(R(2))*R3/DAP)
      TERM4=DCOS (TERM3)
      TERM5=DSIN (TERM3)
      DELTA=DELTAM*TERM2*TERM4
      TERM8=TPI*(RN/DAT+RN*DCOS (R(2))*R3/DAP)
      TERM9=TPI*RN*DSIN (R(2))/DAP
   30 FN2=FC2*TERM6*(1.+DELTA)
      X=FN2/F2
      IF (W(77).EQ.(0.5)) GO TO 964
      PRINT 963,XB,ZB,RB,X,H,G,HY,HO
  963 FORMAT (' ',8(E10.2,3X))
      W(77)=0.5
  964 CONTINUE
      IF(X-1.E-30) 51,50,50
   51 X=0.0
   50 IF(ONLY-1) 21,1000,21
   21 ONLY=1
      IF(X) 22,1000,22
   22 TERM12=TERM7*X
      TERM10=DELTAM*TERM2*X/(1.+DELTA)
      PXPR(1)=TERM12/SCALEH
      IF(TRAVEL) 1000,35,1000
   35 PXPR(1)=PXPR(1)-2.*TERM10*(TERM1*TERM4/HN+PI*TERM5/DAR)
      TERM11=2.*X/FC
      TERM13=TERM5*TERM10
      PXPR(2)=-TERM8*TERM13-TERM12*ETH/SCALEH+TERM11*ETC
      PXPR(3)=-TERM9*TERM13-TERM12*EPH/SCALEH+TERM11*EPC
      PXPT=-TERM13*TPI/PERIOD+TERM11*(EKTCO*R2+EKPCO*R3)-TERM12*(EKTHO*R
     12+EKPHO*R3)/SCALEH
 1000 W(74)=X
      RETURN
   14 READFN=0
      RETURN
   15 RETURN
   16 F2=F*F
```

```
      S1=DSIN(1.57-R(2))
C   W(77)= HEIGHT TC EXOSPHERE
C    W(78)=EXOSPHERIC TEMPERATURE (KELVIN)
      IF (W(77).LT.1.0) GO TO 53
      RB=W(77)+6370.0
      ZB=(W(77)-W(202))/W(203)
      G=9.8E-03*((6370./(RB      ))**2)
      XB=((W(201)/W(3))**2)*DEXP(.5*(1.-ZB-DEXP(-ZB)))
      XBA=XB
      HY=0.848*((   RB/6370.)**2)*W(78)/1.008
      W(77)=0.0
      HO=1.008*HY/16.
   53 CONTINUE
      XB=XBA*1600./(F**2)
      C1=DCOS(1.57-R(2))
      S2=DSIN(1.362DO)
      C2=DCOS(1.362DO)
      S3=DSIN(R(3)-5.09)
      C3=DCOS(R(3)-5.09)
      S12=S1*S2
      C123=C1*C2*C3
      C23=C2*C3
      C12=C1*C2
      BETA=1.-S12*S12-C123*C123-2.*S1*C1*S2*C2*C3
      PXPR(1)=0.0
      PXPR(2)=0.0
      PXPR(3)=0.0
      Z=RB*(((R(1)-RB)/R(1))+(2.675E-09/G)*BETA*((RB**3-(R(1)**3))
     1/RB/R(1)))
      H=R(1)-EARTHR
      IF (H.LT.35800.0) GO TO 612
      X=0.0
      GO TO 1000
  612 CONTINUE
      Q1=1./DEXP(Z/HO)
      Q2=1./DEXP(Z/HY)
      X=XB*DSQRT((Q1+(5.1E-04)*Q2)/(1.00051))
      IF (MONLY-1) 20,1000,20
   20 MONLY=1
      PXPZ=-(XB**2)*(Q1/HO+5.1E-04*Q2/HY)/(2.00102*X)
      PZPR1=RB*((RB/(R(1)**2))-(2.675E-09/G)*BETA*(2.*R(1)/RB
     1+(RB/R(1))**2))
      ALFA=(RB*2.675E-09/G)*(RB**3-(R(1)**3))/(RB*R(1))
      PZPR2=-ALFA*(-2.*S1*S2*S2*C1+2.*C1*S1*C23*C23-2.*C1*C1*S2*C2*C3
     1+2.*S1*S1*S2*C2*C3)
      PZPR3=ALFA*(+2.*C12*C12*C3*S3+2.*S1*C1*S2*C2*S3)
      PXPR(1)=PXPZ*PZPR1
      PXPR(2)=PXPZ*PZPR2
      PXPR(3)=PXPZ*PZPR3
      GO TO 1000
      END
```

LIST OF REFERENCES

Angerami, J. J. and Thomas, J. O., "Studies of Planetary Atmospheres 1. The Distribution of Electrons and Ions in the Earth's Exosphere", Journal of Geophysical Research, Vol. 69, No. 21, Nov. 1, 1964.

Burns, Alan A. and Fremouw, Edward J., "A Real-Time Correction Technique for Transionospheric Ranging Error", IEEE Transactions on Antennas and Propagation, Vol. AP-18, No. 6, November, 1970.

Davies, Kenneth, Ionospheric Radio Propagation, National Bureau of Standards, Monograph 80.

Eshleman, V. R., Gallagher, P. B., Barthle, R. C., "Radar Methods of Measuring the Cislunar Electron Density", Journal of Geophysical Research, Vol. 65, No. 10, October, 1960.

Garriott, Owen K., Da Rosa, Aldo V., Ross, William J. "Electron Content Obtained from Faraday rotation and Phase Path Variations", Journal of Atmospheric and Terrestrial Physics, Vol. 32, 1970.

Jones, R. M., "A Three-Dimensional Ray Tracing Computer Program", Technical Report, Institutes for Environmental Research IER 17-ITSA 17, U.S. Department of Commerce, Environmental Science Services Administration, December, 1966.

Lawrence, R. S., Little, C. G., and Chivers, H. J. A., "A Survey of Ionospheric Effects Upon Earth-Space Radio Propagation", Proceedings of the IEEE, Vol. 52, No. 1, January, 1964.

Park, C. G., "Whistler Observations of the Interchange of Ionization between the Ionosphere and the Protonosphere", Journal of Geophysical Research, Vol. 75, No. 22, August 1, 1970.

Yoh, Philip, "Lunar Radar Measurements of the Diurnal Exchange of Ionization Between the Ionosphere and the Magnetosphere", Scientific Report No. 14 SU-SEL-65-103 Radioscience Laboratory, Stanford Electronics Laboratories, Stanford University, Stanford, California, 1965.

Unclassified
Security Classification

DOCUMENT CONTROL DATA - R&D

(Security classification of title, body of abstract and indexing annotation must be entered when the overall report is classified)

1. ORIGINATING ACTIVITY *(Corporate author)*
University of Illinois
Department of Electrical Engineering
Urbana, Illinois 61801

2a. REPORT SECURITY CLASSIFICATION
Unclassified

2b. GROUP

3. REPORT TITLE
A VERY HIGH FREQUENCY RADIO INTERFEROMETER FOR INVESTIGATING IONOSPHERIC DISTURBANCES USING GEOSTATIONARY SATELLITES

4. DESCRIPTIVE NOTES *(Type of report and inclusive dates)*
Technical Report

5. AUTHOR(S) *(Last name, first name, initial)*
Terry, Robert E.
Flaherty, Bernard J.

6. REPORT DATE	7a. TOTAL NO. OF PAGES	7b. NO. OF REFS
March 1972	63	9

8a. CONTRACT OR GRANT NO.	9a. ORIGINATOR'S REPORT NUMBER(S)
NGR-14-005-002	T. R. 45-1
b. PROJECT AND TASK NO.	
c.	9b. OTHER REPORT NO(S) *(Any other numbers that may be assigned this report)*
d.	UILU-72-2539

10. AVAILABILITY/LIMITATION NOTICES
Available on request until supply is exhausted

11. SUPPLEMENTARY NOTES	12. SPONSORING MILITARY ACTIVITY
	National Aeronautics and Space Administration Washington, D. C. 20546

13. ABSTRACT (Condensed)

The theory, construction, and operation of a VHF correlation type radio interferometer is discussed. The instrument's main use in ionosphere research is to study scintillation, in amplitude and phase, of radio signals received from a synchronous satellite.

The interferometer consists of two superheterodyne receivers with phase coherent local oscillators. The various oscillators are generated by using phase locked loops and a frequency synthesizer.

The interferometer uses the principle of frequency offset to increase the sensitivity of the instrument. This is accomplished by offsetting one of the local oscillators by a small amount. The correlated i.f. outputs of the two receivers contain a signal component whose frequency is equal to the amount of the off-set. Dual channel correlation is accomplished by using quadrature phase detection of the correlated signal. The integrated outputs of the phase detectors represent the sine and cosine components of the correlated signals. The effects of amplitude and phase scintillation can then be separated using coordinate conversion techniques.

DD FORM 1 JAN 64 1473

Unclassified
Security Classification

14. KEY WORDS	LINK A		LINK B		LINK C	
	ROLE	WT	ROLE	WT	ROLE	WT
correlating interferometer						
ionosphere						
scintillation						
geostationary satellite						
frequency offset						
phase locked loop						

INSTRUCTIONS

1. ORIGINATING ACTIVITY: Enter the name and address of the contractor, subcontractor, grantee, Department of Defense activity or other organization *(corporate author)* issuing the report.

2a. REPORT SECURITY CLASSIFICATION: Enter the overall security classification of the report. Indicate whether "Restricted Data" is included. Marking is to be in accordance with appropriate security regulations.

2b. GROUP: Automatic downgrading is specified in DoD Directive 5200.10 and Armed Forces Industrial Manual. Enter the group number. Also, when applicable, show that optional markings have been used for Group 3 and Group 4 as authorized.

3. REPORT TITLE: Enter the complete report title in all capital letters. Titles in all cases should be unclassified. If a meaningful title cannot be selected without classification, show title classification in all capitals in parenthesis immediately following the title.

4. DESCRIPTIVE NOTES: If appropriate, enter the type of report, e.g., interim, progress, summary, annual, or final. Give the inclusive dates when a specific reporting period is covered.

5. AUTHOR(S): Enter the name(s) of author(s) as shown on or in the report. Enter last name, first name, middle initial. If military, show rank and branch of service. The name of the principal author is an absolute minimum requirement.

6. REPORT DATE: Enter the date of the report as day, month, year, or month, year. If more than one date appears on the report, use date of publication.

7a. TOTAL NUMBER OF PAGES: The total page count should follow normal pagination procedures, i.e., enter the number of pages containing information.

7b. NUMBER OF REFERENCES: Enter the total number of references cited in the report.

8a. CONTRACT OR GRANT NUMBER: If appropriate, enter the applicable number of the contract or grant under which the report was written.

8b, 8c, & 8d. PROJECT NUMBER: Enter the appropriate military department identification, such as project number, subproject number, system numbers, task number, etc.

9a. ORIGINATOR'S REPORT NUMBER(S): Enter the official report number by which the document will be identified and controlled by the originating activity. This number must be unique to this report.

9b. OTHER REPORT NUMBER(S): If the report has been assigned any other report numbers *(either by the originator or by the sponsor)*, also enter this number(s).

10. AVAILABILITY/LIMITATION NOTICES: Enter any limitations on further dissemination of the report, other than those imposed by security classification, using standard statements such as:

(1) "Qualified requesters may obtain copies of this report from DDC."

(2) "Foreign announcement and dissemination of this report by DDC is not authorized."

(3) "U. S. Government agencies may obtain copies of this report directly from DDC. Other qualified DDC users shall request through _____."

(4) "U. S. military agencies may obtain copies of this report directly from DDC. Other qualified users shall request through _____."

(5) "All distribution of this report is controlled. Qualified DDC users shall request through _____."

If the report has been furnished to the Office of Technical Services, Department of Commerce, for sale to the public, indicate this fact and enter the price, if known.

11. SUPPLEMENTARY NOTES: Use for additional explanatory notes.

12. SPONSORING MILITARY ACTIVITY: Enter the name of the departmental project office or laboratory sponsoring *(paying for)* the research and development. Include address.

13. ABSTRACT: Enter an abstract giving a brief and factual summary of the document indicative of the report, even though it may also appear elsewhere in the body of the technical report. If additional space is required, a continuation sheet shall be attached.

It is highly desirable that the abstract of classified reports be unclassified. Each paragraph of the abstract shall end with an indication of the military security classification of the information in the paragraph, represented as *(TS), (S), (C), or (U).*

There is no limitation on the length of the abstract. However, the suggested length is from 150 to 225 words.

14. KEY WORDS: Key words are technically meaningful terms or short phrases that characterize a report and may be used as index entries for cataloging the report. Key words must be selected so that no security classification is required. Identifiers, such as equipment model designation, trade name, military project code name, geographic location, may be used as key words but will be followed by an indication of technical context. The assignment of links, rules, and weights is optional.

Unclassified

Security Classification

DOCUMENT CONTROL DATA - R&D

(Security classification of title, body of abstract and indexing annotation must be entered when the overall report is classified)

1. ORIGINATING ACTIVITY *(Corporate author)*
University of Illinois
Department of Electrical Engineering
Urbana, Illinois 61801

2a. REPORT SECURITY CLASSIFICATION
Unclassified

2b. GROUP

3. REPORT TITLE
DETERMINATION OF CHANGES IN EXOSPHERIC ELECTRON CONTENT BY A COMPARISON OF GROUP DELAY AND FARADAY ROTATION

4. DESCRIPTIVE NOTES *(Type of report and inclusive dates)*
Technical Report

5. AUTHOR(S) *(Last name, first name, initial)*
DuBroff, Richard E.

6. REPORT DATE	7a. TOTAL NO. OF PAGES	7b. NO. OF REFS
March 1972	46	9

8a. CONTRACT OR GRANT NO.	9a. ORIGINATOR'S REPORT NUMBER(S)
NGR-04-005-002	T. R. 45-2
b. PROJECT AND TASK NO.	
c.	9b. OTHER REPORT NO(S) *(Any other numbers that may be assigned this report)*
d.	UILU-72-2539

10. AVAILABILITY/LIMITATION NOTICES
Available on request until supply is exhausted

11. SUPPLEMENTARY NOTES	12. SPONSORING MILITARY ACTIVITY
	National Aeronautics and Space Administration Washington, D. C. 20546

13. ABSTRACT

A proposed technique of obtaining the exospheric electron content is by substracting the ionospheric electron content obtained from Faraday rotation measurements of VHF signals from a geostationary satellite, from the electron content obtained simultaneously from group delay measurements of the same signals. In this study, this technique is evaluated by using Faraday rotation data and group delay data simulated by ray tracing for a Chapman layer model extending from the ground to a height h_B, and an exosphere model extending from h_B to the satellite. The effect of varying the boundary height, h_B, is considered and it is shown that the Faraday rotation measurement is not significantly affected by the exospheric region, as expected in view of the rapidly decreasing geomagnetic field in that region. The group delay measurement is then considered in order to determine the size of the errors which would be involved if the electron content were obtained by approximating the group delay as a linear function of the electron content. Based upon the results of the simulation it is found that the accuracy of the technique is sufficient for providing only the changes in the exospheric electron content, but not necessarily the instantaneous values of the exospheric electron content.

DD FORM 1 JAN 64 1473

Unclassified

Security Classification

Unclassified

Security Classification

14. KEY WORDS	LINK A		LINK B		LINK C	
	ROLE	WT	ROLE	WT	ROLE	WT
electron content						
exosphere						
Faraday rotation						
group delay						
geostationary satellite						
ray tracing						

INSTRUCTIONS

1. ORIGINATING ACTIVITY: Enter the name and address of the contractor, subcontractor, grantee, Department of Defense activity or other organization *(corporate author)* issuing the report.

2a. REPORT SECURITY CLASSIFICATION: Enter the overall security classification of the report. Indicate whether "Restricted Data" is included. Marking is to be in accordance with appropriate security regulations.

2b. GROUP: Automatic downgrading is specified in DoD Directive 5200.10 and Armed Forces Industrial Manual. Enter the group number. Also, when applicable, show that optional markings have been used for Group 3 and Group 4 as authorized.

3. REPORT TITLE: Enter the complete report title in all capital letters. Titles in all cases should be unclassified. If a meaningful title cannot be selected without classification, show title classification in all capitals in parenthesis immediately following the title.

4. DESCRIPTIVE NOTES: If appropriate, enter the type of report, e.g., interim, progress, summary, annual, or final. Give the inclusive dates when a specific reporting period is covered.

5. AUTHOR(S): Enter the name(s) of author(s) as shown on or in the report. Enter last name, first name, middle initial. If military, show rank and branch of service. The name of the principal author is an absolute minimum requirement.

6. REPORT DATE: Enter the date of the report as day, month, year, or month, year. If more than one date appears on the report, use date of publication.

7a. TOTAL NUMBER OF PAGES: The total page count should follow normal pagination procedures, i.e., enter the number of pages containing information.

7b. NUMBER OF REFERENCES: Enter the total number of references cited in the report.

8a. CONTRACT OR GRANT NUMBER: If appropriate, enter the applicable number of the contract or grant under which the report was written.

8b, 8c, & 8d. PROJECT NUMBER: Enter the appropriate military department identification, such as project number, subproject number, system numbers, task number, etc.

9a. ORIGINATOR'S REPORT NUMBER(S): Enter the official report number by which the document will be identified and controlled by the originating activity. This number must be unique to this report.

9b. OTHER REPORT NUMBER(S): If the report has been assigned any other report numbers *(either by the originator or by the sponsor)*, also enter this number(s).

10. AVAILABILITY/LIMITATION NOTICES: Enter any limitations on further dissemination of the report, other than those imposed by security classification, using standard statements such as:

(1) "Qualified requesters may obtain copies of this report from DDC."

(2) "Foreign announcement and dissemination of this report by DDC is not authorized."

(3) "U. S. Government agencies may obtain copies of this report directly from DDC. Other qualified DDC users shall request through _____."

(4) "U. S. military agencies may obtain copies of this report directly from DDC. Other qualified users shall request through _____."

(5) "All distribution of this report is controlled. Qualified DDC users shall request through _____."

If the report has been furnished to the Office of Technical Services, Department of Commerce, for sale to the public, indicate this fact and enter the price, if known.

11. SUPPLEMENTARY NOTES: Use for additional explanatory notes.

12. SPONSORING MILITARY ACTIVITY: Enter the name of the departmental project office or laboratory sponsoring *(paying for)* the research and development. Include address.

13. ABSTRACT: Enter an abstract giving a brief and factual summary of the document indicative of the report, even though it may also appear elsewhere in the body of the technical report. If additional space is required, a continuation sheet shall be attached.

It is highly desirable that the abstract of classified reports be unclassified. Each paragraph of the abstract shall end with an indication of the military security classification of the information in the paragraph, represented as *(TS), (S), (C), or (U).*

There is no limitation on the length of the abstract. However, the suggested length is from 150 to 225 words.

14. KEY WORDS: Key words are technically meaningful terms or short phrases that characterize a report and may be used as index entries for cataloging the report. Key words must be selected so that no security classification is required. Identifiers, such as equipment model designation, trade name, military project code name, geographic location, may be used as key words but will be followed by an indication of technical context. The assignment of links, rules, and weights is optional.

Unclassified

Security Classification